Novel Algorithms for Cardiovascular Parameters' Estimation for Long Term Monitoring Systems

By

Moha'med Odeh Al-Jaafreh

Submitted in partial fulfilment of the requirements for the Doctor of Philosophy degree

Faculty of Engineering and Information Technology
UNIVERSITY OF TECHNOLOGY, SYDNEY
2009

CERTIFICATE OF AUTHORSHIP/ORIGINALITY

I certify that the work in this thesis has not previously been submitted for a degree nor has it been submitted as part of requirements for a degree except as fully acknowledged within the text.

I also certify that the thesis has been written by me. Any help that I have received in my research work and the preparation of the thesis itself has been acknowledged. In addition, I certify that all information sources and literature used are indicated in the thesis.

Signature of Candidate

MOHA'MED ODEH AL-JAAFREH

Production Note:
Signature removed prior to publication.

Acknowledgment

Over the last four years I have had the privilege of working with a variety of people who have made my time at University of Technology/ Sydney an enjoyable and intellectually stimulating experience.

I would like to thank all the people who have helped me along the way and contributed to this dissertation. I am especially grateful to my Supervisor Dr. Adel Al-Jumaily. In working with Adel, I have learnt how to pursue research problems with intellectual rigor and how to critically evaluate my work.

I would like to present my appreciations to the committee at Al-Hussain bin Talal University who sponsor me during my master and doctor of philosophy degrees.

I would like to thank the other members of my reading committee, Al-Ani, John and other people at Faculty of Engineering and information technology also CAS centre who provided invaluable guidance.

I have worked in the last couple of years with Akram, Gazi and Osman; they helped me to collect and analyse the data for healthy and unhealthy subjects. Besides, I would like to acknowledge the physio bank centre who offers MIMIC database and other databases for public use.

I would like to thank my friends and colleges who have been encouraged and support me to accomplish my degrees.

Finally, I would like to acknowledge the endless love of my father, my mother, my brothers, my sisters, my daughter and my wife (my life partner); who have been constant source of support also who have provided guidance, love and encouragement throughout my life. This thesis is dedicated to them.

Publications arising from this thesis

Book Chapters:

1. Adel A. Al-Jumaily and Moha'med O. Al-Jaafreh, *Multi – Agent System Concepts: Theory and Application Phases*, Chapter 19 in Book: Mobile Robots: Moving Intelligence, Edit by: Jonas Buchli, ARS International, pp.: 369-392, 2006.
2. Moha'med O. Al-Jaafreh and Adel A. Al-Jumaily, *Blood Pressure Estimation with Considering of Stroke volume Effect*, Encyclopedia of HealthCare Information Systems, N. Wickramasinghe and E. Geisler, Eds.: Idea Group Inc. (IGI Global), pp.: 965-971, 2008.

Conference Papers:

3. Moha'med O. Al-Jaafreh and Adel A. Al-Jumaily, "Type-2 Fuzzy System Based Blood Pressure Parameters Estimation," *2nd Asia International Conference on Modelling and Simulation (AMS 2008)*, May 13 – 15, 2008, Kuala Lumpur, Malaysia, pp.: 953-958, 2008.
4. Usman Mahmood, Adel A. Al-Jumaily and Moha'med O. Al-Jaafreh, "Type-2 Fuzzy Classification of Blood Pressure Parameters", *The third International Conference on Intelligent Sensors, Sensor Networks and Information Processing (ISSNIP 2007)*, December 3-6, Melbourne, Australia, pp.: 595 – 600, 2007.
5. Moha'med O. Al-Jaafreh and Adel A. Al-Jumaily, "Training Type-2 Fuzzy System by Particle Swarm Optimization", *IEEE Congress on Evolutionary Computation (CEC 2007)*, September 25-28, Singapore pp.: 3442-3446, 2007.

6. Moha'med O. Al-Jaafreh and Adel A. Al-Jumaily "Blood Pressure Estimation by Particle Swarm Optimization" *Cairo International Biomedical Engineering Conference 2006 (CIBEC'06)*, December 21-24, Cairo, Egypt, 2006.
7. Moha'med O. Al-Jaafreh and Adel A. Al-Jumaily, "Practical Swarm Optimization based Stroke Volume Influence on Mean Arterial Pressure", *The International Conference in Biomedical and Pharmaceutical Engineering 2006 (ICBPE 2006)*, 11th-14th December, Singapore, pp.: 508-511, 2006.
8. Gazi M. Azmal, Adel A. Al-Jumaily and Moha'med O. Al-Jaafreh, "Continuous Measurement of Oxygen Saturation Level using Photoplethysmography Signal", *The International Conference in Biomedical and Pharmaceutical Engineering 2006 (ICBPE 2006)*, 11th-14th December, Singapore, pp.:504-507, 2006.
9. Moha'med O. Al-Jaafreh and Adel A. Al-Jumaily "New Model to estimate Mean Blood Pressure by Heart Rate with Stroke Volume changing influence", *28th Annual International Conference of the IEEE Engineering in Medicine and Biology Society (IEEE EMBC 2006)*, August 31 - September 3, 2006, New York, USA, pp.:1803-1805, 2006.
10. Moha'med O. Al-Jaafreh and Adel A. Al-Jumaily, " Multi-Agent System for Estimation of Cardiovascular Parameters", *1st International conference on Computers, Communications, and Signal Processing, with special track on Biomedical Technology (CCSP 2005)*, 14-16 Nov, Kuala Lumpur, Malaysia, pp.: 296-299, 2005.
11. Adel A. Al-Jumaily, Joseph M. Azzi and Moha'med O. Al-Jaafreh "Novel Algorithm in Multi-agent Collaboration on Solving Pursuit Problem", *Proceedings of the 2nd International Conference on Mechatronics (ICOM'05)*, 10-12 May, Kuala Lumpur, Malaysia, pp.: 124- 131, 2005.

Table of Contents

List of Figures

Chapter 4

Chapter 5

List of Tables

List of Abbreviations (Acronyms)

ABP	Arterial Blood Pressure
AHA	American Health Association
AC	Alternated Current
BPP	Blood Pressure Parameters
BP	Blood Pressure
B&A	Bland & Altman Plot
CPLTMS	Cardiovascular Parameters Long Term Monitoring System
CO	Cardiac output
DBP	Diastolic Blood Pressure
DC	Direct Current
ECG	Electric cardio graph
EDBP	Estimated Diastolic Blood Pressure
EIP	Electrical Impedance Plethysmography
EMAP	Estimated Mean Arterial Blood Pressure
ESBP	Estimated Systolic Blood Pressure
HbO_2	Oxy-hemoglobin
Hb	De-Oxy-hemoglobin
HR	Heart rate
Hz	Hertz (frequency unit)
I	Circuit Current
IT2FS	Interval Type 2 Fuzzy System
LED	Light Emitting Diode
MAP	Mean Arterial blood Pressure
MF	Membership Function

ml	mile litre
mmHg	mile meter of Mercury (pressure unit)
MPSO	Multi-Particle Swarm Optimization
OS	Oxygen Saturation
PMF	Primary Membership Function
PPG	Photo-Plethysmography
PSO	Particle Swarm Optimization
SBP	Systolic Blood Pressure
SD	Standard Deviation
sec	Second
S_pO_2	Oxygen Saturation
SV	Stroke Volume
T1FS	Type 1 Fuzzy System
T2FS	Type 2 Fuzzy System
TPR	Total Peripheral blood vessel's Resistance
V	Velocity

Abstract

In daily life every person needs continuous monitoring of temperature, heart rate, oxygen saturation level, blood pressure parameters and other parameters to have some idea about one's body systems performance and to assist doctors to diagnose one's health status. This information is more necessary for aged and unhealthy people, while it is also necessary for healthy person, who represents the undiagnosed subject.

Usually, the healthy and unhealthy subjects are advised to measure their cardiovascular parameters at home at various times in a day to avoid any bad developments for their health status. Available self-measurement devices give only discrete readings and have not provided accurate information of heart rate, oxygen saturation level, and blood pressure parameters in many situations since most of them do not consider the body's movement or the uncertainty associated with the reading.

Moreover, Blood pressure parameters (BPP): Systolic, Diastolic, and Mean Blood Pressures, have some types of correlation with the heart rate. This relationship is nonlinear and has many levels of uncertainty. The Type-2 Fuzzy system has a capacity to deal with nonlinear and uncertainty systems. The estimate of Blood pressure parameters based on heart rate can be categorized under such systems that fuzzy system can deal with.

This thesis presents a novel algorithm to measure photo-plethysmography signal, heart rate and the oxygen saturation level and also to estimate BPPs for healthy and unhealthy subjects based on a prototype transducer, particle swarm optimization and type-2 Fuzzy System.

The measured values of heart rate, oxygen saturation level, systolic, diastolic and mean blood pressures by utilizing the novel algorithm are compared with the clinical readings of heart rate, oxygen saturation level, systolic, diastolic and mean blood pressure.

Very encouraging results have been achieved for estimating heart rate, oxygen saturation level, systolic, diastolic and mean blood pressures and the accuracy of estimated results for that parameters for healthy subjects, by our designed algorithm, are 99.53%, 98.91%, 97.76%, 91.81% and 96.43%, respectively.

Add to that, the accuracy of estimated results systolic, diastolic and mean arterial blood pressure for unhealthy subjects are 94.51%, 91.48% and 94.79%, respectively.

On the contrary, the mean arterial blood pressure is estimated based on same heart rate and existing algorithm. This algorithm can only estimate mean arterial blood pressure. The accuracy of estimated mean arterial blood pressure equals 53.83%.

The proposed model achieves very encouraging results; since all accuracies of the blood pressure parameters for unhealthy and healthy subjects are more than 91.4%. Moreover, the proposed algorithm can be utilized to determine heart rate, oxygen saturation level, systolic, diastolic and mean blood pressures.

Chapter 1. Introduction

The main reason for learning or studying is to benefit the world from results that achieved or will be achieved and obtained to satisfy life's requirements. Life's requirements differ personally, socially and regionally. In my opinion, the important requirement of life is health since it assists people to achieve their aims perfectly, smoothly and quickly.

Clinically, health is achieved by protecting all of the body's systems. The cardiovascular system is considered as the second important system after the neural system. Therefore, any imbalance in this system will affect all other systems directly or indirectly, and causes diseases, such as kidney failure and blindness.

This chapter provides research motivations that guide the researcher for investigating cardiovascular system parameters, challenging and interesting concerns, it characterizes research objectives and declares problem statement.

Moreover, contributions of research project will be highlighted to show the quantity and quality of the research's stages were achieved during PhD degree, then the PhD thesis structure will be expressed to simplify thesis reading and understanding.

1.1. Background

As the say "A stitch in time saves nine, Prevention mote Cure" [1], hence preventing and avoiding diseases are better than mitigation. Thus, careful protection and continuous diagnosis are the major issues that help and assist in avoiding many diseases. Moreover, the continuous diagnosis requires reliable, accurate and continuous measurements methods which have to be measured by low cost, non-invasive and user-friendly Instruments.

Cardiovascular diseases have affected more than 17% of Australians. Moreover, these diseases caused 36% of total deaths of Australians (or 47,637 persons) in 2004 [2]. Also

cardiovascular disease is the most expensive health condition, costing 11% of the total allocated health system or $5.4 billion in 2000-01 [3].

The diagnosing process of most of cardiovascular diseases is performed by blood pressure and oxygen saturation instruments. These need a lot of improvements to satisfy the expectations and prospects of subjects, physicians' and clinicians' expectations and prospects. Recent research studies in cardiovascular parameters' measurements aim to offer new instruments had achieved some success, but their measurements need some improvement to be reliable, accurate, continuous of diagnosis, comfortable of subjects and other expectations.

Therefore, trying to find a suitable and fit method and suitable instrument to measure most of cardiovascular parameters is a very interesting and challenging research area.

1.2. Motivation

The inspiration of this research study arose from subjects' requirements and physicians' expectations for measuring most of cardiovascular parameters. Hence, the main target of this research is developing and building a new system to measure most cardiovascular parameters non-invasively, comfortably, continuously, accurately, regularly, conveniently, independently, cheaply and other issues that satisfy the physicians' expectations and prospects.

In blood pressure measurement literature one reads that there are many methods utilized to determine blood pressure parameters' readings such as, Cannulation method, Auscultatory methods and Plethysmography methods. These three main methods will be explained in detail in Chapter 3.

A short description will be given to explain how these main three methods work to find out cardiovascular parameters and what the limitations of available methods are. The Cannulation method estimates blood pressure by measuring blood level on a cannula

which is attached to a flexible tube that is invasively inserted into subject's artery. The blood level is used to compute blood pressure as expressed in next equation:

$$P = \rho \times g \times h \quad \text{..... ..... (1-1)}$$

Where P is blood pressure,

ρ is blood density, g is acceleration of gravity, h is blood level.

Technically, the Cannulation method is avoided due to the painful and invasive feeling. Besides, the cannulation method has caused limb ischaemia, thrombosis, haemorrhage, infection and other side-effects [4].

On other hand, the Auscultatory method depends on a stethoscope to listen to the blood flow sounds through the brachial artery that is gradually liberated of external pressure. This pressure is applied by an air cuff, and the clinician observes the simultaneous changes of the mercury sphygmomanometer readings.

Actually, the Auscultatory method is not completely reliable because of the uncertainty of the stethoscope, uncomfortably of applying an external pressure and discontinuity of measuring blood pressure caused by gradual inflation and deflation of air cuff. Recently, Plethysmography methods have been used to measure most of cardiovascular parameters simultaneously. The Plethysmography methods are based on studying the correlation between Plethysmography's features and cardiovascular parameters. The Plethysmography methods and their measurements need some improvement to be reliable, accurate and other expectations. This motivation based this work to contribute to this research area. And the objectives of this research study can be expressed and determined as stated in next section.

1.3. Objectives

This research study presents a new methodology by designing the Cardiovascular Parameters Long Term Monitoring System (CPLTMS) based on the correlation between

Plethysmography's features and cardiovascular parameters and also by measuring cardiovascular parameters, such as heart rate, oxygen saturation and blood pressure. Based on motivation, the objectives of this research are:

1. Acquire Photoplethysmography (PPG) signal of the subject's finger;
2. Analyse the acquired PPG signal features;
3. Build a system to estimate blood pressure based on PPG signal features;
4. Investigate the deflections of other factors influences on BP estimations, such as stroke volume;
5. Develop the built system to consider the influence of other factors by using intelligent techniques, such as Particle Swarm Optimization;
6. Estimate oxygen saturation based on Photoplethysmography signal features;
7. Designing CPLTMS to measure most of cardiovascular parameters simultaneously;
8. Improve reliability and performance of CPLTMS by utilizing the intelligent techniques; such as Type-2 Fuzzy System and Multi-particle swarm optimization.

1.4. Problem statement

According to the objectives of this research, the main aim of this research is satisfy the requirements of subjects, physicians and clinicians through designing a device for continuous measuring of cardiovascular parameters with cheap sensors, good reliability, accuracy, comfortably and other factors based on finding the relation between Photoplethysmography signal features and cardiovascular parameters through using some intelligent techniques.

1.5. Contribution

During the doctor of philosophy (PhD) degree, these phases have been achieved:

1. Prototype device has been designed to acquire a Photoplethysmography signal (PPG) of the subject's finger.
2. Photoplethysmography signal of the subject's finger has been analyzed to estimate blood pressure based on PPG features
3. The deflections of other factors influences on BP estimations, such as stroke volume, have been investigated.
4. Particle Swarm Optimization (PSO) has been utilized to improve the models by considering the influence of other factors.
5. Near optimal constant values of stroke volume, total peripheral resistance and adjustment of stroke volume have been achieved by multi PSO.
6. A system for estimating oxygen saturation based on PPG features has been built.
7. A fuzzy type-2 system has been designed to estimate blood pressure parameters.

1.6. Thesis Structure

This thesis is organized as follows; the second chapter introduces the cardiovascular system, its parts, blood circulations, cardiovascular parameters, and major diseases that attack the cardiovascular system. The third chapter tracks the methods that are used to measure cardiovascular parameters and explains these methods and shows their drawbacks. The fourth chapter highlights the intelligent software techniques used through this Ph.D. research. The fifth chapter explains the methods that have been developed to measure heart rate and oxygen saturation and illustrates the experiments' results. The sixth chapter explains the methods that have been proposed to measure blood pressure parameters. The results of these methods have been demonstrated by

tables, figures, and graphs. The seventh chapter concludes and summarizes this thesis and suggests some areas of future research.

1.7. Summary

This chapter showed the importance of this research through stated some statistical data about project essential, clarified the research motivations, defined research objectives and stated problem statement.

Moreover, the contributions of research project were highlighted to clear quantity and quality of the stages were achieved during PhD degree, then PhD thesis structure were expressed to simplify thesis reading, evaluation and understanding.

Chapter 2. Cardiovascular system

The cardiovascular system is the second important system of body systems, it is consists of heart, lungs, blood, and blood vessels (arteries, veins and capillaries) and it controls blood flow and circulation in blood vessels by heart beating [5]. It is important to have some operation and biological knowledge about the cardiovascular system and its diseases, since all this research is about the cardiovascular system parameters; so this chapter covers these aspects and provides information about blood pressure diseases and some important advices to assist subjects to avoid these diseases.

2.1. Introduction

Biologically, the cardiovascular system is responsible about blood circulation in all organs of body, delivering oxygen (O_2) and nutrition to cells of all body organs and receiving carbon dioxide (CO_2) and wastes [6].

The blood circulation starts from the heart, which consists of right atrium (RA), right ventricle (RV), left atrium (LA) and left ventricle (LV), where it pumps an oxygenated blood into arteries to all body systems through LV and receives a deoxygenated blood by the veins through RA; this circulation is called a systematic circulatory.

Then the deoxygenated blood is pumped again to lungs through RV to replace CO_2 by O_2, and the lungs return the oxygenated blood to LA; this circulation is called a pulmonary circulatory. These two circulations are shown in figure 2.1 [7].

Through systematic and pulmonary circulations, the blood pressure is high in the arteries and arterioles, then it decreases very quickly in capillaries, and it almost vanishes in the veins, that alteration of blood pressure within blood circulations is shown in figure 2.2 [8].

Clinically, cardiovascular system parameters are the heart rate, oxygen level, pulse wave velocity, peripheral vessel resistance, systolic blood pressure (SBP), diastolic blood pressure (DBP), and mean arterial blood pressure (MAP). From these parameters, blood pressure parameters are considered as important cardiovascular parameters. The Blood pressure is defined as the force of heart beats against the vessels' walls [9]. From this definition blood pressure parameters relay on other cardiovascular parameters such as heart rate, pulse wave velocity, and vessels' resistance.

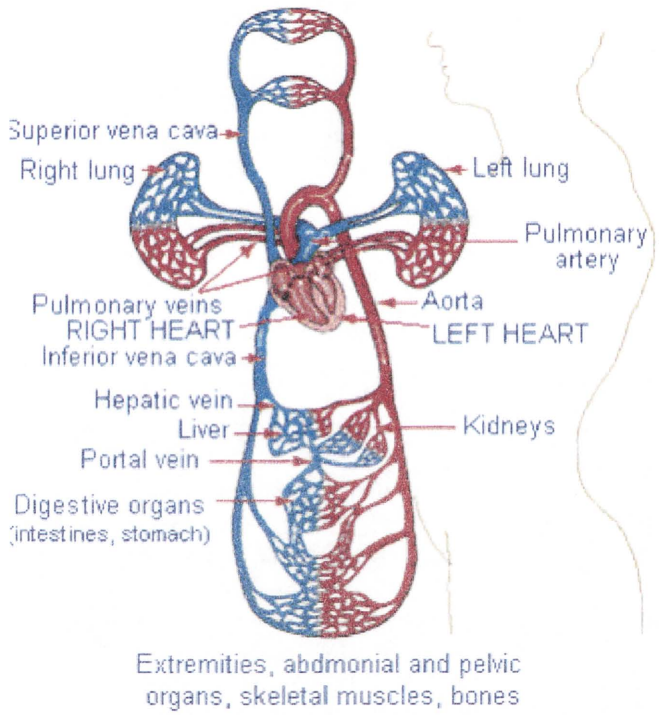

Figure 2.1: Schematic representation of pulmonary and systemic circulations [7]

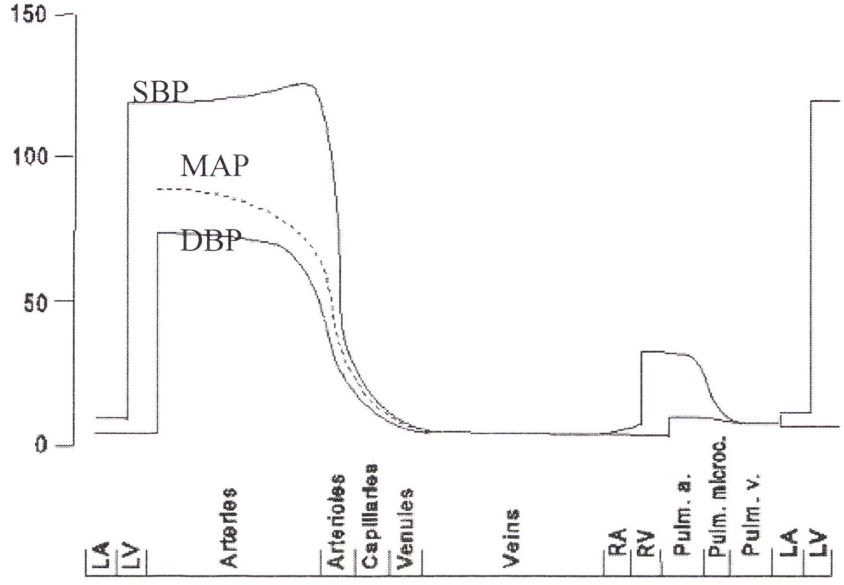

Figure 2.2: Pressure drop in the circulatory system [8]

Also, Blood pressure is identified as the force of blood flow against the arteries' walls. Technically, the blood pressure is divided into three parameters or stages depending upon heart contractions. Since blood pressure is controlled by the heart and its contractions, firstly, SBP which is defined as the pressure when the heart contracts and pushes the blood into the aortic artery, secondly MAP; which is defined as the pressure within heart beat and at maximum blood oscillations in arteries, and DBP which is defined as the pressure when the heart relaxes and receives blood from veins.

MAP is hard to measure by some instruments. Therefore, MAP is calculated from SBP and DBP values as follows [10]:

$$DBP = MAP - ((SBP - MAP) / 2) \text{ [11]} ==>$$

$$2 \times DBP = 2 \times MAP + MAP - SBP ==>$$

$$2 \times DBP + SBP = 3 \times MAP ==>$$

$$3 \times MAP = 3 \times DBP - DBP + SBP ==>$$

$$MAP = DBP + (SBP - DBP) / 3 \quad \ldots\ldots\ldots\ldots\ldots\ldots\ldots\ldots\ldots\ldots \text{(2-1)}$$

Typically, the human body systems work at a high standard in healthy cases; when SBP average value equals 120 mmHg and DBP average value equals 80 mmHg, then any

change in SBP or DBP higher or lower than the average value, it is a sign of disease. In most cases the pressure is higher than the average value that is a sign of Hypertension disease. On the contrary, any value lowers than the average value of blood pressure is a sign of Hypotension disease.

2.2. Hypertension

The normal value of a person's systolic blood pressure is 120mmHg, so any measurements of BP higher than 140 mmHg is hypertension. Thus the body will have some symptoms such as headache, tiredness, confusion, visual changes, nausea, vomiting, anxiety, perspiration, pale skin or redness, crushing substernal chest pain and other symptoms.

When many SBP measurements for the same subject are between (120-139 mmHg) and DBP are between (80-89 mmHg), this indicates a case of prehypertension. This is an indication of increase in the probability of hypertension affection [12].

2.2.1. Factors cause Hypertension

Hypertension can be noticed by increasing of blood amount that is pumped by the heart, with a faster heart beat and a change in the conditions of the arteries. The real reasons of hypertension are undetermined yet, but many physicians state that some cause factors are age, weight, amount of cholesterol, stress, lack of sleep, coffee, fat, salt, and many others. These factors increase the heart rate and the amount of blood which is pumped, thus elevating blood pressure.

These factors cause heart to pump more than sufficient amounts of blood to all body systems. This causes heart fatigue and failure. That vast blood amount will flux quickly in cardiovascular vessels and it causes stiffness in vessels' walls, scratches capillary walls and may lead to brain stroke.

A person's age reduces the arteries' elasticity and their diameter. It also increases the hardness of arteries' walls, so blood pressure is increased because the force of pumped blood which distributed into a smaller area.

High weight increases the amount of blood pumped by the heart during any exercise and coats both sides of arteries' walls with some fat which reduces the area where force of blood is distributed.

Stress, some diseases, and lack of sleep cause muscle contraction and produce many hormones which require a high amount of blood and increase blood density and viscosity; hence, blood pressure will increase.

Coffee, smoking, fat, salt, drugs, and other factors increase the blood density and this increases the blood force which elevates blood pressure.

2.2.2. Diseases due to Hypertension

Patients with hypertension can only perform some exercises with difficulty if hypertension symptoms are not serious, but hypertension affection will be a reason for many diseases, such as headache, ISH, heart problems and failure, kidney failure, artery stiffness, heart attack, brain stroke, blindness, aneurysm, arrhythmias, heart tumour, angina and death.

These diseases are described briefly in the following list [2]:

1. Isolated systolic high blood pressure (ISH) is an elevation in systolic measurement only; this happened mostly in older people >60 years;
2. Heart failure that means the heart misses the ability to pump sufficient blood to the body; this leads to insufficient oxygen percentage and nutrition to body systems;
3. Kidney failure when the kidney loses the ability to draw urine from blood and return back pure blood to body;
4. Artery stiffness that makes the artery lose its elasticity and leads to narrow arteries;

5. Heart attack that happens when the heart muscles are ischemic or injured;
6. Brain stroke which is stopping the brain or part of brain from fulfilling its duties from blood drop on that part, due to hypertension in the cerebral arteries or clotting within these vessels;
7. Blindness;
8. Aneurysm which is an unusual extension of a blood vessel portion. Therefore, that part of artery wall becomes weaker;
9. Arrhythmia which causes an irregular of number of heart beats per minute, which lead to tiredness of the heart muscle;
10. Heart tumour is an abnormal growth of heart tissue;
11. Angina is a strong chest pain due to insufficient blood flow through the arteries, especially the coronary artery and the heart muscle.

2.3. Hypotension

Hypotension is the case when blood pressure in arteries less than normal (<120/80 mmHg); this reduces the blood amount reaching the body systems, especially brain (e.g. extremities). This case has many clear symptoms such as light-headed, a cold feeling, fainting, dizziness, unfasten muscles or coma [13].

2.3.1. Factors causing Hypotension

Hypotension can be noticed when a person changes his position; standing up quickly or starting running. The main reasons of hypotension are drugs, alcohol, and hypertension medicine. In addition, patients of diabetes, arteriosclerosis, bad veins and pregnant women have hypotension due to the effect of progesterone produced by the placenta which causes generalized vasodilatation especially in the second trimester.

The most problematic situation arises if blood cannot reach organs due to artery narrowing (ischemia), or obstruction (clot). Moreover, Hypotension results of many reasons; such as heart attack, severe fever, serious burns, cancer, trauma and extensive blood loss, adrenal failure, serious infection, and shocks.

2.3.2. Diseases due to Hypotension

Patients with hypotension cannot perform any exercise or work since blood cannot reach body organs with low blood pressure. Hypotension patients take medicine or have been quickly transferred to a medical centre to elevate blood pressure immediately. Hence, there is no disease created due to hypotension, because there is no chance for any development of this disease.

2.4. Prevention

Physicians advise hypertension patients and others to decrease their weight, do training exercises and reduce salt, coffee, and active drugs intake, and to stop smoking, to prevent any cardiovascular diseases. In a nutshell, periodic checks of blood pressure and healthy life style are the key for preventing hypertensive disorders.

The American Heart Association presents these ten advices to control BP [12]:

1- Check your blood pressure regularly;

2- Check your weight regularly. Keep it at a balanced level or below;

3- Reduce the amount of salt in cooking or at meals;

4- Eat a low saturated fat diet;

5- Control alcohol intake;

6- Take your medicine exactly as prescribed;

7- Keep appointments with the doctor;

8- Follow your doctor's advice about physical activity;

9- Make certain your parents, brothers, sisters and, children have their blood pressure checked regularly;

10- Live a normal life in every other way.

2.5. Summary:

This chapter provided a brief background about cardiovascular system through describing the blood circulations, clarifying blood pressure parameters and defending blood pressure diseases then providing some important advices to help and assist subjects to avoid these diseases.

As can be notice, the blood pressure and other cardiovascular parameters are very important for the human body operations and it is necessity to check and measure them for healthy and unhealthy subjects. So many methods have been created. The main methods will be highlighted in the next chapter.

Chapter 3. Current methods to measure cardiovascular parameters

In the literature, there are many sensors and instruments used to measure one or more parameters of the cardiovascular parameters, such as heart rate, pulse wave velocity, oxygen saturation level and blood pressure parameters.

These sensors and instruments are developed since the eighteenth century and improved later to offer reliable, computerized, automatic, user-friendly, non-invasive, fast, continuous measurements and considered other issues that satisfy the physicians' expectations and prospects. These sensors are attached to different organs of the body, such as chest, arm, wrist, head, thigh, or finger to acquire data and signals. The acquired data are used to generate the cardiovascular parameters' readings.

3.1. Introduction

Many methodologies and instruments have been developed to be used to measure cardiovascular parameters, the next sections provide historical information and background on various instruments and sensors that have been used to measure cardiovascular parameters to clarify the work that has been done in this wide research area and to discuss some disadvantages and short outcomes that should be addressed to improve the cardiovascular parameters' instruments. These sections are arranged based on the historical sequence (chronically) and classified based on how the data acquired; such as heart sound, blood level, pulses with external blood pressure, pulses with local blood pressure, photo-plethysmography signal, pulse arrival time and other factors.

3.2. Heart sound

In last ages, the heart sound was acquired to sense heart beats by the absolute human ear. This was used to listen to heart beats directly. In 1761, Leopold Auenbragger stated the tapping display any irregularities in heart beat. He named this the "thoracic

percussion" technique. In the beginning of the nineteenth century Nicolas Corvisart, who was a supporter of Auenbragger's technique, raised an auscultation promotion; "listening to the sounds body cavities made when tapped firmly" [13].

In 1819, a new sensor was invented by a French physician R.T.H Laennce, a follower of Nicolas Corvisart. Laennce's sensor consists of a tube of rolled paper used to listen to the heart beats for a young lady instead of laying his head on her chest. He then improved that sensor and replaced a paper tube with perforated wooden cylinder (diameter = 3.5cm, height = 25cm) to form the Stethoscope, as shown in left of figure 3.1. A stethoscope is not more accurate than laying one's head on a patient's chest; it just has a social benefit than clinical benefit because the chest diagnosis becomes more gentle [14].

This instrument was improved with the invention of binaural stethoscope (having two earpieces) in 1852, as shown in middle of figure 3.1. Then it was improved by filtering and amplifying the heart sound, as shown in right of figure 3.1. The developed stethoscope is presently used by most of physicians and it became as a badge for them.

Figure 3.1: Stethoscope's Forms

3.3. Blood level "arterial cannulation"

In 1733, a blood level was measured to estimate blood pressure by Reverend Stephen Hales, an English naturalist. He was. He estimated blood pressure via measuring blood level on a brass pipe, which was inserted into a horse's artery and then connected to a

glass tube to watch the blood level which was caused by blood pressure affection [15]. This method will henceforth be referred to as Hale's method.

Hale's method is illustrated in figure 3.2. Hale calculated the blood pressure of a horse based on next equation:

$$P = \rho \times g \times h \quad \text{..... (3-1)}$$

Figure 3.2:Hale's method [11]

Hale's method was applied on a human body by Carl Ludwig in 1847; it became the first measurement of human blood pressure, but he used a new instrument. Carl's instrument was a kymograph, which means a wave writer in Greek, with catheters inserted into the artery of the chest or arm. A kymograph is composed of a U-shaped manometer tube which was attached to a brass pipe cannula that was invasively inserted into the subject's artery. The manometer tube consists of an ivory float and attached to a rod with a quill which sketches a blood pressure signal on rotating drum as shown in figure 3.3.

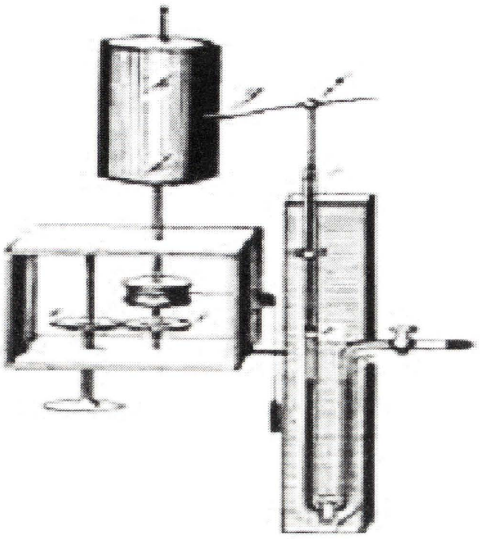

Figure 3.3: Kymograph

Carl's method is developed by reducing the size of catheter and replacing the kymograph by a digital instrument. So, instead of using a quill to sketch a blood pressure signal, the blood pressure signal is sketched on a grided screen or paper or converted to numbers which are shown on a screen.

Nowadays, Carl's method, which is clinically known as "arterial cannulation", is a standard method for measuring blood pressure since it measured blood pressure of the subject directly and invasively, but it is avoided due to the painful and invasive feeling by the subjects. The bad effects of arterial cannulation are limb ischaemia, thrombosis, haemorrhage, infection, and others [4].

Because of the disadvantages and risks of the arterial cannulation method, an estimation of blood pressure by non-invasive indirect methods was required. Researchers depend on other factors instead of blood level to estimate blood pressure.

Despite arterial cannulation's disadvantages, it is still used to measure blood pressure in special cases, such as patients undergoing surgery or high intensive care and as standard measurements to compare the blood pressure recording obtained from other methods and determine the methods' performance.

3.4. Pulses and external pressure

Instead of an invasive method like "arterial cannulation", indirect methods have been developed to measure the blood pressure by measuring a relative external pressure. This pressure was applied on a subject's organ to cease blood flow in that organ. Some of these methods are palpation, auscultatory, oscillometric and local pressurization methods. All these methods measure a relative external pressure that is applied via an air-cuff wrapped around a subject's organ, such as an arm, wrist, finger, head, or thigh.

3.4.1. Palpation method

The palpation method gets its name from the way that has been used to sense heart beat(s). It is implemented by applying an external pressure that obliterates blood flow in brachial artery and eliminates the heart beat. The disappearing of blood flow is palpated or sensed near patient's wrist via physician's fingers as shown in figure 3.4.

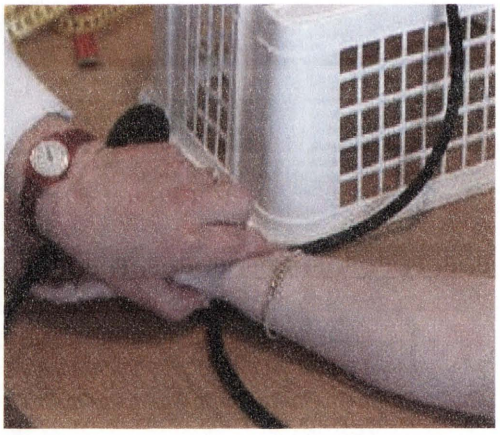

Figure 3.4: Palpation method

At the moment of disappearance of heart beat, that external pressure equals the Systolic blood pressure (SBP) [11].

In 1855, Karl Vierordt invented the palpation method. He found that, if an enough pressure was applied via an air-cuff which was wrapped around subject arm, then the arterial pulse would be eliminated. That applied pressure nearly equals blood pressure that measured by arterial cannulation [11].

Later, Von Basch invented the water-sphygmomanometer, which is composed of a bag joined with a water-manometer to determine the pressure required to eliminate the arterial pulse [11].

In 1896, Scipione Riva-Rocci invented the mercury sphygmomanometer by using a mercury-manometer instead of water-manometer which is better than Von Basch's device because the mercury-manometer is more sensitive than the water-manometer and also the mercury does not stick inside the manometer wall [11].

Actually, this method estimates the SBP only as well as the percentage of error and the uncertainty level are high because of the heart beat sensing based on the sensitivity of physician's fingers. These reasons support and encourage research of blood pressure measurement to develop and improve the palpation method or invent new ways to benefit from the technological development in the field of medical instruments.

3.4.2. Auscultatory method

Nikolai Korotkoff developed the Auscultatory method based on palpation method [15]. He used the stethoscope to sense the heart beat disappearance, which was caused by constriction of blood flow in the brachial artery, instead of fingers' touching sense. He found five characteristic sounds at certain points during the deflation of air-cuff caused by the irregular passage of blood through the brachial artery. The Korotkoff's sounds are classified as:

1.Sharp sound: It is a faint sound that firstly appears. Its intensity is increased regularly;

2.Swishing sound: It is a softened sound that may become "swishing in quality" [15];

3.Crisper sound: It is the sharp sound again, but its intensity is reduced;

4.Muffled sound: It is the swishing sound again but with less intensity;

5.Silence: The sound disappears completely.

Korotkoff's technique is called "auscultatory method" since it depends on a stethoscope to listen for the blood flow sounds through the brachial artery and to observe the change on the mercury sphygmomanometer as shown in figure 3.5.

The blood pressures parameters are measured according to characteristic sounds; the sphygmomanometer record at sharp sound is registered as systolic blood pressure while the sphygmomanometer record at silence is registered as diastolic blood pressure. This technique becomes more reliable and more trustworthy than the palpation method [11].

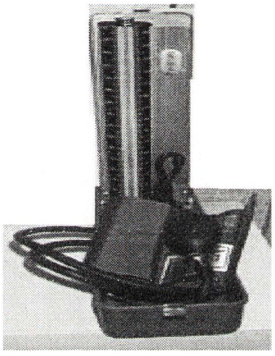

Figure 3.5: Sphygmomanometer

The Korotkoff's characteristic sounds and the correspondingly decreasing of pressure in sphygmomanometer by deflating cuff pressure that wrapped around patient's arm as well as the Korotkoff's technique "auscultatory method" are shown in figure 3.6 [15].

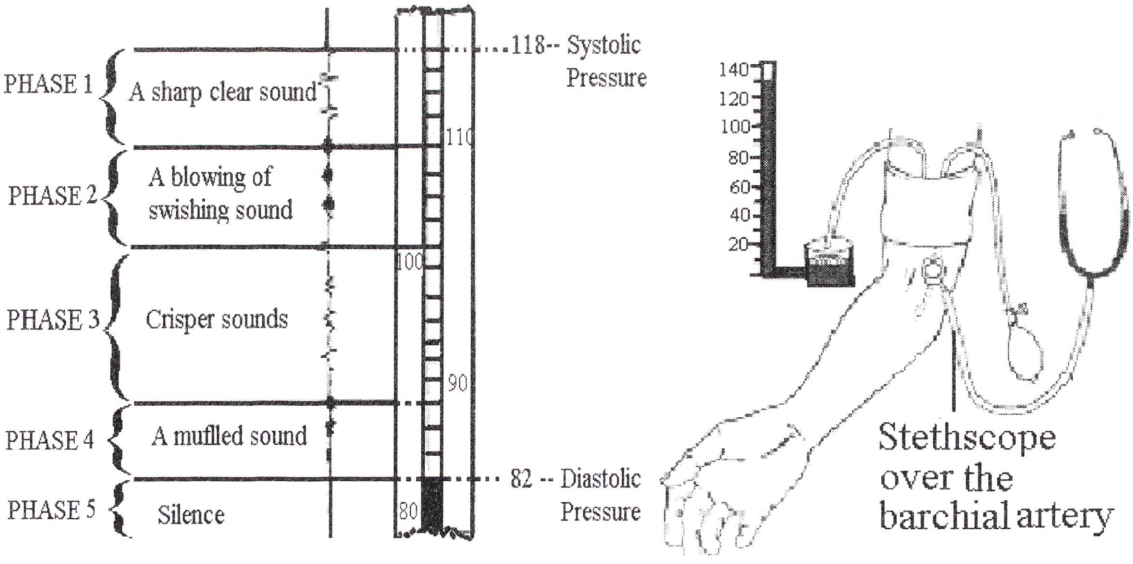

Figure 3.6: Korotkoff's characteristic sounds and auscultatory method

Currently, this method is used mostly in many medical centres instead of "arterial cannulation" since blood pressure is non-invasively estimated and auscultatory methods results are nearly equal the results of "arterial cannulation". This method is not completely reliable because of the uncertainty of the stethoscope and external pressure. Therefore, researchers developed the oscillometric method based on palpation method. It depends on sensing the blood flow oscillation in brachial artery.

3.4.3. Oscillometric method

The oscillometric method differs from the auscultatory method in the way that the heart beat or blood flow is sensed. The blood flow oscillations are measured by a device located under a warped occluding cuff.

The procedure of oscillometric method depends on applying an external air pressure by an air-cuff wrapped around forearm of the patient or subject. When the pressure decreases during the deflation process, the blood starts flowing in the brachial artery, the oscillations are started, small amplitude, and that pressure is SBP. Continuously decreasing that pressure increases the oscillations' amplitude. At maximum oscillations' amplitude, the applied pressure is equal to mean blood pressure (MAP). Finally, the DBP is calculated by equation [15] :

$$DBP = MAP - ((SBP - MAP)/2) \quad \text{..... (3-2)}$$

This method decreased the uncertainty in the measurement compared with auscultatory or palpation methods because an automatic or semi-automatic device is used to detect the blood flow in the brachial artery [11].

3.4.4. Local pressurization methods

These methods depend on applying an external pressure on a segment of such arteries by using a small size of air-cuff instead of occluded all vascular vessels under a normal

air-cuff. The main methods of local pressurization are volume-compensation and volume-oscillometric methods which are described in the next subsection.

3.4.4.1. Volume-compensation method

This technique is called volume-compensation since it is based on compensating the volume of occluded artery segment (V_a) by applying an external pressure. V_a equals the artery's cross-sectional area multiplied by cuff width. V_a is compensated by the cuff pressure (P_c) which equals the mean intra-arterial pressure (P_a) when the transmural pressure (P_{tr}) equals zero; P_{tr} calculated by:

$$P_{tr} = P_a - P_c \quad \text{..... (3-3)}$$

When P_{tr} equals zero, the artery is at an unloaded state (indirect unloading).

P_c is changed by deducting the difference between V_a changes and the unloaded volume (V_{ref}); which is considered as an error fed to volume-servo system (VSS). Hence, the changes in blood pressure (intra artery volume) will directly transfer as changes in P_c. This method is illustrated in the hand clarification drawing shown in figure 3.7.

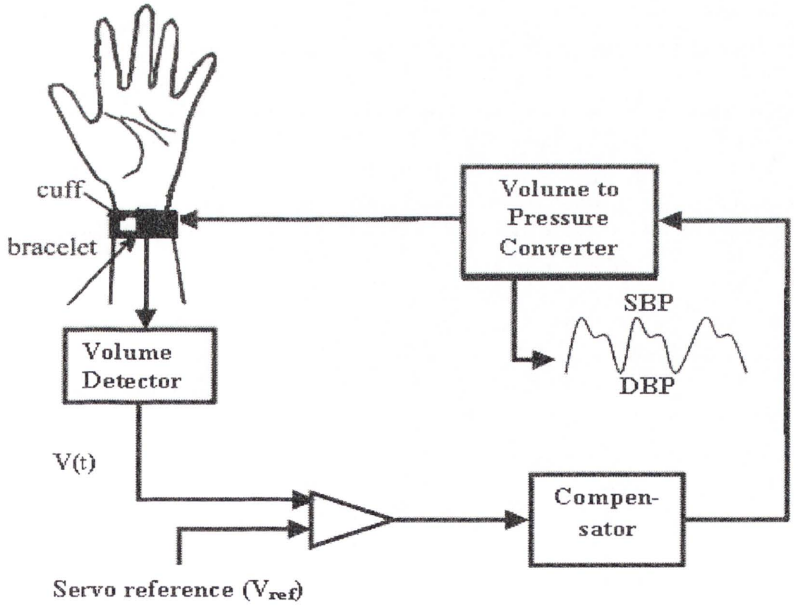

Figure 3.7: Volume-Compensation method

P_c is changed by VSS according to the P_a changes to compensate V_a changes from the unloaded state. The SBP, MAP and DBP can be determined by Volume-compensation

method depends on P_c; where P_c at unloaded state equals relative MAP and the maximum P_c equals relative SBP and the minimum P_c equals relative DBP [17, 18] .

Many research studies estimate blood pressure based on volume-compensation methods by utilizing such arteries: the radial artery in the wrist or a superficial temporal artery in the head.

For the radial artery in wrist, the occluding cuff is included at a wrist bracelet. This bracelet has to be located in a suitable place to optimize pressure on the radial artery so the cuff is located exactly to occlude the radial artery in the wrist only. The part of the radial artery in that location was proposed since it is close to the skin and the radial artery can be completely occluded by a square-cuff with radius bone assistance [19].

For a superficial temporal artery in head, the occluding cuff is included in a circular belt which is tied around the forehead. The cuff is designed to occlude the superficial artery with skull bone assistance [20].

3.4.4.2. Volume-Oscillometric method

This technique is the same as the Oscillometric method but a local pressure is applied instead of general pressure to reduce the disadvantages and risks of the Oscillometric method. The "volume" word comes from the changes of artery volume by applying an external pressure (P_c). Volume changes can be detected by photoplethysmography (PPG) sensor which consists of a near-infrared light emitting diode (LED) as a light-source and a sensitive photodiode as a photo-detector [18, 21].

The Volume-Oscillometric method is based on applying an external pressure (P_c) that equals the mean intra-arterial pressure (P_a) when the transmural pressure (P_{tr}) equals zero, P_{tr} is calculated by equation (3-3).

When P_c decreases during the deflation process, the blood starts flowing in the artery and the oscillations of volume signal are started. The SBP, MAP and DBP can be

determined by the Volume-oscillometric method which depends on P_c; when the amplitude of volume signal is small then P_c equals relatively to SBP. A continuous decrease of P_c increases the oscillations' amplitude. At maximum oscillations' amplitude, P_c equals relatively to MAP. Finally, the DBP is calculated by equation (3-2). This method is illustrated in the hand clarification drawing shown in figure 3.8.

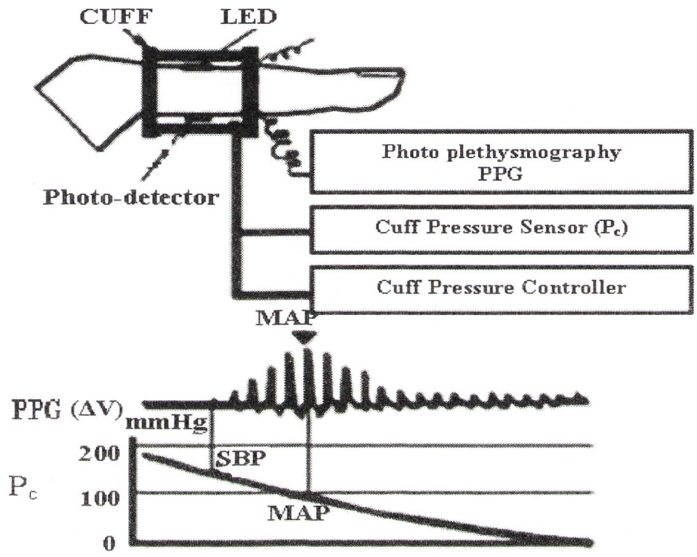

Figure 3.8: Volume-Oscillometric method

Many research studies estimate blood pressure based on volume-oscillometric methods by utilizing palmar digital artery in the finger or femoral artery in the thigh

For palmar digital in the finger, the occluding cuff is included in a cuff-supporter tied around finger's joint. The cuff-supporter consists of two holding plates; a hinge like a paper clip and a screw to fix the hinge and a PPG sensor. The cuff is designed as a disk to occlude the digital palmar artery with basal phalanx bone assistance [22].

For the femoral artery in the thigh, there is no need for an occluding cuff since the posterior of the thigh, while sitting on a chair seat (toilet seat), contains small arteries of perforation. These arteries are used as a site to measure the volume pulsation by using PPG sensors. Then by using Volume-oscillometric method, the blood pressure was

estimated. These sensors are arranged on a plate in a toilet seat beneath the area of skin contacts [23].

Nowadays, many instruments, which were based on local pressurization methods, are widespread and consist of an air-cuff wrapped around wrist or finger. Some of these models are illustrated on figure 3.9.

Figure 3.9: Local pressurization instruments

The methods, which have been described in this section, depend on Pulse and applying an external pressure. Therefore, these methods need some components, such as an air-cuff, motor, controller and others which cause instruments to be heavy, large and power consumption instruments. As well, these instruments consume time for inflation and deflation of the cuff.

Moreover, applying external pressure causes side effects; such as:

1- Discomfort and trouble for the subject;

2- Blood pooling or venous congestion;

3- Redness skin where the cuff is wrapped;

The consumed time may be reduced but not cancelled by using local pressurization techniques. This causes discontinuous of measurements that measure beat-by-beat blood pressure by using an air-cuff. One of the problems can be noticed when time is consumed for inflation and deflation is constant but the beat-by-beat time is changed according to the subjects' activities.

These disadvantages encourage researchers to find new factors and methods to estimate blood pressure non-invasively and continuously as the next section highlights.

3.5. Pulse arrival time

The new trend has been adopted because of many studies of estimating blood pressure depending on measuring the pulse arrival time or/and pulse wave velocity. The relationship between blood pressure and the pulse wave velocity can be derived from the Moens-Korteweg formula [24] :

$$v = \sqrt{\frac{gEa}{\rho d}} \ , \ v = \frac{K}{T} \quad \text{..... (3-4)}$$

Where v is the pulse velocity

g is the gravitational constant

E is the elastic modulus

a is the wall thickness of the vessel

ρ is the blood density inside specified vessel

d is the interior diameter of the vessel

K is a proportional coefficient of the specific distance for the pulse wave

T transit time in seconds; pulse arrival time

The elastic modulus of the vessel is increased exponentially with blood pressure [25] as in next equation:

$$E = E_0 e^{\gamma P} \quad \text{..... (3-5)}$$

Where P is the blood pressure

E_0 is the elastic modulus at zero pressure

γ is the coefficient vessel elasticity (0.016 - 0.018 $mmHg^{-1}$).

Then from equations (3-4) and (3-5) blood pressure can be estimated by next equation:

$$P = \frac{1}{\gamma}\left[\ln\left(\frac{K^2 \rho d}{gaE_0}\right) - 2\ln T\right] \quad \text{..... (3-6)}$$

The blood pressure changes only when the pulse time arrival changes, the changes in wall thickness and artery diameter are negligible as well as the changes of E_0 is slow enough, hence:

$$\frac{dP}{dT} = -\frac{2}{\gamma T} \text{ or } \Delta P = -\frac{2}{\gamma T}\Delta T \quad \text{..... (3-7)}$$

From the above equations and assumptions, the relationship between the blood pressure and pulse arrival time is shown in following equation:

$$P_e = P_b - \frac{2}{\gamma T_b}\Delta T \quad \text{..... (3-8)}$$

Where P_e is the estimated blood pressure

P_b is the base blood pressure

T_b is the pulse arrival time corresponding to P_b

ΔT is the change in the pulse arrival time

The systolic blood pressure has been estimated by Chen [26] based on subject-dependent information of series of SBP values. He used the higher frequency component (HFC) and lower frequency component (LFC).

HFC has been found from converting the filtered re-scaled pulse arrival time by an infinite impulse response narrow band-pass filter by using equation (3-8).

The pulse arrival time is the time interval from the appearing of QRS apex of the R wave to the appearing of onset point in the same heart beat as shown in figure 3-10.

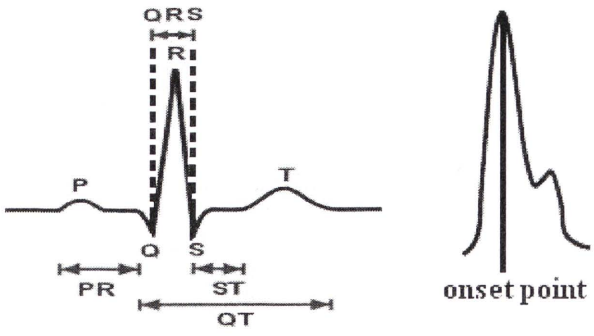

Figure 3.10: QRS apex of R wave and onset point of PPG signal

The onset point was detected by a PPG sensor at the finger tip via an ox-metric sensor. LFC was extracted from a series of SBP values, which were interpolated at sampling rate of 1Hz by using a linear look-up table method. SBP values were measured via an automatic measuring system, arterial cannulation, at an interval T_C of 5 minutes as intermittent calibrations. The estimated SBP equals the HFC plus LFC.

The correlation coefficients, root mean square error and arithmetic mean error methods were used to evaluate the performance of estimated systolic blood pressure and calculate the estimation errors. The mean and standard deviation of correlation coefficients of estimated SBP and invasive SBP among twenty patients, root mean square error and arithmetic mean error are tabled in table (3-1):

Table (3-1): Statistical amounts of Chen's method

Statistical amounts	Mean	Standard deviation
Correlation coefficient	0.97	0.02
Root mean square error	3.7	1.85
Arithmetic mean error	0.06	0.68

This method has some drawbacks, such as applying the measurement on unhealthy subjects and within operations time. The elasticity of the arterial wall was neglected, the LFC values are subject dependent and the study showed a linear relationship between

systolic blood pressure and also the pulse arrival time within the frequency band (0.53 mHz – 4 mHz).

Therefore, other researchers adopted different methods that utilizing different sensors to estimate more reliable and subject independent blood pressure. Some of these sensors are explained in next section.

3.6. Existing proposed methods based on photo-plethysmography signal

Photo-plethysmography (PPG) signal is acquired by a PPG sensor; which consists of infrared light emitting diode LED as transmitter and a photo-diode as a receiver. The PPG sensor is attached to the subject's finger. The output of PPG sensor is a pulse wave signal. That signal has been known as PPG signal. Heart beat is calculated according to the number of pulses of PPG signal within each minute.

There are two types of PPG's sensors:

1. Reflective PPG sensor: this type is based on the reflected optical beam of finger's bone and tissues; because both Optical diode and LED are located on front side of finger, as shown in figure 3.11(a);
2. Transmissive PPG sensor: this type is based on the penetrated and transmitted optical beam through the finger's bone and tissues, since Optical diode and LED are located on opposite sides of the finger, as shown in figure 3.11(b);

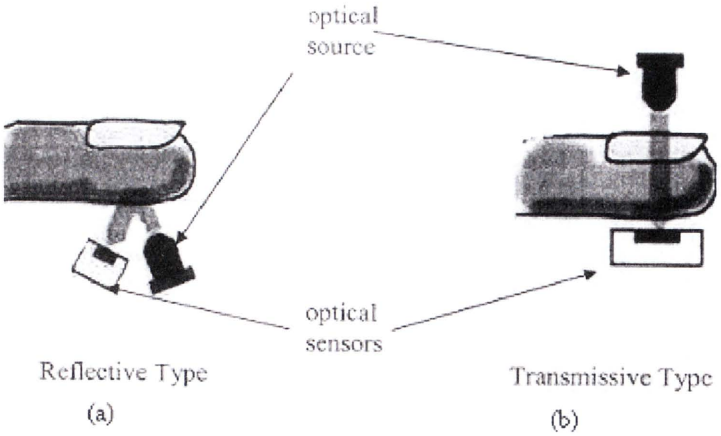

Figure 3.11 Photo-plethysmography Types

The output of photodiode, which is shown in figure 3.12, has a high DC level. Therefore, a filter is used to remove DC level. Then, an amplifier is used to amplify the filtered PPG signal.

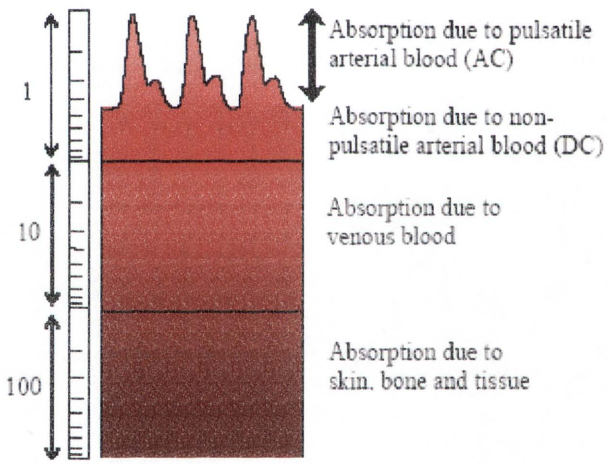

Figure 3.12: PPG signal

3.6.1. Existing proposed methods to measure Oxygen Saturation Level

Oxygen Saturation level (SpO2) is measured by a pulse Oximeter, which has been used as a standard measure during neonatal care, anesthesia and post-operative recovery [27]. Pulse oximeter uses PPG that is described above to measure the SpO2 by a non-invasive spectrophotometric method and it is used to estimate the heart rate and the blood oxygen saturation level of an individual [28].

Current Pulse Oximeters perform well when a monitored subject is in a resting position. Their reliability, however, is notably reduced when the subject moves, even when movements are only involuntary, such as shivering. Therefore, the reduction of motion artifacts is one of the main concerns in the development of pulse oximeters [29].

Measuring Oxygen Saturation level based on the ratio of the optical absorption of hemoglobin and oxy-hemoglobin. It is based on the Beer-Lambert Law, which establishes a relationship between absorbance and concentration of an absorbing liquid. More details about this method are presented in Chapter 5.

3.6.2. Existing proposed methods to measure Blood pressure

Based on PPG signal and other factors, Yang, Asada and Zhang [30] developed a method to measure the blood pressure and electro-cardiograph (ECG) signal by using a finger's artery. Their method's sensor is called a "ring sensor". Figure 3.13 shows a prototype of ring sensor.

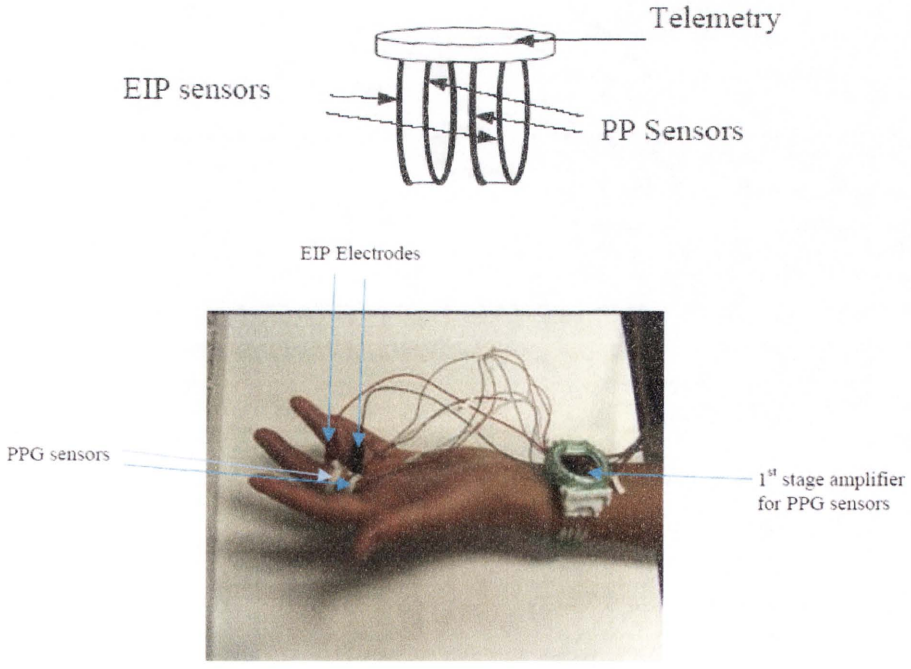

Figure 3.13: Ring sensor

Ring sensor structure depends on two types of plethysmographys; photo-plethysmography (PPG) and electrical impedance plethysmography (EIP); where EIP is implemented by two impedance electrodes as shown in figure 3.13.

PPG signal and two arterial diameters have been measured by two reflective PPG sensors and volumetric change of the arterial segment has been measured by two EIP's sensors. Therefore, PPG signal, the cross sectional area and volume change of artery are the major factors that measured to estimate blood pressure.

Asada's team employed four Hemodynamic models: local, upstream, down stream, arterial, and visco-elastic of arterial wall models based on PPGs and EIP signals. Then they use the Kalman filter to estimate blood pressure.

The artery model for the parameters of four hemodynamic models is demonstrated in figure 3.14:

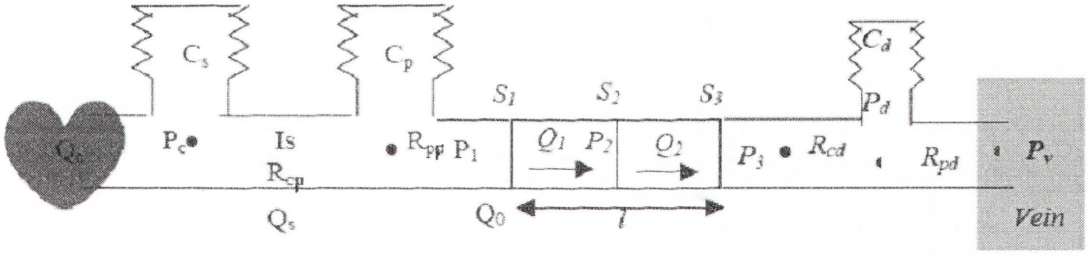

Figure 3.14: Artery Model and parameters of four Hemodynamic models

This ring sensor minimizes the sensor's effects on human daily life and provides a continuous self and safe blood pressure measurement and cancelling stethoscope or palpating duty and their uncertainties; since it is based on PPG and EIP sensors, also it is not applying an external pressure and estimates the systolic and diastolic blood pressure values with the Kalman filter [31].

Also, there is a partial decrease of the venous occlusion problem which is presented by using local pressurization. This is due to the fact that the local external pressure is

applied by a band with a small spring around the palmar digital artery only where the sensors are located.

On the contrary, this design has some limitations, such as lack of reliability of its measurements which were caused by the Kalman filter estimation, low signal-to-noise ratio, lack of motion detection, scratch of the surface tissue (gangrene), ambient light and management of wires.

Also, this design does not present any suggestion for the different volume of fingers for different persons and the requesting mechanical isolation.

This wired sensor has been improved to become a wireless sensor with PPG sensors only to increase signal-to-noise ratio and reduce the unarranged wires' effect. Wireless ring-sensor design is modelled by Rhee, Yang, and Asada in 2001 [32]. Their objectives were to reduce motion detection and achieve reliable measurements of vital signs for long-term use. Also, this design convenes varied and differing requirements, such as compactness, minimum loading effects, and low battery power consumption. The real shape and a block diagram of wireless ring sensor are shown in figure 3.15.

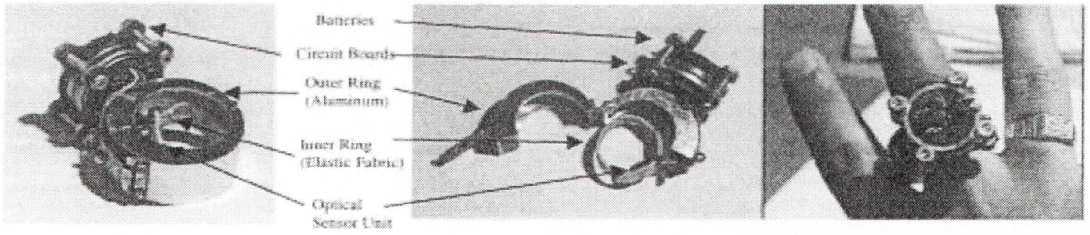

(a)

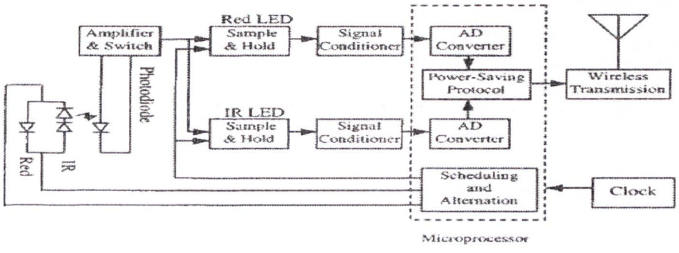

(b)

Figure 3.15: Wireless ring sensor

The wireless ring sensor is emitted a light by LED through the subject's pressurized finger by elastic fabric. The received signal of photodiode is changed by the blood flow on the digital artery. Then the PPG signal is amplified, sampled, digitized, and transmitted to the host computer for processing and to estimate the blood pressure by using a Kalman filter based on the hemodynamic models of the systemic blood circulation.

Wireless ring sensor consists of a double ring configuration as shown in figure 3.15 (a). The double ring configuration is modelled to reduce the affect of:

1- The force of the mechanical contact since this force is produced by an outer ring and this uncoupled design will not transmit this influence to the inner ring;
2- The acceleration of finger movement because the inertia force of small inner ring is small and negligible;
3- The pressure applied on the skin because of a light inner ring;
4- The ambient light because the outer ring provides an optical shield.

The battery power consumption of the components, which is embedded in the ring sensor, is estimated. Then a balancing strategy between the performance and the power consumption is used. There are, however, some cons of a wireless sensor that are produced by a big size of ring, a heavy mass of outer ring and battery weight [32].

Furthermore, low signal-to-noise ratio and lack of motion detection drawbacks were studied by the Asada team [33]. They designed a wearable biosensor (WBS). This design is used to measure heart rate, oxygen saturation, heart rate variability, and blood pressure.

This sensor differed from the previous ring sensor on the components' performance, such as type of light emitting diode (LED), to improve the signal-to-noise ratio. Also, the mechanical configuration of sensor was improved, to reduce the finger movement

effect by using a small screw instead of the spring, which has applied a local pressure on 5mm. Figure 3.16 shows the new design configuration. The LED and photo detector were located on the finger flank to emit a large amount of light close to digital arteries and detect a good amount of light through a thin epidermal tissue layer.

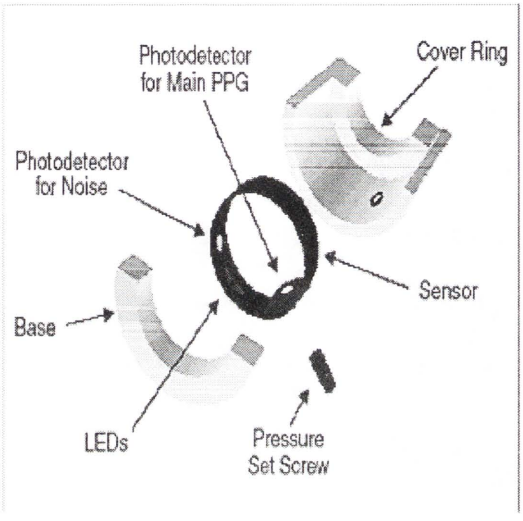

Figure 3.16: Wearable sensor

The WBS needs some improvement to meet the critical, contradictory design specification for out-of-hospital environment. The understanding of the physiology and mechanism of the cardiovascular signals will assist to design a cost-effective and acceptable cardiovascular diagnostic [33].

On other hand, the disadvantages of using a finger for cardiovascular measurements, such as mechanical isolation, scratch of the surface tissue and finger movement, were studied in depth by Cheang and Smith [34]. They designed a non-contact sensor which consisted of a PPG sensor in transmission mode.

A non-contact PPG sensor was implemented by considering these issues:

1- The detected signal, which consisted of a very small AC component compared with a DC component, was logarithmically amplified by a nonlinear optical preamplifier to detect AC component and extract the cardiovascular parameters;

2- Ambient light effect, which is produced from the space between the probes and the finger surface, was reduced by additional sampling of the surrounding lights and subtracted it from the intensity sampling;

3- Finger movements' effect was reduced by extending the field of the light source and the detector view;

4- Direct coupling effect, which is related to the direct illumination of the detector without any light/tissue interaction, was controlled by following equations:

$$PPG_{Signal} = DC_{blood\ \&\ tissue} + AC_{blood\ modulation} + DC_{direct\ coupling} \quad \ldots\ldots\ldots (3\text{-}9)$$

$$\hat{s}_{AC}(t,x) \cong \frac{\hat{\gamma}\hat{p}}{\hat{\beta}}\left(1+\frac{\alpha(x_0)}{\beta(x_0)}-\frac{\alpha(x)}{\beta(x)}\right) \quad \ldots\ldots\ldots\ldots\ldots (3\text{-}10)$$

Where s_{AC} is arterial pulsation

x_0 is centre position where the light source and detector are aligned

α is interpreted as direct coupling between source and detector

β corresponds to light coupled via DC (static) blood and tissue

γ corresponds to light coupled via AC blood modulation.

Only these variables are defined by the authors [34].

On the contrary, the Cheang and Smith design require many issues to be considered which were partially controlled. Besides, the acquired PPG signal of Non-contact PPG sensor was not accurate as shown in figure 3.17.

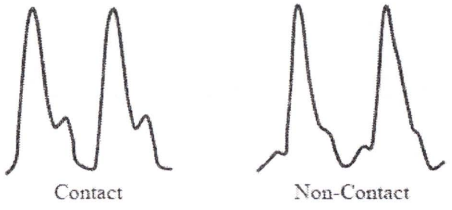

Figure 3.17: PPG signals

Continuously, the relationships of four certain features of photo-plethysmography (PPG) signal with arterial blood pressure (ABP) have been examined by Teng [35]. The PPG signal was measured by a reflectance PPG probe on the right hand index finger. ABP was measured by an oscillometric BP set (Model BP-8800, COLIN).

Four features of the PPG signal have been examined: systolic time (t_1), diastolic time (t_2), width of half of pulse amplitude ($width_2$) and width of two third of pulse amplitude ($width_1$). The correlation analysis was performed for the relationship between these features and arterial blood pressure to find the highest mean correlation coefficient. The linear regression line of ($y = ax + b$) form was derived from comparing two trials of ABP and certain feature; then ten other trials were used for validating the estimated ABP values which were obtained from the regression line. The diastolic time (t_2) has been the best feature to estimate ABP because its mean and standard deviation are the lowest values. The four features are illustrated in figure 3.18.

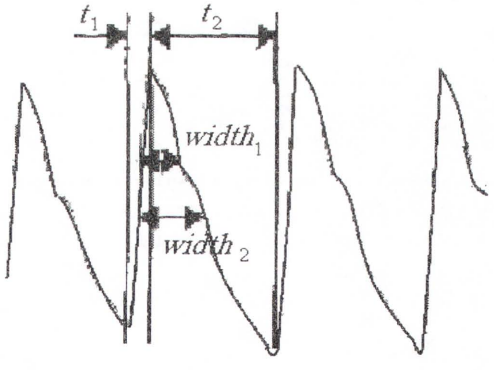

Figure 3.18: Photo-plethysmography features

Also based on the PPG signal, Pulse transit time (PTT) was used to estimate blood pressure based on wavelet transform modulus maxima by Lee [36]. Pulse transit time is the time difference between the ECG characteristic point, the position of Q wave of the ECG signal, and the PPG characteristic point is the position of the PPG signal's foot.

The ABP of subject at three states: resting, running on a trail-mill and after twenty minutes rest from running, has been measured by a standard BP occluding cuff meter

and estimated from the regression line of relationship between ABP and 1/PTT, which was calculated based on the first measurement at a resting state [36].

Although Teng's and Lee's methods have achieved good results, these methods have some disadvantages, such as:

1. Foot shift and unclear foot of the measured PPG signal form problems in reflectance PPG;
2. The regression line is changed based on subjects and sites of measurement;
3. Necessity of new calibration or backward signal to update the regression line;

Moreover, Yan and Zhang [37] stated that the normalized harmonic area of a discrete period transform of PPG signal has a high correlation with blood pressure.

In addition, Ma and Zhang [38] stated that the blood pressure variability has a high correlation with pulse time interval (PTT), which is the time interval between peak of electrocardiograph (ECG) and front foot of PPG signal, also known as the (PTT_f).

In addition, another model has been developed by Poon and Zhang [39] to estimate blood pressure by using a weighted PTT (PTT_W); these parameters' estimations are subject-dependent because they required a calibrating procedure to be obtained.

These three relations, however, are based on measuring two signals simultaneously which increase the measurement error and increase the process time.

As another trend, Shalitis, Reisner, and Asada presented a hydrostatic method: modification of the volume-oscillometric technique. The hydrostatic method reduces the inflatable pressure cuff and captures natural hydrostatic pressure advantage which is caused by movements of the subject's arm.

They developed the transmural pressure equation (3-3) by considering the hydrostatic pressure (P_{HYD}) effect as shown in next equation:

$$P_{tr} = P_a - P_{HYD} - P_c \quad \text{..... (3-11)}$$

Where $P_{HYD} = \rho \times g \times h$

and h equals the height offset of the measurement site relative to the proximal aorta.

They calculated the MAP by following equation:

$$MAP = \rho \times g \times h_{zero\_Ptr} + P_c \quad \text{..... (3-12)}$$

While they said SBP is equal P_c when the cuff oscillation amplitude equals 0.55 times of its peak, MAP oscillation amplitude, then DBP is calculated based on equation (3-2).

They suggested that hydrostatic changes caused an error in blood pressure (BP) measurements, enhance an absolute gauge pressure reference for BP measurements, caused a battery-free actuation, and recover the signal quality because PPG sensor is sensitive for motion and position changes.

The hydrostatic method may be used as alternative method to measure MAP, SBP and DBP. Nevertheless, the hydrostatic method is limited for continuous monitoring of SBP and DBP. Also, it needs to improve the BP measurements accuracy, energy efficiency, and comfort the presenting devices [40].

Furthermore, Carr produced a mathematical model based on high correlation between MAP and PPG signal frequency. He considered the cardiovascular system as an electric circuit. Therefore, Ohms' law, as shown in next equation, can be adopted on the cardiovascular system [41].

$$\text{Ohms' law: } V = I \times R \quad \text{..... (3-13)}$$

Where V is voltage potential difference

I is circuit current

R is circuit resistance

Carr matched the mean arterial blood pressure (MAP) to voltage potential difference, the Cardiac output (CO) of heart to circuit current, and the total peripheral blood

vessel's resistance (TPR) against blood flow to circuit resistance. Therefore, as Ohm's law, the mean arterial blood pressure, is calculated based on:

$$MAP = CO \times TPR \quad \text{..... (3-14)}$$

Physically, cardiac output can be calculated by measuring the volume of blood which is pumped by each heart beat. This volume, which is known as stroke volume (SV), is equal to the difference between end-diastolic-volume (EDV) and end-systolic-volume (ESV) as expressed in next equation:

$$SV = EDV - ESV \quad \text{..... (3-15)}$$

The heart pumps this amount of blood with every heart beat. Thus, the cardiac output for every minute can be computed based on next equation:

$$CO = HR \times SV \quad \text{..... (3-16)}$$

Then equation (3-14) can be written as [5, 41]:

$$MAP = HR \times SV \times TPR \quad \text{..... (3-17)}$$

Carr's model stated a linear relationship between MAP and the variable factor HR with constant values for SV and TPR factors. This mathematical model is the benchmark of our proposed method as it will be explained, demonstrated and tested in Chapter 6.

3.7. Summary

The chapter described the instruments and sensors that have been used to measure cardiovascular parameters, explained the various techniques that developed in this research area and discussed some drawbacks and weakness points that need to be addressed for further improvements to cardiovascular parameters' instruments. The chapter was arranged chronically and classified based on the data acquired; such as heart sound, blood level, pulses with external blood pressure, pulses with local blood pressure and PPG signal, pulse arrival time and other factors.

Chapter 4. Intelligent Techniques

Physical phenomena, social behaviour, engineering and universe systems are nonlinear, multimode, noisy and nondifferentiatable with high levels of uncertainties, these systems are called natural problems [42]. Nature problems depend on one or many variables, which are changed within different ranges. This dependency between problems and related variables are expressed by functions.

Functions are classified to Mathematical Formulas and Multi-objective arrays [42]. The Mathematical Formulas represent the relationship between system variables that are well expressed by a mathematical expression, hence the unknown variable(s) is directly calculated by that mathematical expression. An example of that is the relationship between value of object mass (m), an unknown variable, and the value of an object's material density (ρ) and object volume (V) as known variables, where they are mapped by mathematical expression as expressed in equation (4-1):

$$m = \rho \times V \text{ --- } (4\text{-}1)$$

On other hand, the multi-objective arrays maps between variables of system by unknown or difficult specified mathematical expression. Experimentally, they are related by bounded, nonlinear, multimode and noisy sampling for input, known, and output, unknown, variables on the same grid. Therefore, output variable(s) can be estimated or predicted upon existing multi-objective array by intelligent techniques, such as Neural Network, Fuzzy System, Genetic Algorithm, Particle Swarm Optimization and others.

4.1. Introduction

According to many researchers the relationship between physical phenomena of Systolic, Diastolic, and mean blood pressures with the heart rate is nonlinear, multimode

and noisy and does not have a specified mathematical expression [43]; therefore, two intelligent techniques are used through this research to achieve a good and reliable function or relationship to map between Systolic, Diastolic, and mean blood pressures with the heart rate depending on multi-objective arrays of all variables.

These two intelligent techniques are Interval Type-2 Fuzzy System (IT2 FS) and Particle Swarm Optimization (PSO). The following sections of this chapter define IT2FS, present a brief history and theory of IT2FS, its main parts as well as its applications and benefits. Besides, introduce a short literature of PSO, its major parts also its applications and advantages.

4.2. Interval Type-2 Fuzzy system

IT2 FS deals with nonlinear, multimode, noisy, and high uncertainty systems; also they do not have a specified mathematical expression such as the relationship of Systolic, Diastolic, and Mean blood pressures with the heart rate.

Actually, IT2 FS is extended from Type-1 Fuzzy system, ordinary Fuzzy system, to handle more levels of uncertainties, to determine a membership function for difficult circumstances, and to deal with incorporating uncertainties [44]. To give a good view about IT2 FS, a brief introduction of Type-1 Fuzzy system would be required as presented in following subsection.

4.2.1. Type-1 Fuzzy System

Type-1 Fuzzy control System (T1 FS) is defined as a control system based on fuzzy sets theory and fuzzy logic to design a model that maps between system variables through investigating the analogy variable values in terms of logical variables and linguistic expressions that has its own continuous distribution which represents all values between 0 and 1 [45]. The designed model is used to predict and estimate the output variables, depending on input variables.

The Fuzzy sets theory was inspired by Professor L. A. Zadeh [46] in 1965 to effectively and quantitatively deal with objects which have a "matter-of-degree" with all possible degrees of reality between Yes and No and also between True or False, in contrast with mathematical logic which divides the world into Yes and No, True or False, only.

Theoretically, Fuzzy sets out to establish the principle for computing by linguistic terms. These terms reflect people and specialist opinions about any system and its variables according to their perspectives, outlooks and experiences. Then the collected terms are expressed by linguistic expressions to represent the fuzzy sets of the system variables.

Fuzzy sets include some of uncertainty levels which were produced by specialist opinions, by generalizing the 0 and 1 membership values to a membership function (MF) according to linguistic expressions.

As an example, the relationship between age and "*young*" is represented by a crisp value that will be either 0 or 1. 0 means no association at all between young and sector of age, while 1 indicates complete association between young and a sector of age. As shown in figure 4.1, while, in Fuzzy set theory, the "*young*" association membership set is generalized to MF according to linguistic expressions that reflect people aged 10, 30, 50 and 70, as shown in figure 4.2, where age 0-10 is "*young*" with membership value of 1, then the graph is gradually reduced to membership value of 0.75 with age 30, membership value of 0.1 with age 50 and membership value of 0 with age 70 [47].

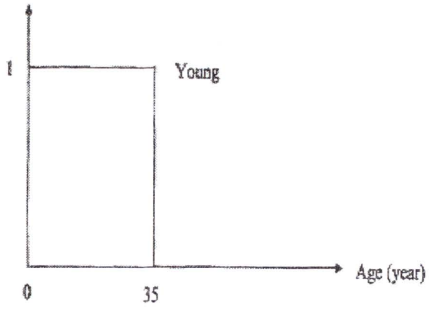

Figure 4.1: Crisp set MF

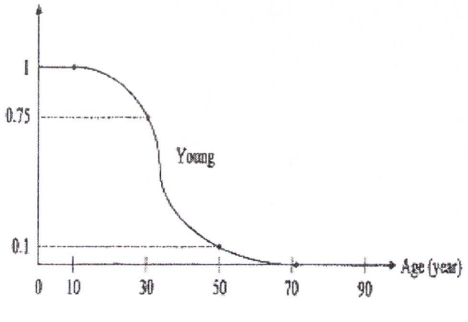

Figure 4.2: Type-1 MF

This simple example expresses the age description as young, so this Fuzzy system can be used to predict the age description as young for other values of age from the graph in Fig. 4.2; such as age 20 is described as 0.9 young, age 40 is described as 0.4 young, and age 60 is described as 0.05 young.

From the last example, some of the uncertainty levels are included in the gradual graph as distribution. Essentially, there are different distributions which are used for Fuzzy sets to express the linguistic expressions based on specialist opinions and to include some of uncertainty levels, such as piecewise linear distribution, Gaussian distribution, sigmoid curve, quadratic ,and cubic polynomial curves.

Actually, the Gaussian distribution is most common distribution used in Fuzzy system to express the linguistic expressions because it achieves the smoothness of linguistic expressions representation, expresses the probability density of problem in an understandable way and mimics the central method theorem [48].

Technically, the T1 FS consists of four parts; firstly, Fuzzifier initializes the fuzzy sets (A_x) of known, input, variables according to linguistic expressions then represent these sets as Membership Functions (MFs) $\mu_A(x)$ with specified distribution.

Secondly, "IF ..., THEN ..." rules control the connections between MFs of input and output variables. These rules consist of an antecedent part for fuzzy set of input(s) and a consequent part for fuzzy set of output(s).

Thirdly, the Inference engine combines the nonzero membership values by interface methods, such as maximum, minimum, max-product, averaged, root-sum-squared, and others, to produce an output fuzzy set of input variables.

Finally, the Defuzzifier that produces crisp values of output by defuzzifying the output of fuzzy set to crisp value by Defuzzification method; such as Centroid of gravity, Bisector, Mean of Maximum, Smallest of Maximum, Largest of Maximum and others.

The block diagram of Fuzzy system is illustrated in figure 4.3 [49].

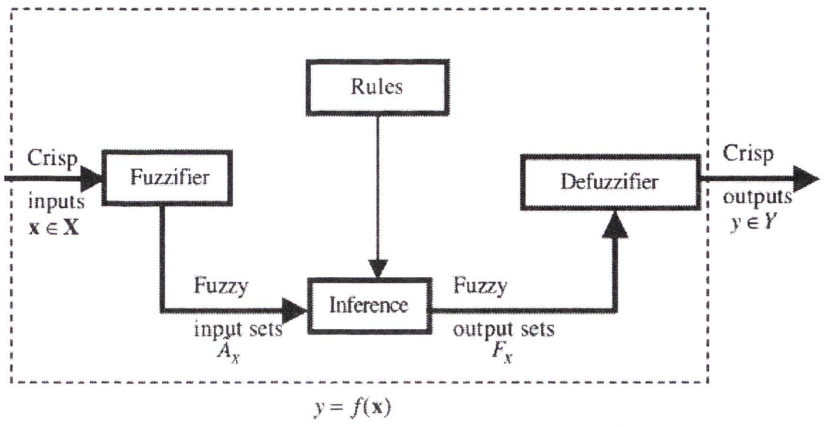

Figure 4.3: Block diagram of Fuzzy System

For more clarification, the T1 FS block diagram stages are described in next paragraphs: A type-1 fuzzy system (T1 FS) is designed to predict one output (U) based on two inputs (X and Y). The range of X variable is fuzzified to few fuzzy sets according to linguistic expressions based on specialist opinions. Then these sets are represented as Membership Functions (MFs) $\mu(x)$ with triangle distribution, such as A and N sets, while the range of Y variable is fuzzified to a few fuzzy sets according to linguistic expressions then these sets are represent as Membership Functions (MFs) $\mu(y)$ with triangle distribution, such as I and O sets. "IF …, THEN …" rules of this T1 FS are set between inputs and output as shown in figure 4.4.

This T1 FS is tested by two instant numbers x and y.

The instant number x belongs to X variable range while instant numbers y belongs to Y variable range are supplied to T1 FS.

Firstly, according to the Fuzzification process, the instant number x has two fuzzy values $\mu_A(x)$ and $\mu_N(x)$ while the instant number y has two fuzzy values $\mu_I(y)$ and $\mu_O(y)$. Secondly, the rules of this T1 FS are fired, the $\mu_A(x)$ fuzzy value combines with $\mu_I(y)$ fuzzy value to form U_1 set and the $\mu_N(x)$ fuzzy value combines with $\mu_O(y)$ fuzzy value to form U_2.

Thirdly, the Inference engine combines the nonzero membership values of x and y, where the minimum combination of $\mu_A(x)$ and $\mu_I(y)$ are formed U_1 set and the minimum combination of $\mu_N(x)$ and $\mu_O(y)$ are formed U_2 set, then the maximum combination of U_1 set and U_2 set are formed U_C set.

Finally, the formed U_C set is defuzzified by a centre of gravity method to find the crisp value u. These four steps are illustrated graphically as shown in figure 4.4 [50].

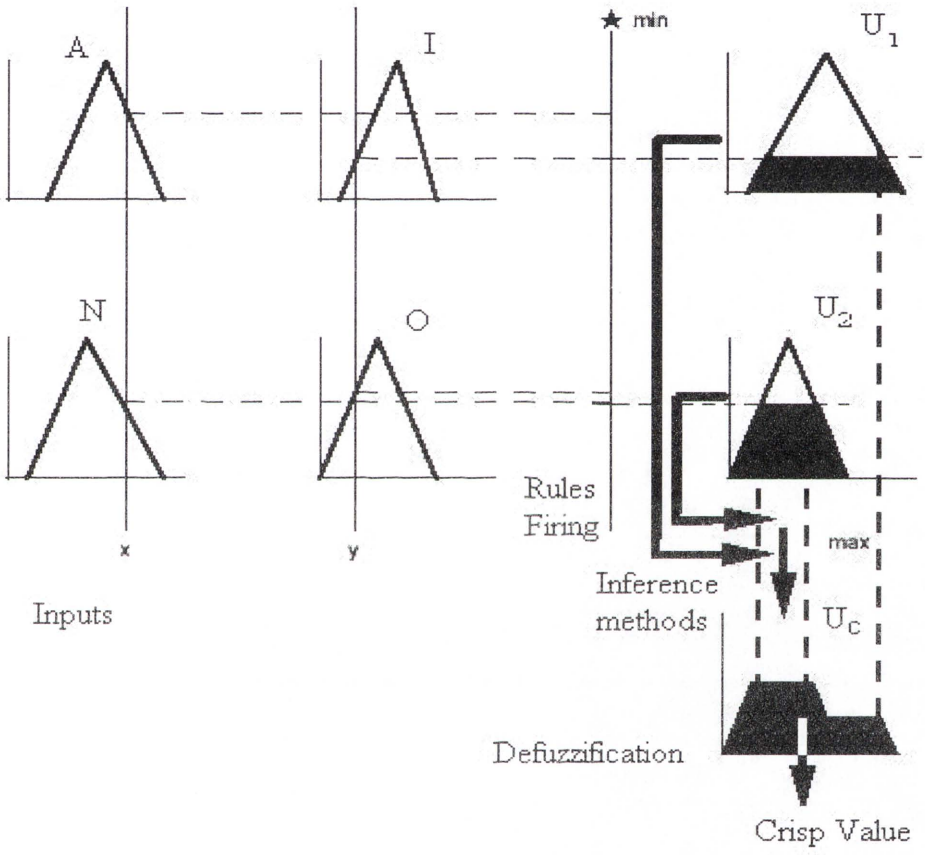

Figure 4.4: Stages of Type-1 fuzzy system

The designed IT1FS model is trained by available database of input variables and output variables to minimize the error between the estimated output variables by FS and the real output variables by adjusting the MFs' parameters.

Afterwards the designed IT1FS model is used to estimate and predict output variables depend on an available database of known input variables only.

After this introduction of Type-1 Fuzzy system, the history and the theory of Type-2 Fuzzy system are presented in the next subsection.

4.2.2. History and Theory of Interval Type-2 Fuzzy System

The motivation of Type-2 fuzzy system was proposed by Zadeh in 1975 [51]. Then, Mizumoto and Tanaka presented some properties of fuzzy sets of type-2 [19]. Later in 1999, Karnik, Mendel and Liang introduced T2 FS comprehensively [44]. The developments and applications of type-2 fuzzy logic are increased and varied in many fields; hundreds of publications are listed on type-2 fuzzy logic organization web site.

Theoretically, T2 Fuzzy sets are represented by the same distributions mentioned for T1 fuzzy sets. The T2 Fuzzy set is characterized by a $\mu_{\tilde{A}}(x)$ as Primary Membership Function (PMF) for set $\tilde{A}$ and the membership value for each element of $\tilde{A}$ is fuzzy set; which is called a secondary membership function or membership grade [52].

As an example of the Type-2 system, Gaussian type-2 set is formed by moving the Gaussian type-1 set to left and right in a non-uniform manner as shown in figure 4.5.

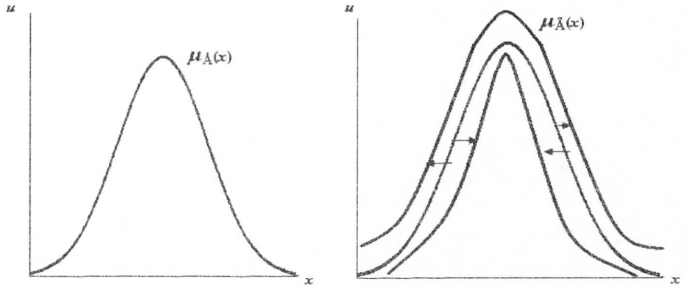

Gaussian Type-1 MF Gaussian Type-2 PMF

Figure 4.5: Extension Type-1 MF to Type-2 PMF

As a practical case of the general T2 FS, the Interval T2 FS (IT2 FS) is proposed to avoid the terrible and horrendous of the non-uniform sides of T2 FS PMF, by bounding the sides of T2 MF by Upper MF and Lower MF to form the Footprint of Uncertainty (FOU) of the IT2 PMF.

Moreover, the Gaussian IT2 PMF depends on these main parameters:

1- Lower mean m_l.

2- Upper mean m_u.

3- Lower standard deviation σ_l.

4- Upper standard deviation σ_u.

These parameters control the shape of primary membership functions and FOU of IT2 FS and are shown in figure 4.6.

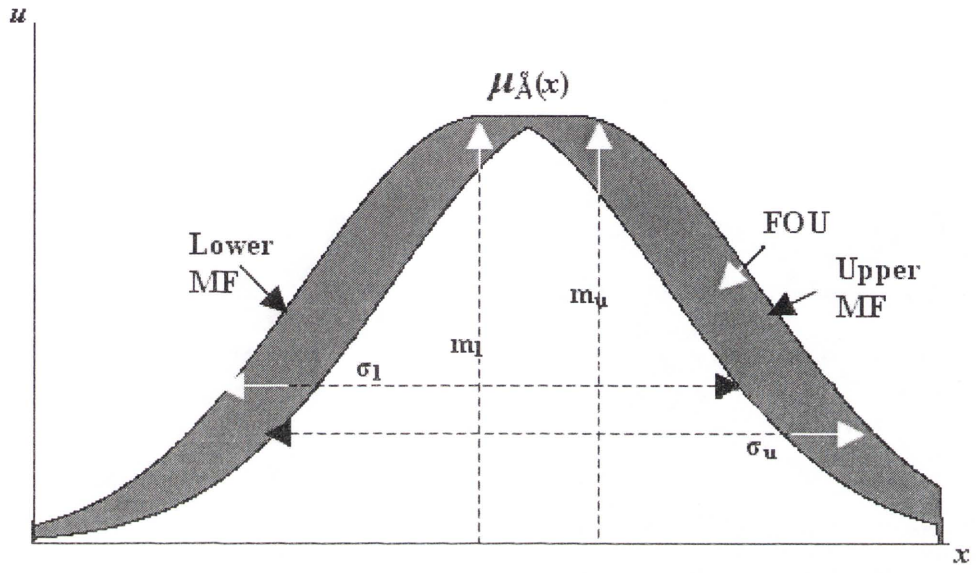

Figure 4.6: Gaussian Interval Type-2 PMF

4.2.3. Parts of Interval Type-2 Fuzzy System

T2 FS model, similar to T1 FS model, consists of four parts; firstly, Fuzzifier represents the input into T2 fuzzy sets by Primary Membership Function (PMFs) and initializes input PMFs' parameters.

Secondly, "IF …, THEN …" rules to connect fuzzified sets ($\tilde{A}_x$) of input with represented sets of output ($\tilde{U}_x$).

Thirdly, an inference engine which combines the rules and forms a mapping between the input sets and the output sets.

Finally, there is a Defuzzification process to produce crisp values of output by two stages. The first stage is descending the type-2 fuzzy set to type-1 fuzzy set by type reduction methods; such as centroid, centre-of-sums and height. The second stage is using the T1 Defuzzifier to find the output crisp value [44].

The block diagram of T2 FS is illustrated in figure 4.7.

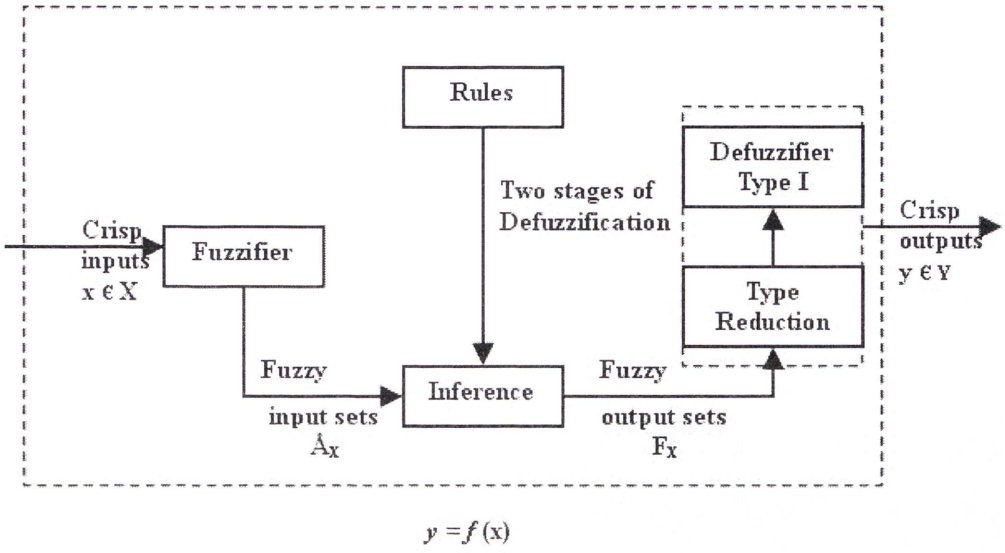

Figure 4.7: Block diagram of Type-2 Fuzzy System

For more explanation, IT2 FS block diagram stages are detailed in next paragraphs:

An IT2 FS is designed to predict one output (Ũ) based on two inputs (X and Y). The range of X variable is fuzzified to a few fuzzy sets according to linguistic expressions based on specialist opinions. Then these sets are represented as Primary Membership Functions (PMFs) $\mu(x)$ with triangle distribution dependent on different means and same σ; such as Ã and Ñ sets, while the range of Y variable is fuzzified to a few fuzzy sets according to linguistic expressions. These sets then are represented as PMFs of $\mu(y)$ with triangle distribution dependent on different means and same σ; such as Ĩ and Õ sets. "IF …, THEN …" rules of this IT2 FS are set between inputs and output.

This IT2 FS is tested by two instant numbers x and y.

The instant number x belongs to X variable range while instant numbers y belongs to Y variable range are supplied to IT2 FS.

Firstly, according to the Fuzzification process, the instant number x has two membership grades $\mu_{\tilde{A}}(x)$ and $\mu_{\tilde{N}}(x)$ while the instant number y has two membership

grades $\mu_{\tilde{I}}(y)$ and $\mu_{\tilde{O}}(y)$. Secondly, the rules of this IT2 FS are fired; the $\mu_{\tilde{A}}(x)$ combines with $\mu_{\tilde{I}}(y)$ to form $\tilde{U}_1$ set and the $\mu_{\tilde{N}}(x)$ combines with $\mu_{\tilde{O}}(y)$ to form $\tilde{U}_2$.

Thirdly, the Inference engine combines the nonzero membership grades of x and y; where the minimum combination of $\mu_{\tilde{A}}(x)$ and $\mu_{\tilde{I}}(y)$ are formed $\tilde{U}_1$ set and the minimum combination of $\mu_{\tilde{N}}(x)$ and $\mu_{\tilde{O}}(y)$ are formed $\tilde{U}_2$ set, then the maximum combination of $\tilde{U}_1$ set and $\tilde{U}_2$ set are formed $\tilde{U}_C$ set.

Finally, the formed $\tilde{U}_C$ set is defuzzified by a centre of gravity method to find two crisp values C_1 and C_2 and then by a centre of sums method to find one crisp value C. These four steps are illustrated graphically as shown in figure 4.8 [50].

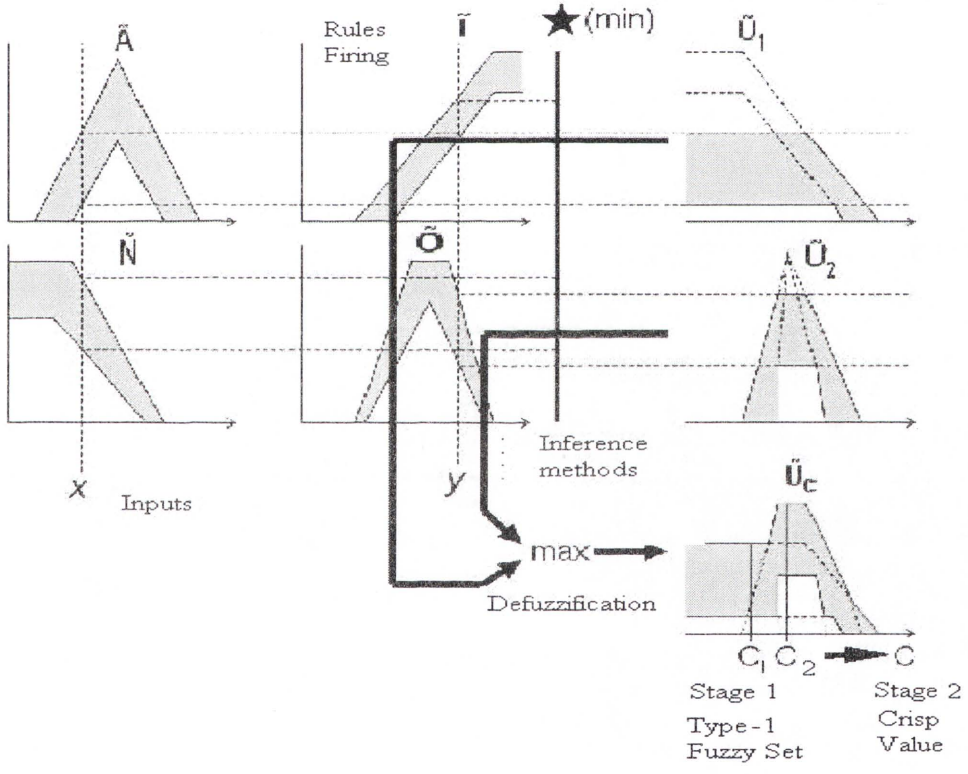

Figure 4.8: Stages of Type-2 Fuzzy System

The designed IT2FS model is trained by an available database of input variables and output variables to minimize the error between the estimated output variables by FS and the real output variables by adjusting the PMFs' parameters.

Afterwards, the trained IT2FS model is used to estimate and predict output variables dependent on an available database of known input variables only.

4.2.4. Applications and benefits of Type-2 Fuzzy System

Recently, the applications of the Fuzzy System are increased extensively. These applications differ from consumer products, such as camcorders, washing machines, cameras, and microwave ovens, to industrial process control systems, such as decision-support systems and medical instrumentations [53].

In this brief subsection, it is hard to express all applications of the type-2 Fuzzy System that is listed in the type-2 fuzzy logic organization web site, or discuss in detail single application. Therefore, four applications are reviewed in a small sample through following paragraphs.

The first application was mentioned by John and Czarnecki who presented "An Adaptive Type-2 Fuzzy System for Learning Linguistic Membership Grades". Their system represented the uncertainty in both the representation and inference. According to their results, they found that their system offered the capability to allow linguistic descriptors to be learnt by an adaptive network [54].

The second application was expressed by Mendoza, Melín and Sandoval, who set up some T2 Fuzzy Inference Systems for Edge Detection of Digital Images. Their method was implemented for the detection of edges and they achieved quite good results [55].

The third application was invented by John, Innocent, and Barnes, who designed a Type-2 Fuzzy and Neuro-Fuzzy Clustering system for Radiographic Tibia Images. They stated and discussed the results of using type 2 sets and Neuro-Fuzzy Clustering for clustering of radiographic tibia images. Their system assisted the experts to analyse different sets of images that were unable to analyse with the type-1 fuzzy system [56].

The fourth application was done by Own, Tsai, Yu, and Lee who created an Adaptive T2 Fuzzy Median (A2FM) filter for impulse noise removal. Their filter depended on the uncertainty of the type-2 fuzzy sets' capacity. Their proposed method of designing an

A2FM filter assumes a powerful scheme to reduce the restrictions of the type-1 FM filter membership function and include a flexibility inference mechanism by reducing the memory usage of the filter [57].

Finally, there are many benefits and reasons of utilizing and using T2 Fuzzy system. The most important seven T2 Fuzzy System advantages are [49]:

1- T2 Fuzzy system directly handles many levels and types of uncertainties more than T1 Fuzzy system can handle;
2- T2 Fuzzy system is able to design a system to map between the inputs and the outputs of nonlinear, multimode and noisy systems;
3- T2 Fuzzy system provides an easy contact with public people through its linguistic expressions; such as low, normal, high and, other expressions;
4- T2 Fuzzy system offers a continuous domain of problem through the generalization of crisp set to a two dimensional set;
5- T2 Fuzzy is inherently robust because it does not need strict or noise-free inputs;
6- T2 Fuzzy can be designed to protect system if a feedback sensor quits;
7- T2 Fuzzy is a multi-inputs and multi-outputs control system.

4.3. Particle Swarm Optimization

The Particle Swarm Optimization (PSO) is a new intelligent technique that was inspired by the social actions of bees flocking, food seeking by birds, and fish crowding together. These actions are applied to the many insights of persons' actions and cognitions [58]. Generally, PSO is linked to artificial life while, in particular, it is linked to bird flocking, fish schooling, and swarming theory. Also PSO is related to other computation and programming evolutionary techniques and has relations with evolution strategies [59].

4.3.1. History and theory of Particle Swarm Optimization

The inspiration of the Particle Swarm Optimization (PSO) algorithm is stated by Dr. Russell Eberhart and Dr. James Kennedy in 1995 based on the social behaviours of bird flocking, bees congregation and fish schooling [60].

In 1996, Eberhart and Kennedy developed a discrete binary version of the particle swarm algorithm. This version operates on discrete binary variables, where the particle take a zero or one value on the problem space. Besides, some of main algorithm parameters were detected depending on trial and error and to produce a very simple and easy implemented version of PSO algorithm [59].

Theoretically, PSO contributes many attributes with Genetic Algorithms (GA) because it is initialized by a population with random solutions and searches the optimal solution(s). However, PSO is unlike GA because it does not have crossover operators that GA has.

Moreover, the potential solutions of PSO are called particles. Each particle flies, moves, and searches through the problem space by tracking its best solution and global best solution that is achieved by a whole swarm population.

The PSO tracking process is depends on the updated velocity and updated position of each particle, every iteration, toward the best solution through problem domain. The

velocity is weighted, with separate numbers being generated toward two best locations based on evaluation functions.

The two best values are tracked by particle swarm are the particle best and the global best, the particle best (pbest) is the best location that the particle has achieved so far in the problem space. Global best (gbest) value is the best value obtained so far by any particle of the whole population.

4.3.2. Parts of Particle Swarm Optimization

Particle Swarm Optimization parts are population of particles, interconnection topologies, search algorithms, and evaluation functions. These fundamentals cooperate together to find the optimum solution of problem.

The normal population of PSO is twenty to fifty particles [61, 62]. This number is determined according to the problem size. This population, however, is far less than the usual population of other evolutionary algorithms.

PSO particles have interconnection topologies describing the communication among them to move within the problem domain to find an optimum solution. There are two topologies:

1. Sociometry topology or global best topology (gbest) where every particle is connected with all particles of population and influenced by the particle which has found best problem solution;
2. Local best topology (pbest) where every particle is affected by its previous position value.

Local best topology can converge separately on various optima solutions in problem space and it has less complexity than global best topology. Global best topology, however, is faster in finding an optimum solution to the problem.

The main fundamental of PSO is the search algorithms which adjust particles' velocities and positions by equations (4-2) and (4-3) respectively to move toward pbests and gbest within domain boundaries as shown in figure 4.9 [62]:

$$V_n(t+1) = \chi \times V_n(t) + \varphi_1 \times rand_1 \times (pbest_n - X_n) + \varphi_2 \times rand_2 \times (gbest - X_n) \text{ -- (4-2)}$$

$$X_n(t+1) = X_n(t) + V_n(t+1) \text{ ----- (4-3)}$$

V_n is the displacement of particle's movement

n is the current particle

t is the iteration number

χ is the constriction coefficient

$\varphi_{1,2}$ are the acceleration constants

$rand_{1,2}$ are random numbers in range [0,1]

$pbest_n$ is the particle's best position

X_n is particle's position within problem domain

gbest is the global best within all particles

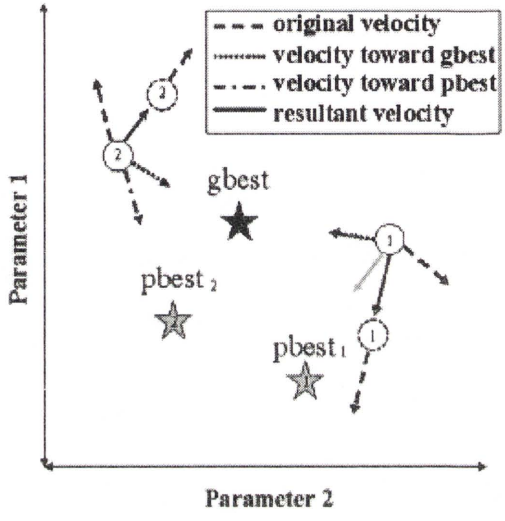

Figure 4.9: Particles movements in Problem domain

Firstly, parameters' values of n, $V_{n=1}$ (t=1), $X_{n=1}$ (t=1), $\varphi_{1,2}$, χ, pbest and gbest are initialized to start particles' movements within problem space. Then particles' displacements are updated by equation (4-2) then the particles' positions are updated by equation (4-3).

Acceleration constants' values $\varphi_{1,2}$ manage particles' movements and the probability of finding optimum solution slowly with high accuracy or quickly with less accuracy; increasing φ_1 supports exploration and leads particles' movements towards pbest, while increasing φ_2 supports exploitation and particles' movements towards gbest. On the other hand, the construction coefficient χ balances between the effect of previous displacement, which is referred to cognitive rates, and the effect of interconnection topologies local and global best on current displacement, which is referred to social

rates. Also, $rand_{1,2}$ are used to stochastically change the relative pull of pbest and gbest and to imitate the sight unpredictable element of nature swarm behaviour. Besides these algorithms and their parameters, the particles' movements are surrounded by problem space - Maximum displacement (V_{max}) and boundary wall that control the particles' movement within problem space. There are three types of boundary wall:

1. Absorbing Wall: when a particle steps out the boundary of the solution space, the velocity value is changed to zero and the particle will eventually be pulled back toward the allowed solution space. In this sense the boundary "walls" absorb the energy of particles trying to escape the solution space;
2. Reflecting Wall: when a particle steps out the boundary, the sign of the velocity is changed and the particle is reflected back toward the solution space;
3. Invisible Wall: It is a wall that allows particles to move without any physical restriction. However, particles that wander outside solution space are not evaluated for fitness [59].

Finally, the evaluation functions appraise the obtained solution success by adjusting global and local best values according to new best particles' positions. This operation is reiterated till the particles or some of them reached the optimum solution. The optimum solution goal is achieved by three ways:

1. Maximum Iteration: The PSO will stop when number of iterations reaches the number defined by the user;
2. Target fitness termination: The PSO is executed by a number of iterations that are defined by the user, PSO will stop when the target fitness reaches the target defined by the user, or when the number of iterations reaches the number defined by the user;

3. Minimum standard deviation (STD): The PSO is executed by number of iterations that defined by the user, PSO will stop when the computed STD of all particles' fitness are less or equal to the user-defined min-STD or when the number of iterations reaches the number defined by the user.

In summary, PSO search algorithms and interconnection topologies control the particles' movements within the problem domain to find the optimum problem solution that is evaluated by evaluation rules. Stages of PSO algorithm are simply expressed on the flowchart as shown in figure 4.10.

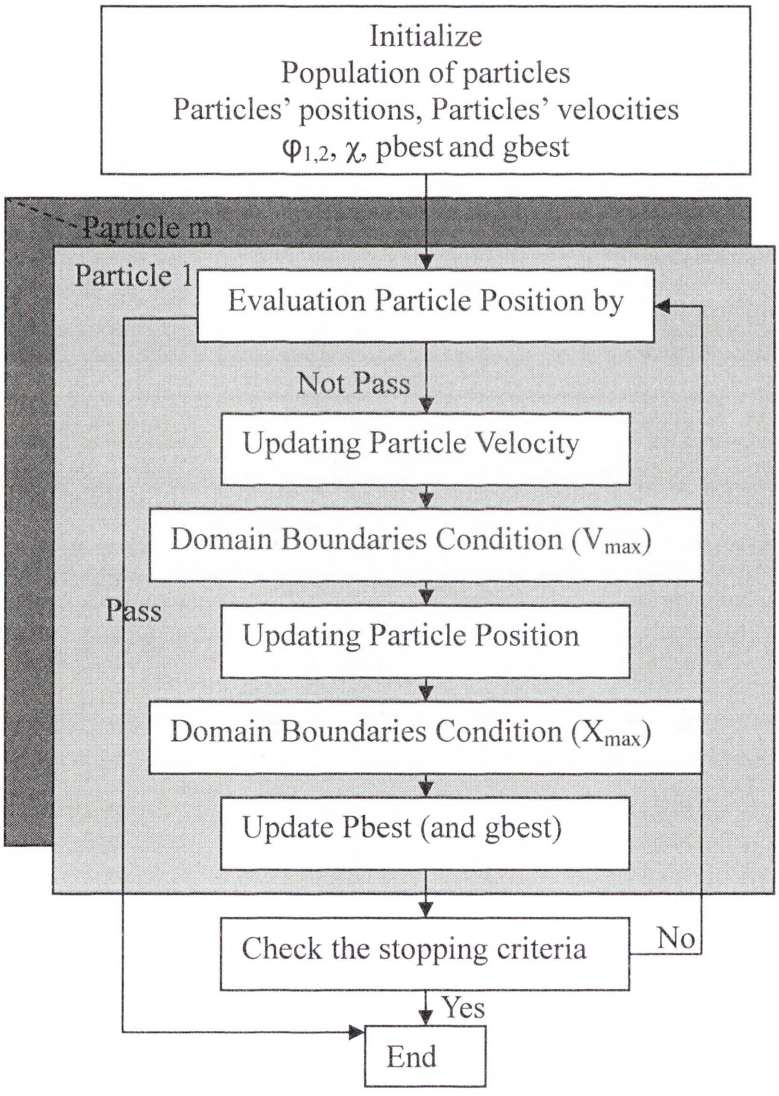

Figure 4.10: Flowchart of Particle Swarm Optimization Algorithm

4.3.3. Applications and benefits of Particle Swarm Optimization

Already, PSO is being utilized in many applications because it has very few parameters to adjust comparison with other population based algorithms. In this concise section, it is hard to describe all applications of PSO that recorded in swarm intelligence area, or discuss in detail single application. Therefore, four applications are summarized in a small sample throughout the following paragraphs.

The first application was mentioned by John Salerno, who utilized PSO to train the recurrent neural model. He initialized a number of models for a neural network. Then he found the suitable model which generated the best results. Overall, he yielded better results by PSO than other available techniques [63].

The second application was presented by Russell Eberhart and Xiaohui Hu who offered methods for the human tremor analysis by using PSO. They dealt with Parkinson's disease and essential tremor. They achieved quite promising results from this investigation [64].

The third application was introduced by Fukuyama, Takayama, Nakanishi, and Yoshida, who designed a particle swarm optimization for reactive power and voltage control in electric power systems. They expand the original PSO algorithm to handle mixed-integer nonlinear optimization problem and decide an online voltage control strategy with both discrete and continuous control variable [65].

The fourth application was executed by Kannan, Slochanal, Subbaraj, and Padhy who utilized PSO and its variants to deal with generation expansion planning problem. They introduced a virtual mapping procedure to improve the efficiency of the PSO. In addition to simple PSO, many variants such as constriction factor approach, Lbest model, hybrid PSO and composite PSO are also applied to test systems [66].

In the end, there are many benefits and reasons of utilizing and using PSO algorithm, the important five PSO benefits are listed here [59]:

1- PSO has very few parameters to adjust comparing with other population based algorithms;

2- PSO achieved quite good results in many applications as mentioned before;

3- PSO has a very simple and easy implemented algorithm;

4- PSO computational time is very small because PSO only has two main equations and two tracking values pbest and gbest;

5- The two tracking values, which are produced from PSO topologies, assist in finding the best solution of the whole system and not being stuck in local solutions.

4.4. Summary

An introduction of Interval type-2 Fuzzy System (IT2FS) and Particle Swarm Optimization (PSO) were presented. These two intelligent techniques are utilized during the research to deal with nonlinear, noisy and multi- uncertainty relationship between heart rate and Blood pressure parameters; Systolic, Diastolic and Mean blood pressure. This chapter presents a good justification for using these particular intelligent techniques; IT2FS and PSO, through the advantages and benefits of each technique that mentioned in section 4.2.4 and 4.3.3.

Chapter 5. Cardiovascular Parameters Long Term Monitoring System

Cardiovascular Parameters' measurements are very important to diagnose the subject's health situations. In this research, a Cardiovascular Parameters Long Term Monitoring System (CPLTMS) is designed to measure cardiovascular parameters using Photo-plethysmography (PPG) sensor. Thus the researcher suggested a frame work to deal with such system. The proposed frame work are divided the Cardiovascular Parameters to three levels based on fusion and processing of PPG signal as shown in figure 5.1. This chapter presents the design and implantation of our proposed frame work for the CPLTMS.

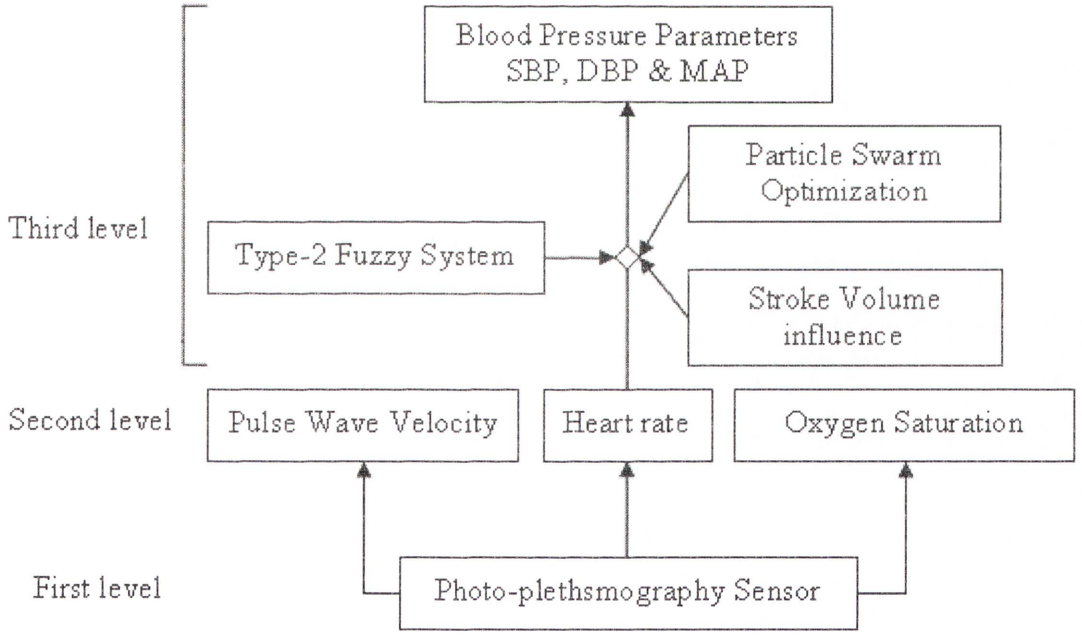

Figure 5.1: The Cardiovascular Parameters structure

5.1. Introduction:

The Cardiovascular Parameters structure considers the PPG signal as the first level because it is a direct output of PPG sensor that is attached to the subject's finger. The PPG sensor types, circuit and shape of outputs are discussed in section 5.1. Besides,

heart rate, pulse wave velocity, and oxygen saturation level are directly dependent on the PPG signal; hence, they are classified as the second level of cardiovascular parameters structure. The measuring procedure of second level parameters are clarified and illustrated in section 5.2. Further, the blood pressure parameters' (BPPs) estimations are based on second level parameters and some intelligent techniques; thus, BPPs are classified as the third level of cardiovascular parameters. The BPPs estimations methods, utilizing of intelligent techniques and the results of these methods will be explained in chapter 6.

5.2. Photo-plethysmography signal

The PPG signal is the first level of our CPLTMS structure because it is directly measured from the subject's finger by a PPG sensor. The PPG sensor consists of an optical source and an optical sensor; the optical source is an infrared light emitting diode (LED) that acts as an optical transmitter and the optical sensor is a photo-diode that acts as an optical receiver. Actually, there are two types of PPG sensors [67]:

1. Reflective PPG sensor: this type is based on the reflected optical beam of the finger's bone and tissues; because both Optical diode and LED are located on the front side of finger, as shown in figure 5.2 (a);
2. Transmissive PPG sensor: this type is based on the penetrated and transmitted optical beam through finger's bone and tissues; since Optical diode and LED are located on opposite sides of the finger, as shown in figure 5.2 (b).

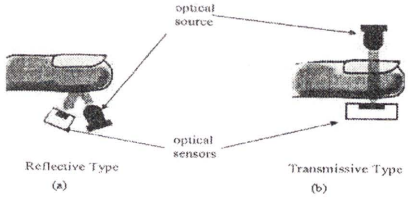

Figure 5.2: Photo-plethysmography Types

The circuit model of PPG Sensor consists of infrared light emitting diode (LED) and a photo-diode with other supporting components to form a PPG Sensor circuit as shown in figure 5.3.

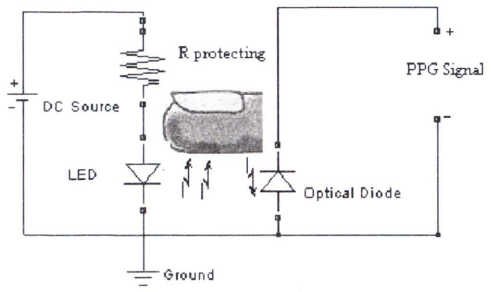

Figure 5.3: Circuit Model of PPG Sensor

The PPG signal detected from the reflective PPG sensor has a lower ratio of power consumption compared to that used by the Transmissive PPG sensor which consumes extra power to assist the beam penetration to the other side of organ. Also the Reflective PPG sensor can be attached to additional parts of the subject's body, such as the wrist and neck [68]. Therefore the Reflected PPG sensor is preferred for use in CPLTMS.

A prototype of PPG sensor's circuit is configured, as shown in figure 5.4 based on the PPG circuit model that shown in figure 5.3.

Figure 5.4: A proto-type of PPG sensor's circuit

The PPG prototype; which is shown in figure 5.4, is utilized to acquire the PPG signals of four healthy subjects. This experiment is based on ethical approval that attached as

Appendix 1. The PPG sensor's output is connected to an oscilloscope to analyze the PPG Signal. The general shape of the PPG signal is shown in figure 5.5.

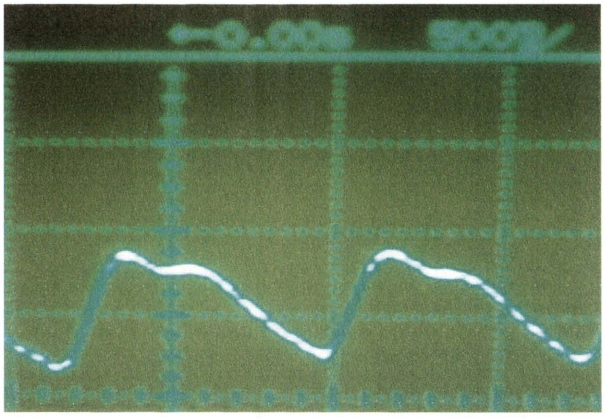

Figure 5.5: PPG signal as sketched by the oscilloscope

The readings for four PPG signals' are analyzed, based on oscilloscope parameters to detect the DC component and AC component. The values of DC, AC components of PPG signals and frequencies of AC components are listed in table (5.1).

Table (5.1): DC, AC components and frequencies of AC components of PPG signal

Component of PPG	Subject 1	Subject 2	Subject 3	Subject 4
DC Component (V)	3.89911	3.55509	3.69003	4.04749
AC Component Amplitude (V)	0.02614	0.09732	0.05037	0.03589
AC Component Frequency (Hz)	1.12	1.48	1.32	1.25

The PPG signal, as noticed in table (5.1), has high DC part (3.5 - 4) V and very low AC part (10 - 100) mV; this means that the PPG signal is influenced by the absorption of the finger's bone, arteries, veins, tissues, and skin; hence, the PPG signal is structured of four portions:

1- Absorption due to pulsated arterial blood; AC component;

2- Absorption due to non-pulsated arterial blood;

3- Absorption due to venous blood;

4- Absorption due to skin, bone, and tissues.

The listed portions are shown in figure 5.6 [34]:

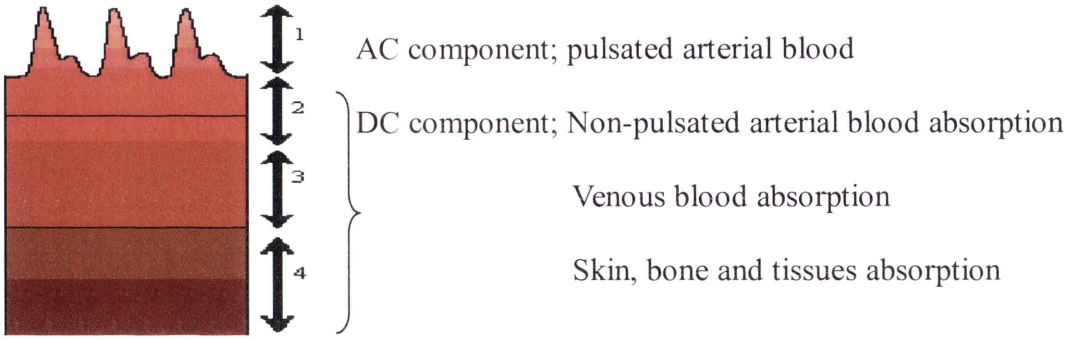

Figure 5.6: Structure of PPG signal

The results of the PPG signal will be used to compute the values of other cardiovascular parameters, such as heart rate, pulse wave velocity, oxygen saturation level, and blood pressure parameters, depending upon the methodologies and equations which will be discussed later.

Moreover, there are many other applications of PPG signal, such as human verification and recognition approach [69] and respiratory rate monitoring [70].

5.3. Second level of Cardiovascular Parameters

Heart rate, pulse wave velocity and oxygen saturation level are measured depending on the PPG signal. Thus, they are classified as the second level of our CPLTMS. The relationships between these parameters and PPG signal as well as the procedures to evaluate these parameters will be clarified in the following subsections:

5.3.1 Heart rate

Heart rate (HR) is a very important parameter for subject health situation because, if the heart beats regularly, then almost the other body's organs will work properly; but if the heart does not beat regularly, then other body's organs will not work normally.

Heart rate is the first cardiovascular parameter which has been sensed [71] because it is observed by touching the surface of big arteries. Clinically, HR equals the number of

heart beats during one minute. In our CPLTMS, HR is measured using PPG signal by next equation [72]:

$$HR = 60 \times \text{frequency of PPG signal} \quad \text{..... (5-1)}$$

This equation is utilized to evaluate the HR values of healthy subjects. HR values are evaluated based on the AC component frequencies of four PPG signals; which can be seen in the third row of table (5.1). The computed HR values are shown in table (5.2).

Table (5.2): AC component frequency of PPG signal and Heart rate

Component of PPG	AC Component Frequency (Hz)	Heart rate
Subject 1	1.12	67.2
Subject 2	1.48	88.8
Subject 3	1.32	79.2
Subject 4	1.25	75

Moreover, the MIMIC database has been utilized to verify equation (5-1). The MIMIC database is available in a web site for Physio-bank database and it includes continuous clinical records from some subjects at the intensive care unit (ICU) for every second more than 10 hours; that means 36000 records for each case, at least. In addition, these records include many types of cardiovascular signals and interrupted measurements, such as PPG signal and HR records for each case. These are extracted from bedside monitors attached to the subjects and from the subjects' medical records.

PPG signal frequencies have been computed for some subjects of database of subjects that extracted from MIMIC database. These frequencies are utilized to evaluate HR values by equation (5-1). The average of PPG signal frequencies and HR values for subjects of MIMIC database are listed in table (5.3):

Table (5.3): PPG signal frequencies and HR values for subjects of MIMIC database

Case	Period of PPG cycle from Chart of Bedside monitor (sec)	PPG frequencies (Hz)	Real HR from subjects' records (60/sec)	Computed HR (CHR) (60/sec)	Absolute difference |CHR– Real HR|
1	0.70	1.42	85	85.33	0.33
2	0.62	1.62	98	97.41	0.59
3	0.85	1.18	71	70.58	0.42
4	0.76	1.31	79	78.48	0.52
5	0.72	1.38	83	82.98	0.02
6	0.63	1.60	96	95.77	0.23
7	0.69	1.45	87	86.93	0.07
8	0.80	1.26	76	75.32	0.68
9	0.77	1.29	78	77.43	0.57
10	0.65	1.54	93	92.46	0.54
11	0.64	1.56	94	93.88	0.12
12	0.71	1.41	84	84.5	0.5
13	0.62	1.63	97	97.55	0.55
14	0.67	1.50	90	89.87	0.13
15	0.83	1.21	72	72.49	0.49
16	0.74	1.34	81	80.57	0.43
17	0.63	1.59	96	95.11	0.89
18	0.60	1.68	101	100.57	0.43
19	0.68	1.48	88	88.51	0.51
20	0.66	1.51	91	90.8	0.2
Average			87	86.83	0.41

The accuracy of equation (5-1) is computed based on following equation [73]:

$$\text{Accuracy} = 100\% \times \left(1 - \frac{\text{average of absolute difference between Estimated and Real values}}{\text{average of Real values}}\right) \quad \ldots\ldots\ldots (5\text{-}2)$$

$$\text{Accuracy} = 100\% \times \left(1 - \left(\frac{0.41}{87}\right)\right) = 99.53\ \%$$

The results of table (5.3); are illustrated in figure 5.7:

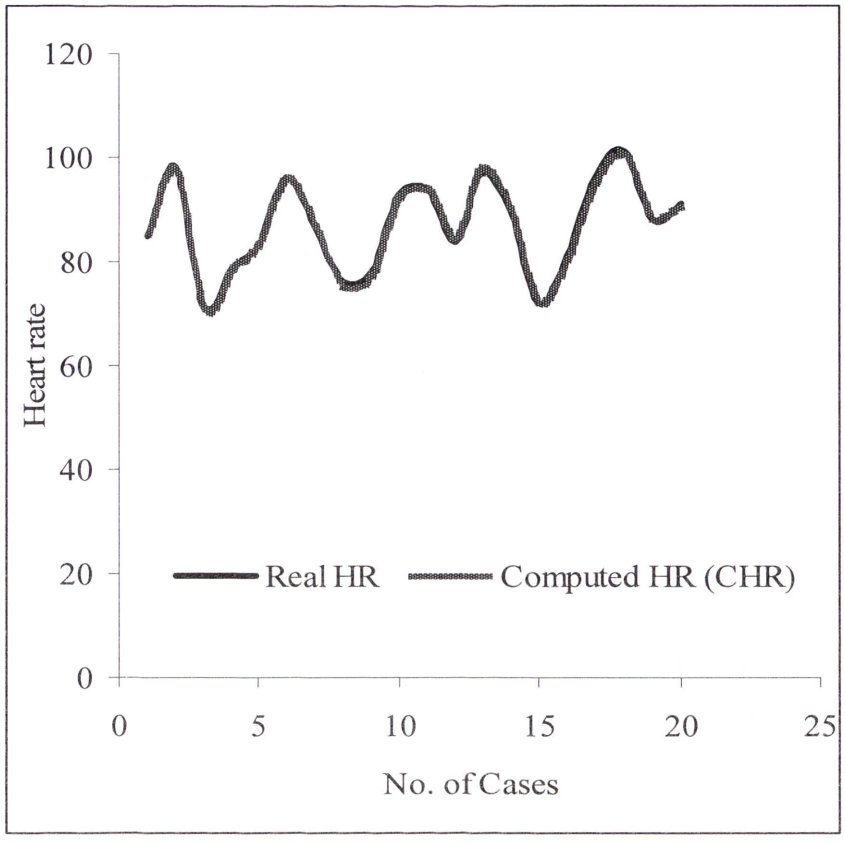

Figure 5.7: Real HR and computed HR Values

As noticed in figure 5.7, all computed HR values are close or equal to Real HR and the accuracy of equation (5-1) equals 99.53%. These results support the utilization of equation (5-1) to evaluate HR values.

Also, the good performance of equation (5-1) is illustrated graphically by the Bland and Altman (B&A) plot method. The B&A plot makes a graphic comparison between any two methods to check the accessibility if the second method can be used as an alternative method instead of the other method based on calculating mean and standard deviation of the differences between results of both methods.

The B&A plot is established for the HR values that are obtained from subjects' medical records (Real HR) and HR values that are computed by equation (5-1) (computed HR) by calculating the Mean and the standard deviation (SD) of the difference between Real

HR and computed HR that are shown in table (5.3). The Mean and SD values are -0.173 and 0.44 respectively. Then the B&A plot for HR Values are shown in figure 5.8.

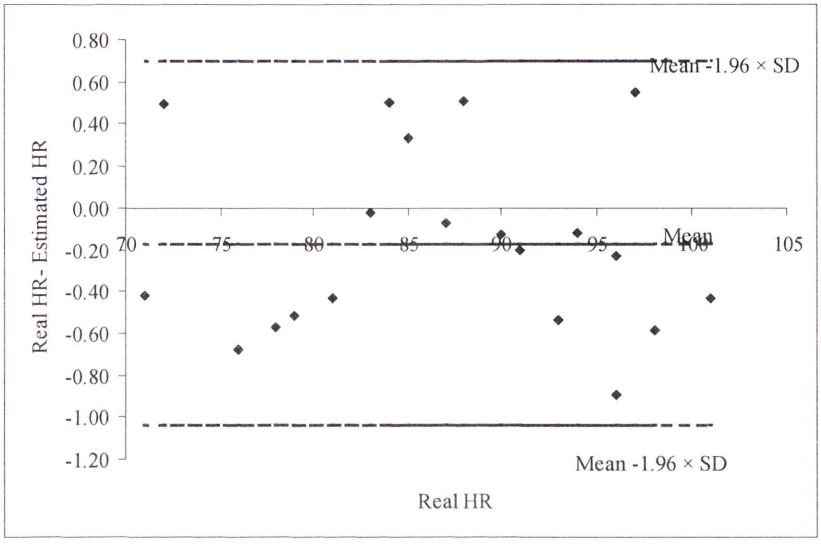

Figure 5.8 B&A plot for computed HR Values

As can be observed from the B&A plot, figure 5.8, the mean of differences between Real HR and computed HR is very small; mean = -0.173 only, and all differences between Real HR and computed HR are lying within the limits of agreement; which represents the Mean ± 1.96 × SD, so the new method matches and agrees well with the standard method [74].

5.3.2 Pulse wave velocity

The second parameter of cardiovascular parameters that depends on PPG signal is the Pulse wave velocity (PWV) which measures the velocity of the heart beat based on the standard expression for velocity calculation where the *average* velocity v of an object moving through a displacement (ΔD) during a time interval (ΔT) is described by the formula [75]:

$$V = \Delta D/\Delta T \quad \text{(5-3)}$$

To measure the Pulse wave velocity two PPG sensors are required. The PPG sensors are attached to the subject's finger with known distance (ΔD), see figure 5.9 (a).

Figure 5.9 (b) shows the two PPG signals sketch as acquired by oscilloscope where the normal signal represents the output$_1$ whereas the dashed signal represents the output$_2$. Therefore, PWV can be calculated based on next expression:

$$PWV = \frac{\Delta D}{\Delta T} = \frac{\text{Distance between two PPG sensors}}{\left|\text{Time of beginning of output}_2 - \text{Time of beginning of output}_1\right|} \quad \ldots. (5\text{-}4)$$

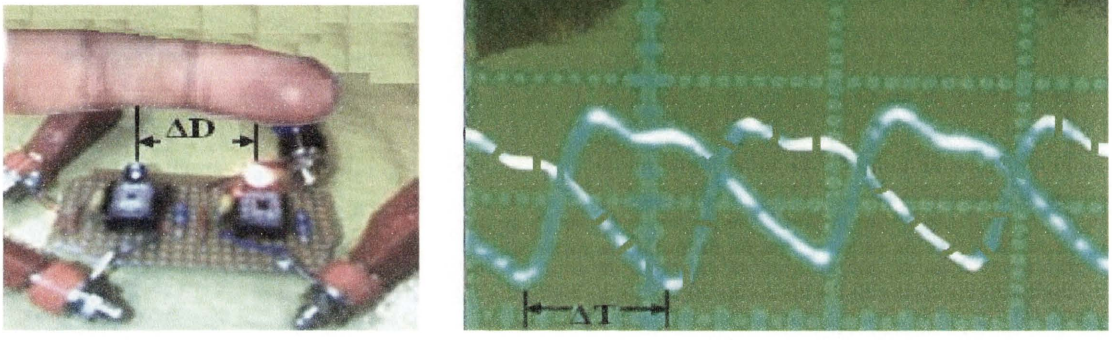

(a) (b)

Figure 5.9 Two PPG sensor circuit and PPG signals as sketched by the oscilloscope

5.3.3 Oxygen Saturation level

Oxygen Saturation level (S_pO_2) is the third parameter of cardiovascular parameters and can be measured directly depending on the PPG signal. Clinically, Oxygen Saturation level (OSL) is known as S_pO_2 or Sa O_2 and it represents the amount of oxygen saturation in the vessel's blood.

There are two sensors which were used to measure S_pO_2: oxygen sensor and pulse oximeter. The drawback of the oxygen sensor is the consumption of oxygen from the vessel's blood during the measurement based on the rate of the probe diffusion, while the drawback of the pulse oximeter is the high sensitivity to the small subject of the subject, such as shivering [76]; to deal with these drawbacks, the reflected mode of the

PPG sensor is used in CPLMTS to measure S_pO_2 relies on the Oxy-hemoglobin and De-Oxy-hemoglobin optical absorption ratio, where S_pO_2 is calculated by:

$$SpO2 = \frac{HbO_2}{HbO_2 + Hb} \times 100\% \quad \text{..... (5-5)}$$

Where, S_pO_2 = Oxygen Saturation,

HbO_2 = Oxy-hemoglobin,

Hb = De-Oxy-hemoglobin

The oxygen saturation, which is defined in equation (5-5), can also be defined in terms of concentrations as:

$$SpO2 = \frac{c_{HbO_2}}{c_{HbO_2} + c_{Hb}} \times 100\% \quad \text{..... (5-6)}$$

from equation (5- 4) and after ignoring the percentage part:

$$c_{HbO_2} = S_pO_2 \left(c_{HbO_2} + c_{Hb}\right) \quad \text{..... (5-6a)}$$

$$c_{Hb} = (1 - (S_pO_2)) \left(c_{HbO_2} + c_{Hb}\right) \quad \text{..... (5-6b)}$$

The optical absorption ratio, which depends on medium concentration, of Oxy-hemoglobin and De-Oxy-hemoglobin is acquired by PPG sensor(s) based on the Beer-Lambert law [77]. This is stated as if the light travels through a uniform medium as shown in figure 5.10, then its intensity will attenuated by a predictable rate based on the extinction coefficient of the medium absorption ($\varepsilon(\lambda)$), concentration of the medium (c), and the length of optical path (d); so the intensity of the light after travelling (I_{out}) is related to the original intensity of the light (I_{in}) as shown in equation (5-7):

$$I_{out} = I_{in} e^{(\varepsilon(\lambda) \times c \times d)} \quad \text{--- (5-8)}$$

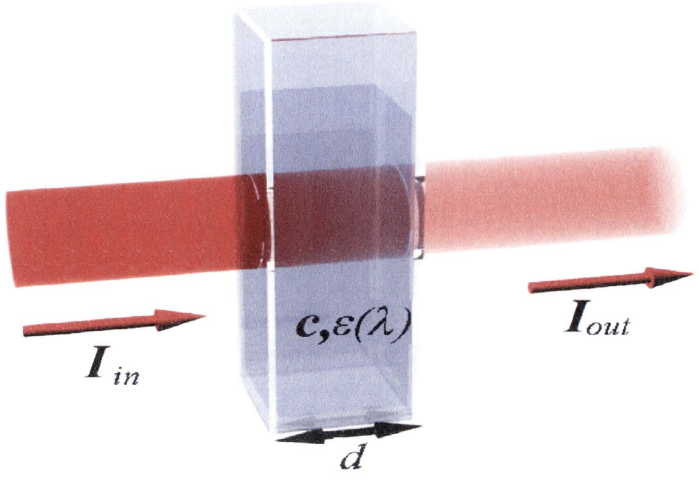

Figure 5.10 Graphical presentation of Beer-Lambert law

Hence, when the optical light travels through the subject's finger, then the light intensity after travelling, can be found based on Beer-Lambert law by next formula:

$$I_{out} = I_{in} e^{(\varepsilon_{HbO_2}(\lambda)\times c_{HbO_2}\times d + \varepsilon_{Hb}(\lambda)\times c_{Hb}\times d)} \quad \text{... (5-8)}$$

After substituting the values of c_{HbO_2} and c_{Hb} in terms of S form equations (5-6a) and (5-6b), respectively, then simplifying the whole expression of equation (5-8) produces:

$$\Rightarrow \ln\frac{I_{out}}{I_{in}} = d\times\left(c_{HbO_2} + c_{Hb}\right)\times[\varepsilon_{HbO_2}(\lambda)\times S_pO_2 + \varepsilon_{Hb}(\lambda)(1-(S_pO_2))] \quad \text{... (5-9)}$$

Now, to find S_pO_2 of equation (5-9); the ratio between light intensities of two PPG sensors with different wavelengths (Infrared and red) are required. The ratio (R) between light intensities of Red and IR diodes are expressed by:

$$R = \frac{\ln\left(\frac{I_{out}}{I_{in}}\right)_{Red}}{\ln\left(\frac{I_{out}}{I_{in}}\right)_{IR}} \quad \text{..... (5-10)}$$

After simplifying equation (5-8) by substituting ($\frac{I_{out}}{I_{in}}$) value of equation (5-9) for both PPG sensors and rearranging the whole expression to easily calculate the S_pO_2 value by:

$$\Longrightarrow \quad S_pO_2 = \frac{\varepsilon_{Hb}(\lambda_R) - \varepsilon_{Hb}(\lambda_{IR}) \times R}{\varepsilon_{Hb}(\lambda_R) - \varepsilon_{HbO_2}(\lambda_R) + ([\varepsilon_{HbO_2}(\lambda_{IR}) - \varepsilon_{Hb}(\lambda_{IR})] \times R)} \quad \text{..... (5-11)}$$

The Ratio (R) in equation (5-11) is calculated by DC and AC components of two different PG signals:

$$R = \frac{AC_R/DC_R}{AC_{IR}/DC_{IR}} \quad \text{..... (5-12)}$$

The values of the extinction coefficients (ε_{HbO2} and ε_{HB}) for both wavelengths; can be obtained from Spectrum graph [78] as shown in figure 5.11:

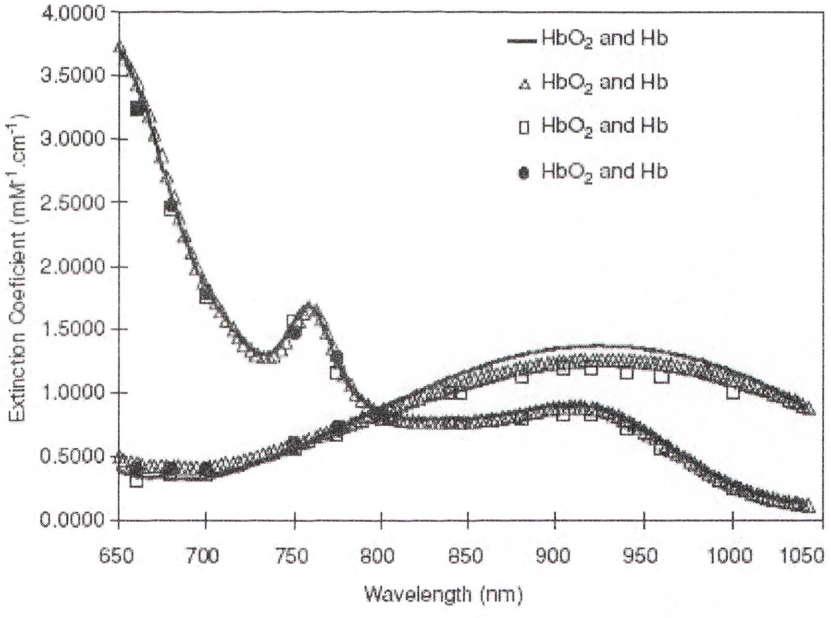

Figure 5.11: Absorption Spectrum graph for Oxy-hemoglobin and De-Oxy-hemoglobin [78]

The extinction coefficients (ε_{HbO2} and ε_{HB}) values are detected from Spectrum graph, shown in figure 5.11. These values are then demonstrated in table (5.4):

Table (5.4): LEDs' Wavelengths and their corresponding Extinction Coefficient [78]

Wavelength (nm)	Extinction Coefficient (L/mmol/cm)	
	Hb	HbO_2
660 (Red)	0.81± 0.006	0.08 ± 0.005
940 (IR)	0.18 ± 0.003	0.29 ± 0.002

Therefore, after substituting extinction coefficients values from table (5.4) in equation (5-11), the equation (5-11) can be written as:

$$S_pO_2 = \frac{0.81 - (0.18 \times R)}{0.73 + (0.11 \times R)} \times 100 \quad \text{..... (5-13)}$$

Furthermore, equation (5-13) is illustrated graphically as shown in figure 5.12 to simply obtain S_pO_2 value if Ratio (R) has been known.

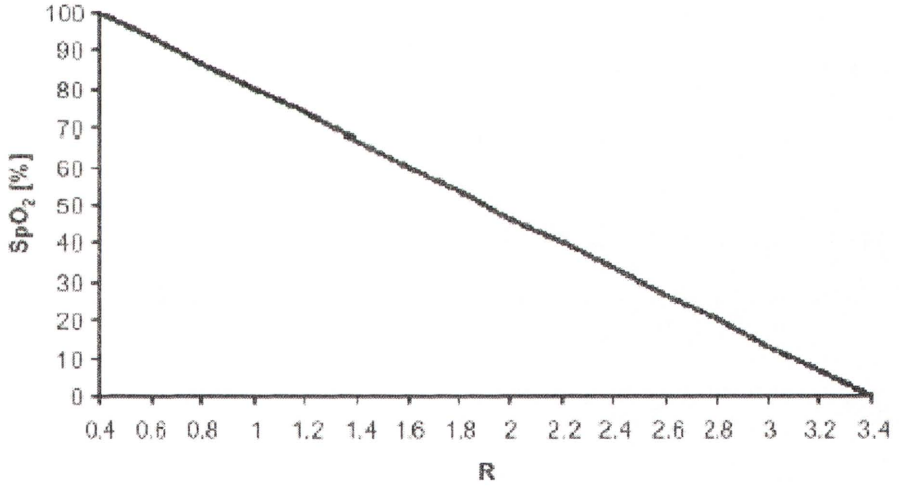

Figure 5.12: Graphical illustration of equation (5-13)

An experiment has been conducted by researcher on four healthy subjects in sitting posture, based on ethical approval in appendix 1. Oxygen Saturation level was measured depending upon two PPG signals. They are acquired by attaching two PPG sensors on the subject's finger as shown in figure (5.9a). These PPG sensors are based on different type of Light Emitting Diodes (LED); Infrared (IR) and Red (R). Hardware circuit of these two PPG sensors is shown in the figure 5.13.

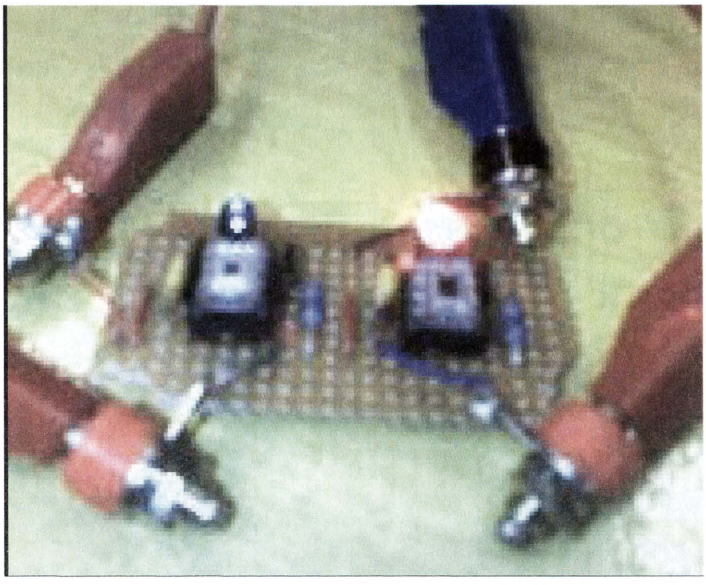

Figure 5.13: Hardware Circuit of Two PPG sensors to measure OS

The OS level measurements are required two PPG sensors to be attached to subject's finger. A few minutes are needed to get stable PPG signals. The output of the circuit is analysed to measure OS and is evaluated by the substituted the AC and DC components values in the equations (5-12) and (5-13).

The achieved results of DC and AC components of PPG signals for RED and IR LEDs also the calculated ratio (R), which was obtained from equation (5-12), and Oxygen saturation level value, which was found by equation (5-13), for each subject are shown in table (5.5):

Table (5.5): Experimental Values of Four Healthy Subjects

Component	Subject1	Subject 2	Subject 3	Subject 4
DC level IR	3.89911	3.55509	3.69003	4.04749
AC level IR	0.02614	0.09732	0.05037	0.03589
DC level Red	3.71914	3.49037	2.78973	3.31003
AC level Red	0. 01059	0.03762	0.01221	0.00916
RATIO	0.424771	0.39372	0.32068	0.31215
Oxygen Saturation	94.4%	95.5%	98.3%	98.6%

From table (5.5), all calculated values of Oxygen Saturation Values are clinically accepted for healthy subjects with healthy haemoglobin levels since all values are located between (94.4%) and (98.6%) and these values are close (or more than 95 %) which is clinically acceptable for a healthy subject in [79].

Another experiment was carried out to compare the measurements of CPLTMS with pulse oximeter (Mallinckrodt N-20E). Two healthy subjects were involved in the measurement with two readings for each subject; the first reading was taken in a healthy condition and the second reading was taken after deep breathing for each subject. The results of comparison between two devices are shown in the table (5.6).

Table (5.6): Comparison between CPLTMS and Standard Device

Subject	Condition	Built Transducer Result	Standard Device Result
1	Healthy	96.56%	98%
	Deep Breath	97.33%	99%
2	Healthy	96.82%	98%
	Deep Breath	100%	100%
Average		97.68%	98.75%

The accuracy of oxygen saturation level (OS) results is computed by equation (5-2):

$$\text{Accuracy} = 100\% \times \left(1 - \left(\frac{1.07}{98.75}\right)\right) = 98.91\ \%$$

Practically, a subject with a healthy haemoglobin level of OS value around 95% or over is clinically accepted [79]. Hence, the results that have been shown in table (5.6) are within a healthy range. A comparison between CPLTMS and standard device, as shown in table (5.6), shows that the accuracy for CPLMTS and the standard device are close enough. This comparison is demonstrated graphically in next figure.

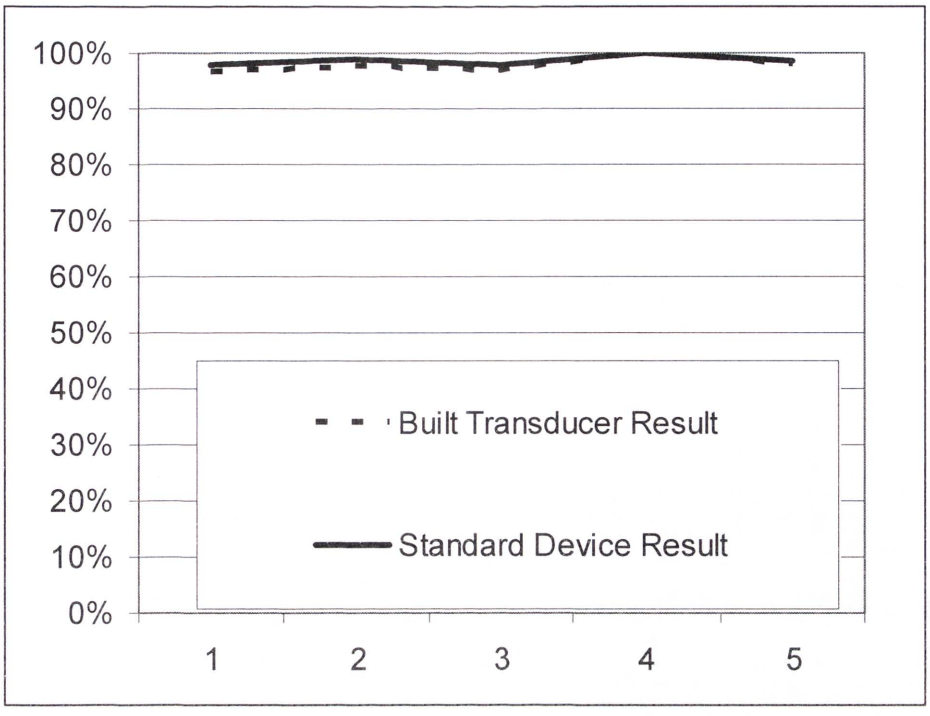

Figure 5.14: Comparison between CPLTMS and standard device

The accuracy of our Built system is very close to the accuracy of the standard device hence, our device performance is accepted.

5.4. Summary

In conclusion, the experiments performed on CPLMTS, which were utilized to estimate HR and Oxygen saturation values, clarify the conformity of implementing the method that has been described because those experiments gave expected results.

In the next chapter, The BPPs estimations methods, the use of intelligent techniques and the results of these methods will be explained.

Chapter 6. Blood Pressure Estimations Methods

The blood pressure measurements were started in 1733 [41] by an invasive method since that blood pressure measurement have been developed over years by using new methods and new sensors to satisfy the subjects, physicians and clinicians expectations. The details of blood pressure measurement developments and limitations were presented and discussed on chapter 3.

6.1. Introduction

This chapter will present our proposed novel algorithms to deal with some of blood pressure measurement limitations by designing Cardiovascular Parameters Long Term Monitoring System (CPLTMS) based on heart rate (HR) and Photo-plethysmography (PPG) signal.

Clinically, the blood pressure has three parameters: mean arterial blood pressure (MAP), Systolic blood pressure (SBP) and Diastolic blood pressure (DBP). These parameters will henceforth be referred to as blood pressure parameters (BPPs). BPPs are estimated by many methods.

The development of methods, performing experiments and achieved results of these methods will be clarified, explained, discussed and illustrated by procedures steps, flowcharts, tables, figures and discussion arguments in following sections.

The first section presents our proposed methods that are used for MAP estimations; the second section provides our proposed methods that are used type-2 fuzzy system to estimate BPPs for unhealthy and healthy subjects.

6.2. Mean arterial blood pressure estimation methods

The Mean Blood Pressure estimation methods in this research are based on PPG signal frequency which is equal to HR. The relationship between MAP and HR, however, is very complicated has a nonlinear relationship and without a standard expression. Carr

provided an expression to estimate MAP based on HR values. Carr's expression is detailed in next subsection [41].

6.2.1. Carr's expression

As has been mentioned in Chapter 3, Carr specified an expression to state the relationship between MAP and HR depending on Dynamic blood flow in the body. He considered the cardiovascular system as an electric circuit [41]. Therefore, Ohms' law, as shown in next equation, can be adopted on the cardiovascular system.

$$\text{Ohms' law: } V = I \times R \quad \text{..... (6-1)}$$

Where V is voltage potential difference

I is circuit current, R is circuit resistance

Carr matched the mean arterial blood pressure to voltage potential difference, the Cardiac output (CO) of heart to circuit current and the total peripheral blood vessels resistance (TPR) against blood flow to circuit resistance. Therefore, as Ohm's law, the mean arterial blood pressure is calculated based on following equation [5]:

$$MAP = CO \times TPR \quad \text{..... (6-2)}$$

Physically, the cardiac output can be calculated by measuring the volume of blood which is pumped by each heart beat. This volume is equal to the difference between end-diastolic-volume (EDV) and end-systolic-volume (ESV). This volume is known as stroke volume (SV) [5].

$$SV = EDV - ESV \quad \text{..... (6-3)}$$

The heart pumps this amount of blood with every heart beat. Thus, the cardiac output for every minute can be computed based on next equation [5]:

$$CO = HR \times SV \quad \text{..... (6-4)}$$

Then equation (6-2) can be re written as:

$$MAP = HR \times SV \times TPR \quad \text{..... (6-5)}$$

Carr's expression [41], as stated in equation (6-5), is investigated during this research based on real HR values and real MAP values of Mimic database [80]. The MIMIC database is available in the Physio-bank web site, and it includes continuous records of cardiovascular signals and interrupted measurements, such as HR and MAP values of subjects at an intensive care unit (ICU) for every second during more than 10 hours. This means 36000 records for each case, at least. These records are extracted from bedside monitors that were attached to subjects and from subjects' medical records.

The SV and TPR values of healthy subject; SV = 70 ml and TPR = 0.018 mmHg. min/ml [5], are utilized with the mean of real HR records for each case of Mimic database to estimate MAP values by equation (6-5). This method will henceforth be referred to as Meth1.

The mean of estimated MAP values based on Carr's expression, mean of clinic HR records, mean of MAP records of Mimic database [80] (clinic MAP) and the absolute differences between estimated MAP and real MAP values are illustrated in table (6.1).

The accuracy of Carr's method is calculated based on equation (5-2) [73]:

$$\text{The Carr's method Accuracy} = 100\ \% \times \left(1 - \left(\left|\frac{34.63}{74.99}\right|\right)\right) = 53.83\%$$

Table (6.1): mean of HR values, mean of estimated MAP1 values based on Meth1, mean of real MAP and absolute difference between real and estimated MAP1 values

Case	HR	Estimated MAP1 (mmHg)	Real MAP (mmHg)	|EMAP1- Real MAP| (mmHg)
1	85.33	107.1	63.45	43.65
2	97.41	123.48	80.03	43.45
3	70.58	89.46	75.34	14.12
4	78.48	99.54	80.81	18.73
5	82.98	104.58	72.98	31.6
6	95.77	120.96	75.62	45.34
7	86.93	109.62	72.28	37.34
8	75.32	95.76	79.45	16.31
9	77.43	98.28	75.64	22.64
10	92.46	117.18	77.60	39.58
11	93.88	118.44	74.21	44.23
12	84.5	105.84	76.80	29.04
13	97.55	122.22	81.20	41.02
14	89.87	113.4	75.32	38.08
15	72.49	90.72	71.25	19.47
16	80.57	102.06	71.58	30.48
17	95.11	120.96	69.75	51.21
18	100.57	127.26	69.46	57.8
19	88.51	110.88	84.54	26.34
20	90.8	114.66	72.54	42.12
Average	86.83	109.62	74.99	34.63

Mean values of the estimated MAP and mean values of the real MAP of table (6.1) are illustrated graphically in figure 6.1:

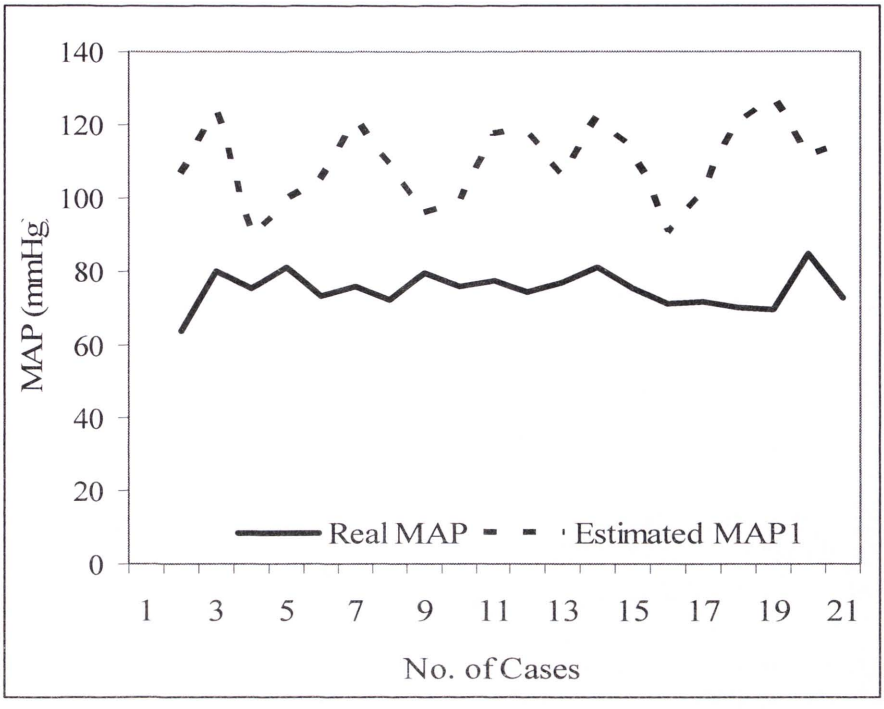

Figure 6.1: The estimated MAP1 values and real MAP values

As can be observed from figure 6.1, most of the mean of estimated MAP1 values are far from the mean of real MAP values and its accuracy equals 53.83%; hence, Carr's method cannot be considered as a practical or reliable method to estimate MAP values.

Moreover, Carr's expression of results are illustrated graphically by the Bland and Altman (B&A) plot method [74]; B&A plot compares graphically between two methods to check if the second method can be used as an alternative method based on calculating mean and standard deviation of the differences between results of both methods.

Therefore, mean of estimated MAP values by Carr's expression are compared with the mean of real MAP values that were obtained from subjects' medical records of Mimic database. The B&A plot is arranged by calculating the Mean and SD of the differences between estimated MAP values by Carr's expression and real MAP values that were obtained from subjects' medical records of Mimic database [80], which were shown at table (6.1). The Mean and SD values of the differences between mean of estimated

MAP and real MAP are 34.63 and 12.20, respectively. Also the B&A plot for the mean of the MAP values for Carr's method is illustrated in figure 6.2.

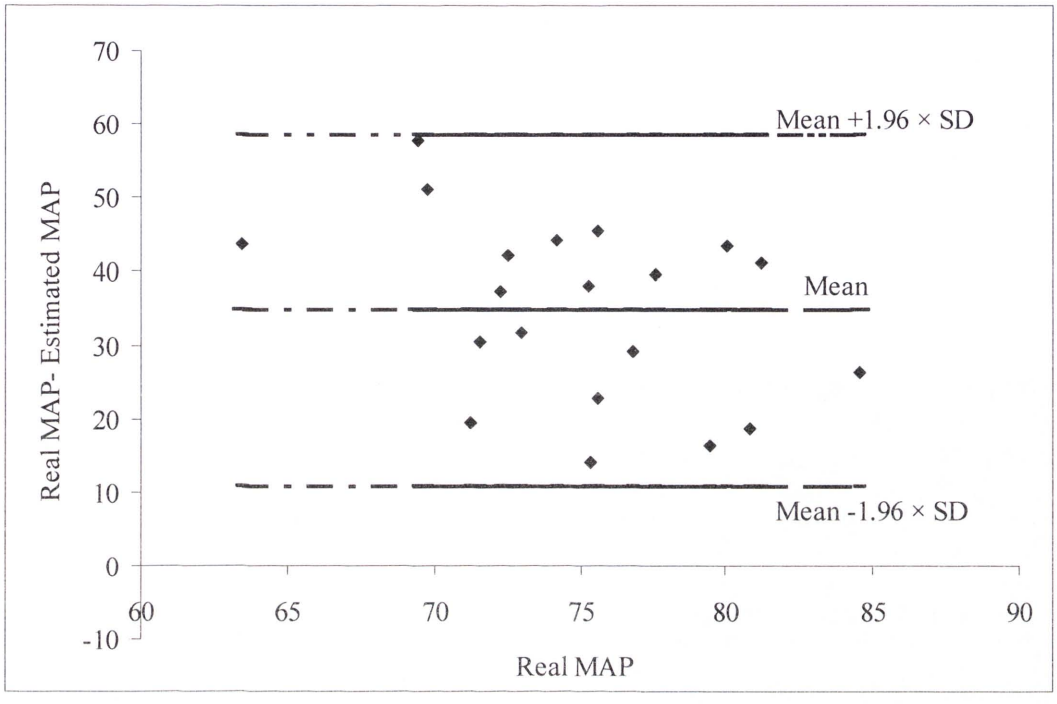

Figure 6.2: B&A plot for estimated MAP by Carr's Method

As can be observed from plot figure 6.2, all the differences between measurements of two methods are located within the limits of agreement: Mean ± 1.96 × SD. These differences, however, are not close to the mean of differences as well as the mean of differences is very high which equals 34.63. That mean is not close to zero and Carr's method accuracy is small, which equals 53.83%. Hence, Carr's method is not accepted as an alternative method instead of the bedside monitor and benchmark methods that are used in ICU to register subjects' medical records.

Therefore, the researcher develops new methods to overcome these limitations and to achieve a low mean of differences between estimated and real MAP values and low SD through improving Carr's formula by considering the effects of other factors as explained in next subsection.

6.2.2. Proposed Methods

In Carr's expression, stroke volume is considered as constant value, but actually SV is a function related to HR variability [81]. Therefore, the researcher takes the effect of the SV changes in account by specifying the SV value as a function of HR as follows:

$$SV = SV_0 + A \times SV_0 \times HR \quad \text{..... (6-6)}$$

Where SV_0 is a constant stroke volume.

A is an adjustment coefficient of SV variability influence

After substituting the value of SV of equation (6-6) in equation (6-5):

$$MAP = HR \times (SV_0 + A \times SV_0 \times HR) \times TPR$$

$$MAP = HR \times SV_0 \times (1 + A \times HR) \times TPR$$

$$MAP = SV_0 \times TPR \times HR \times (A \times HR+1) \quad \text{..... (6-7)}$$

The value of adjustment coefficient of SV influence (A) will be determined by:

i- Optimize SV influence (A) by fit value:

The coefficient (A) is optimized by fit value method depending on the database of twenty cases; which were chosen randomly of MIMIC database where each case has 36000 readings at least; the following procedure has been followed to optimize the coefficient A by fit value method:

Firstly, since, the effect of HR on SV is small, so a small range between (-0.1, 0.1) with 0.00001 as step change, is proposed for coefficient (A). Therefore, there are twenty thousand and one values for coefficient (A).

Secondly, the optimized coefficient (A) value was generated by using a fit value method based on substituting each value of coefficient (A) for twenty thousands values in equation (6-7) with the mean of HR and MAP values for each case of ten cases' records of MIMIC Database with the SV_0 and TPR values of healthy subject; where SV_0 = 70 ml and TPR = 0.018 mmHg. min/ml.

Thirdly, the average of absolute differences between estimated and real MAP values for ten cases' records were computed and the value of coefficient (A) that achieves the smallest average of absolute differences between real and estimated MAP values for ten cases' records is assigned as optimized value of coefficient (A).

The procedure of Fit method is represented by flowchart as shown in figure 6.3.

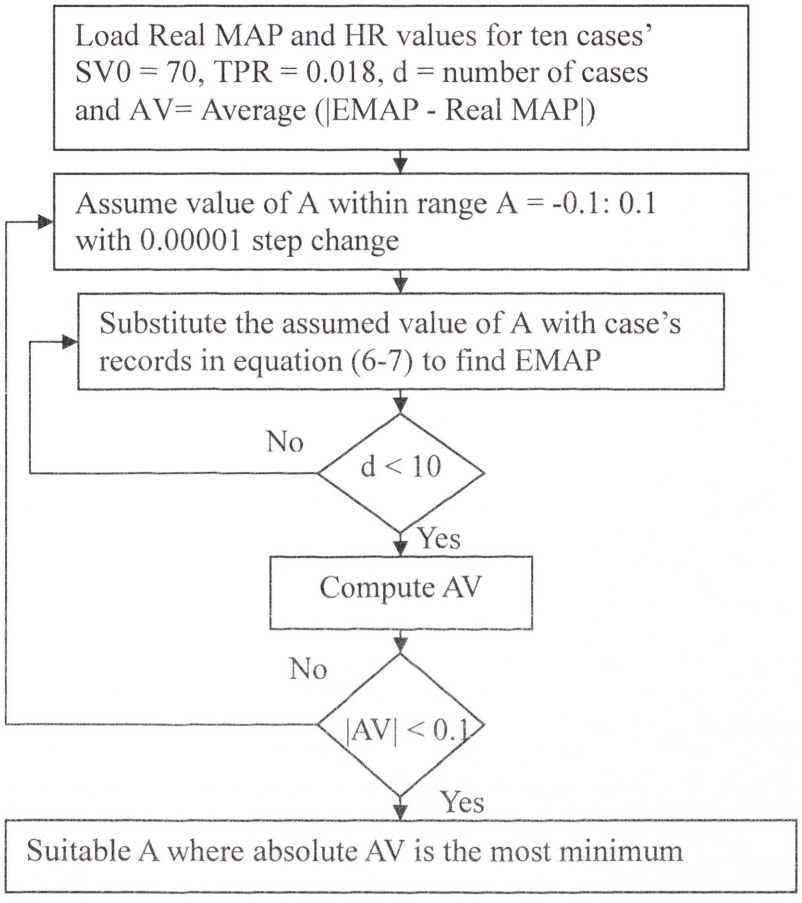

Figure 6.3: Flowchart of Fit method

Finally, the optimized value of coefficient (A), where A = -0.00331 is utilized with the SV_0 and TPR values of healthy subject, and with mean of HR values of remaining ten cases' records, as test cases, to estimate MAP values for the remaining ten cases by equation (6-7). This method will henceforth be referred to as Meth2.

The mean of estimated MAP values by Meth2 (EMAP2) for the remaining ten cases, as test cases, mean of estimated MAP values for the remaining ten cases by Meth1

(EMAP1), mean of real MAP values and absolute differences between mean of real and estimated MAP values of Meth1 and Meth2 are listed in table (6.2).

Table (6.2): mean of HR values, mean of real MAP, mean of estimated MAP values by Meth1 and Meth2, and absolute differences between their values of Meth1 and Meth2

Case	HR	Real MAP (mmHg)	EMAP2 (mmHg)	|EMAP2 – Real MAP | (mmHg)	EMAP1 (mmHg)	|EMAP1 - Real MAP | (mmHg)
11	93.88	74.21	81.64	7.43	118.44	44.23
12	84.50	76.80	76.78	0.02	105.84	29.04
13	97.55	81.20	83.28	2.08	122.22	41.02
14	89.87	75.32	79.65	4.33	113.4	38.08
15	72.49	71.25	69.4	1.77	90.72	19.47
16	80.57	71.58	74.53	2.95	102.06	30.48
17	95.11	69.75	82.53	12.78	120.96	51.21
18	100.57	69.46	84.66	15.2	127.26	57.8
19	88.51	84.54	78.95	5.59	110.88	26.34
20	90.80	72.54	80.13	7.59	114.66	42.12
Average	89.39	74.67	79.16	5.97	112.64	37.98

The accuracy of Meth2 is calculated based on equation (5-2) [73]:

$$\text{The Meth2 Accuracy} = 100\ \% \times \left(1 - \left(\frac{5.97}{74.67}\right)\right) = 92.00\%$$

Mean of estimated MAP values of Meth2, Meth1 and real MAP values that were shown at table (6.2) are illustrated graphically in figure 6.4:

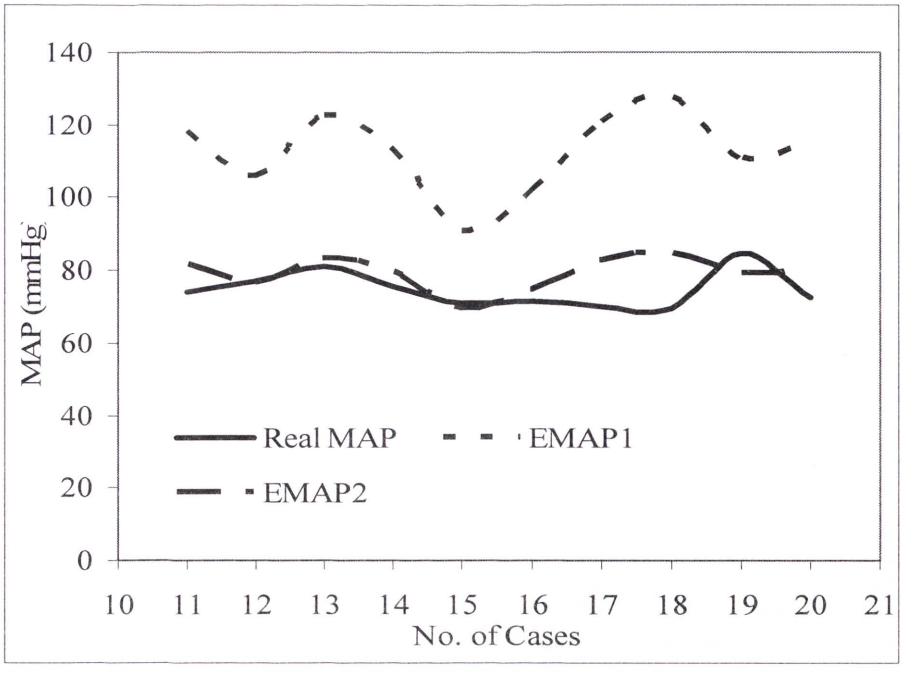

Figure 6.4: The estimated MAP values of Meth2, Meth1 and real MAP values

As can be noticed from figure 6.4, the estimated MAP values by Meth2 are closer to real MAP values than estimated MAP values by Meth1; and Meth 2 accuracy equals 92.00% is higher than the accuracy of Meth1; hence, Meth 2 can be considered as a practical method.

Moreover, the achievements of Meth2 and Meth1 for last ten cases' records are illustrated graphically by the B&A plot method [74]; the B&A plot is arranged by calculating the Means and SDs of (EMAP1 - Real MAP) and (EMAP2 - Real MAP). The Mean and SD values of (EMAP1 - Real MAP) are 37.979 and 11.77 respectively, while the Mean and SD values of (EMAP2 - Real MAP) are 4.499 and 6.42 respectively, then the B&A plot for MAP values for Meth1 and Meth2 are shown in figure 6.5.

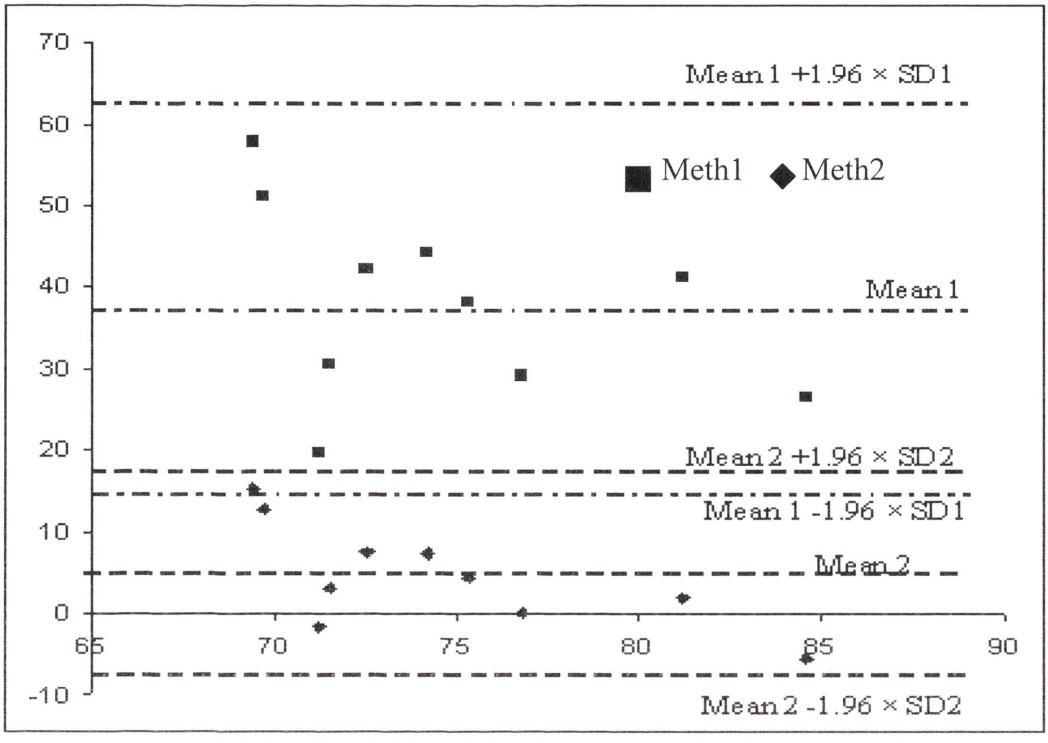

Figure 6.5: B&A plot for MAP Values for Meth1 and Meth2

As can be observed from the B&A plot that are shown in figure 6.5; all the differences between measurements of two methods are located within the agreement limits; (Mean ± 1.96 × SD), however, the absolute mean and SD of difference for Meth2 is smaller than the absolute mean and SD of difference for Meth1 as well as the differences for Meth2 are closer to mean2 and to zero than the differences for Meth1, so the Meth2 is accepted as an alternative method instead of the bedside monitor and benchmark methods that are used in ICU to register subjects' medical records.

Actually, optimizing the adjustment coefficient of SV influence (A) by Fit method value achieved good results; however, the mean and SD of the differences between estimated and real MAP values are still high. Therefore, the researcher overcomes these limitations by utilizing Particle Swarm Optimization (PSO), an intelligent technique, to optimize the value of adjustment coefficient of SV influence (A) as explained next.

ii- Optimize SV influence coefficient (A) by PSO:

The coefficient (A) is optimized by PSO algorithm depending on the same twenty cases that were used before, in which each case has 36000 records at least. The PSO algorithm that optimizes coefficient (A) value consists of the following steps:

1- Divide the twenty cases to ten cases for training PSO to find the optimal value for coefficient (A) and ten cases for testing the achieved value of coefficient (A);

2- Set the problem domain for PSO algorithm as the database of ten cases of MIMIC database and coefficient (A) range as suggested before in Meth2 procedure the range of coefficient (A) is (-0.1, 0.1) with 0.00001 change step;

3- Set the number of particles; which is known as Swarm population, for the coefficient (A) within the recommended range of particles (20-50) particles [61, 62]. 24 particles are proposed for this method; n = 1 … 24;

4- Initialize random position for each particle of 24 particles within the suggested range (-0.1, 0.1) and initialize random velocity for each particle within fraction range of the particles' range; (1/swarm population) × (-0.1, 0.1);

5- Set constant values for Swarm parameters; $\chi = 1$ and $\varphi_1 = \varphi_2 = 2$, to use them in equation (4-2) and Set constant values for boundaries of the problem domain; $X_{max} = \pm 0.1$ $V_{max} = \pm 0.03$, to use them in steps 9 and 10;

6- Utilize two particle topologies gbest and pbest; which explained in Ch4 section 4.3, to achieve the optimal solution for coefficient (A). Where the initial value for pbest equal the initial random position for that particle. Also generate initial value of gbest based on equation (6-7) that is calculated Estimated MAP (EMAP), where (A) has 24 values stands on 24 particles initial random positions, HR and MAP values equal the mean of real HR and Real MAP records for each case of the ten cases' records. Also the SV_0 and TPR values for healthy subject are chosen as constant

values for SV_0 and TPR; so SV_0 = 70 ml and TPR = 0.018 mmHg. min/ml [5]. The initial particle position, which achieves the smallest average of absolute differences between EMAP and Real MAP values of ten cases, is assigned as initial value for gbest;

7- Start the searching part of PSO; where maximum iterations is 100; t = 1 … 100;

8- Evaluate the initial value for gbest by equation (6-7). If the mean of absolute differences between EMAP and Real MAP values for ten cases is zero, where real HR, real MAP, SV_0 and TPR values equal the values as described in step 6. If this value of gbest passes the evaluation check, the optimal value is achieved so the algorithm processing is stopped or else the algorithm processing continues;

9- Update particle's velocity by equation (4-2) [62] to use it as the new V_n value in next iteration:

$$V_n(t+1) = \chi \times V_n(t) + \varphi_1 \times rand_1 \times (pbest_n - X_n) + \varphi_2 \times rand_1 \times (gbest - X_n) \text{ -- (4-2)}$$

Absorbing wall is used to keep the particle within problem domain as it is explained. The Absorbing wall changes the velocity value to zero and the particle position will be frozen inside the allowed solution space; in other words, if $V_n(t+1)$ is less than V_{max} continue the algorithm processing else new $V_n(t+1) = 0$;

10- Update particle's position by equation (4-3) [62] to use it as the new X_n value in equations (4-2) and (4-3) for the next iteration:

$$X_n(t+1) = X_n(t) + V_n(t+1) \text{ ----- (4-3)}$$

Absorbing wall is used to keep the particle position within problem domain; in other words, if absolute ($X_n(t+1)$) is less than X_{max} continue the algorithm processing else $X_n(t+1) = Xn(t)$;

11- Update the particle's $pbest_n$ value, which will be used as the new $pbest_n$ value in equation (4-2) in the next iteration, based on substituting the updated particle's

position; which achieved from equation (4-3), instead of ($A = X_n (t+1)$) in equation (6-7) to estimate EMAP values; where real HR, real MAP, SV_0 and TPR values equal the values as described in step 6. If the average of absolute differences between EMAP and Real MAP values for ten cases records is less than the average of absolute differences between EMAP and Real MAP values for ten cases records; when $A = X_n (t)$, then the new particle's value; $X_n(t+1)$, is assigned as a new value for $pbest_n$ to use it for the next iteration, else $pbest_n (t+1) = pbest_n (t)$;

12- Repeat steps 8, 9, 10 and 11 with other particles to update the value of pbests for other 23 particles and assign the $pbest_n$ value that achieves the smallest mean of absolute differences between EMAP and Real MAP values for the ten cases records, as a new value of the gbest. This will be used as a new value of gbest in equation (4-2) for next iteration;

13- Finally, repeats steps 8, 9, 10, 11 and 12 to update the values of $V_n (t+1)$, $X_n (t+1)$, $pbest_n$ for each particle and update the value of gbest for whole system in every iteration till it reaches a maximum iteration ($t = 100$), and assigns the gbest value as value of coefficient (A). This method will henceforth be referred to as Meth3.

The flowchart in figure 6.6 highlights the twelve steps of the PSO procedure.

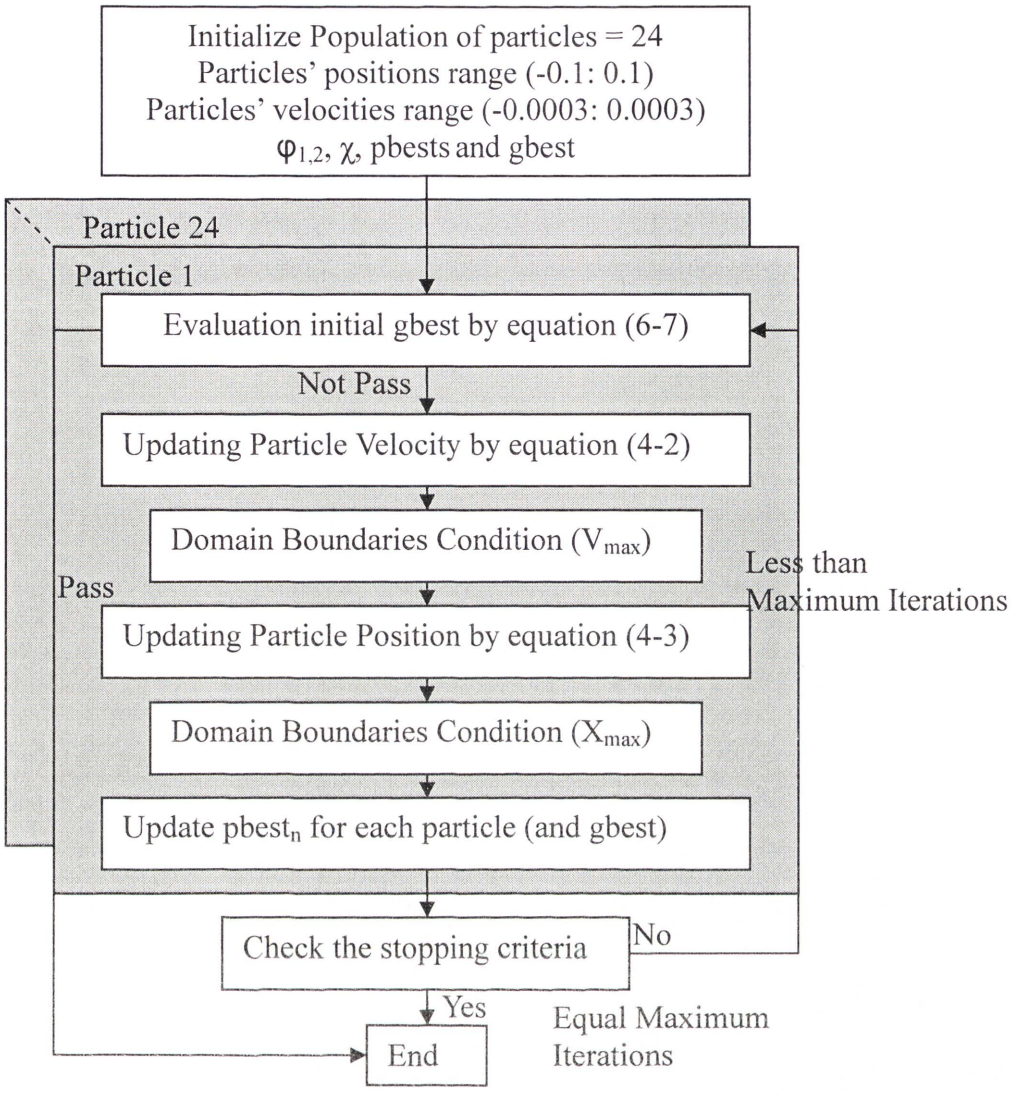

Figure 6.6: Flowchart of PSO procedure

The mean of MAP values for the remaining ten cases' records, as test cases, are estimated to examine the value of (A = -0.0034139) that are achieved by PSO algorithm. The new value of (A) that are achieved by Meth3 minimizes the difference between EMAP and Real MAP values for remaining ten cases more than Meth1 and Meth2 performed.

The HR values and real MAP values, estimated MAP values by three methods for remaining ten cases' records and the absolute differences between real and estimated MAP for the three methods are illustrated in table (6.5).

Table (6.3): mean of HR values, real MAP, estimated MAP by Meth1, Meth2 and Meth3, and absolute differences between mean of real and estimated MAP by Meth1, Meth2 and Meth3

Case	HR	Real MAP (mmHg)	EMAP3 (mmHg)	|EMAP3-Real MAP| (mmHg)	EMAP2 (mmHg)	|EMAP2-Real MAP| (mmHg)	EMAP1 (mmHg)	|EMAP1-Real MAP| (mmHg)
11	93.88	74.21	80.43	6.22	81.64	7.43	118.44	44.23
12	84.50	76.80	75.49	1.31	76.78	0.02	105.84	29.04
13	97.55	81.20	81.75	0.55	83.28	2.08	122.22	41.02
14	89.87	75.32	78.56	3.24	79.65	4.33	113.4	38.08
15	72.49	71.25	68.42	2.83	69.48	1.76	90.72	19.47
16	80.57	71.58	73.84	2.26	74.53	2.95	102.06	30.48
17	95.11	69.75	81.32	11.57	82.53	12.78	120.96	51.21
18	100.57	69.46	83.38	13.92	84.66	15.20	127.26	57.8
19	88.51	84.54	77.57	6.97	78.95	5.59	110.88	26.34
20	90.80	72.54	79.04	6.50	80.13	7.59	114.66	42.12
Average	89.39	74.67	77.98	5.54	79.16	5.97	112.64	37.979

The accuracy of Meth3 is calculated based on equation (5-2) [73]:

$$\text{The Meth3 Accuracy} = 100\ \% \times \left(1 - \left(\frac{5.54}{74.67}\right)\right) = 92.58\ \%$$

Mean of estimated MAP values of Meth3, Meth2, Meth1 and real MAP values that were shown at table (6.3) are illustrated graphically in figure 6.7:

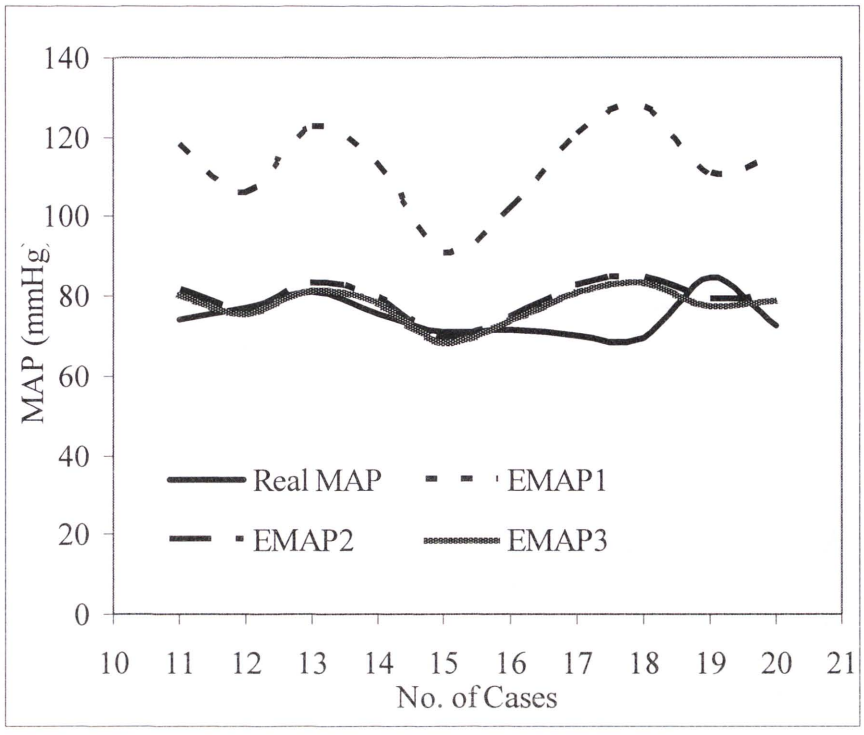

Figure 6.7: Mean of estimated MAP values of Meth3, Meth2, Meth1 and real MAP values

As observed in figure 6.7, the estimated MAP values by Meth3 are closer to real MAP values than estimated MAP values by Meth1 and Meth2, also Meth3 accuracy equals 92.58% is higher than the accuracy of Meth2 and meth1; hence, Meth3 can be considered as more practical method than Meth2.

Moreover, the achievements of Meth3 for remaining ten cases' records, as test cases, are illustrated graphically by the B&A plot method [74]. Then the B&A plot is arranged by calculating the Mean and SD of (EMAP3 - Real MAP), of table (6.5). The Mean and SD values of (EMAP3 - Real MAP) are 3.314 and 6.44 respectively, then the B&A plot for MAP Values for Meth3 is shown in figure 6.8.

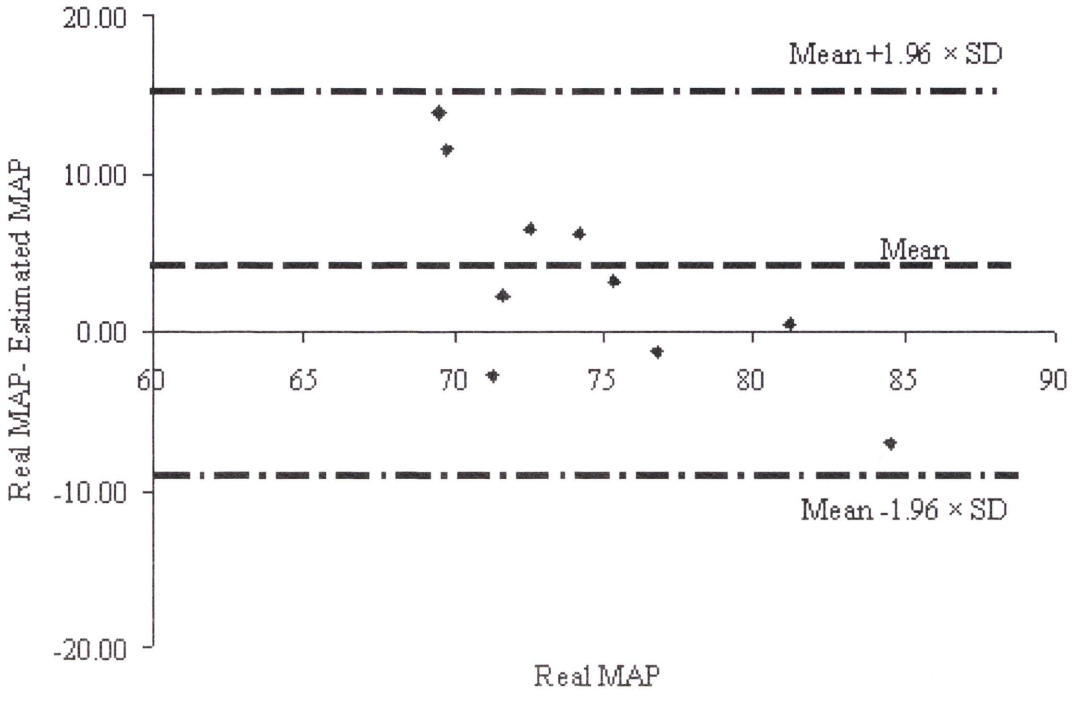

Figure 6.8: B&A plot for MAP Values for Meth3

Although the absolute mean and standard deviation of error between estimated values of MAP by Meth3 and real records of MAP were 3.314 mmHg and 6.4, respectively, it was more accurate than Meth2 and Meth1, but it was still high since the optimal values of SV, TPR and coefficient (A) are not optimized, simultaneously.

6.2.3. Optimizing A, SV_0 and TPR by Multi PSO

In literature, SV and TPR have ranges of values; where SV range is (35, 170) ml and TPR range is (0.015, 0.02) mmHg.min/ml [5]. Therefore, the researcher utilizes Multi Particle Swarm Optimization (PSO), to optimize the values of adjustment coefficient of SV influence (A), SV_0 and TPR simultaneously to achieve more accurate MAP values depending in equation (6-7).

The multi PSO (MPSO) procedure to optimize constant values of adjustment coefficient of SV influence (A), SV_0 and TPR is implemented as described in following procedure:

1- Divide the twenty cases of Mimic database [80] into ten cases for training MPSO to find the optimal value for the coefficient (A), SV_0 and TPR, and the other ten cases' records for testing the achieved values;

2- Set the problem domain for the MPSO as the database of ten cases of MIMIC database, coefficient (A) range is as suggested before within (-0.1, 0.1) period, SV range is (35, 170) ml and TPR range is (0.015, 0.02) mmHg.min/ml [5];

3- Assign one swarm population for each parameter; coefficient (A), SV_0 and TPR. Also set the number of particles, which is known as Swarm population, within the recommended range (20 -50) particles [61, 62], 24 particles for each swarm are proposed for this method; n = 1 … 24;

4- Initialize random position and initialize random velocity for each particle as well as set constant value of V_{max} and X_{max} for each parameter;

   a- For each particle's position of coefficient (A) within range (-0.1, 0.1); where $X_{max}= \pm 0.1$and for each particle's velocity within fraction of particle's range (-0.0003, 0.0003); where $V_{max}= \pm 0.0003$.

   b- For each particle's position of SV_0 within range (35, 170) ml; where $X_{max}=35$ or $X_{max}=175$ and for each particle's velocity within fraction range of particle's range; (-3, 3) where $V_{max}= \pm 3$.

   c- For each particle's position of TPR within range (0.015, 0.02) mmHg.min/ml; where $X_{max}=0.015$ or $X_{max}=0.02$ and for each particle's velocity within fraction range of particle's range; (-0.00003, 0.00003); where $V_{max}= \pm 0.00003$.

5- Set constant values for: $\chi = 1$ and $\varphi_1 = \varphi_2 = 2$, to use them in equation (4-2) for each Swarm;

6- Utilize two particles' topologies gbest and pbest to achieve the optimal solutions for coefficient (A), SV_0 and TPR. Where the initial vectors for pbests are equal to the

combination of initial particles' random positions. Also generate initial values of gbest for each swarm to form initial vector of gbest based on equation (6-7) that is Estimated MAP (EMAP), where (A), SV_0 and TPR have 24 values stands on 24 particles initial random vectors, HR and MAP values equal the mean of real HR and Real MAP records for each case's of the ten cases' records.. The initial particle's vector, which achieves the smallest average of absolute differences between EMAP and Real MAP values for the ten cases' records is assigned as initial vector of gbest;

7- Start the searching part of MPSO; where the maximum iteration is 100;

8- Evaluate the initial vector of gbest by equation (6-7). If the average of absolute differences between EMAP and Real MAP values for the ten cases' records is zero, where real HR and Real MAP values equal the mean of each case's records for the ten cases' records. If this initial vector of gbest passes the evaluation check, then the optimal value is achieved so the algorithm processing is stopped or else the algorithm processing continues;

9- Update the particle's velocity for each swarm separately by following step 9 as mentioned in page 90;

10- Update the particle's position for each swarm separately by following step 10 as mentioned in page 90;

11- Update the particle $pbest_n$ vector; which will be used as the new $pbest_n$ vector in equation (4-2) in next iteration, based on substituting the combination of updated particles' values; which are achieved from step 11, instead of A, SV_0 and TPR in equation (6-7) that is estimated EMAP values; where real HR and real MAP equal the mean of real HR and Real MAP records for each case of the ten cases' records.. If the average of absolute differences between EMAP and Real MAP values is less than the average of absolute differences between EMAP and Real MAP values for

the ten cases records, where A, SV_0 and TPR values of the previous iteration; then new particles' positions are assigned as a new vector for $pbest_n$ or else there is no change for $pbest_n$ vector values.

12- Repeat steps 9, 10 and 11 with other particles to update the pbests' vectors for other 23 particles and assign the $pbest_n$ vector that achieves the smallest mean of absolute differences between EMAP and Real MAP values for ten cases, as vector of gbest which will be used as new gbest in equation (4-2) in the next iteration;

13- Repeat steps 8, 9, 10, 11 and 12 to update the values of $V_n(t+1)$, $X_n(t+1)$, and the vector of $pbest_n$ for each particle also update gbest for whole system in every iteration till it reaches a maximum iteration (t = 100) or passes the evaluation check in step 8;

14- Finally, assign final gbest vector values to corresponding values of coefficient (A), SV_0 and TPR, respectively. This method will henceforth be referred to as Meth4.

The achieved optimal values of A = -0.0048, SV_0 = 81.67 ml and TPR = 0.01844 mmHg.min/ml are substituted in equation (6-7) to estimate the MAP values for remaining ten cases' records.

The mean of real HR values and real MAP values, estimated MAP values by Meth4 for remaining ten cases' records and the absolute differences between real and estimated values of MAP for the Meth.4 are illustrated in table (6.4).

Table (6.4): mean of HR values, real MAP, estimated MAP by Meth4 and absolute differences between real and estimated MAP by Meth4

Case	HR	Real MAP (mmHg)	EMAP4 (mmHg)	|EMAP4- Real MAP| (mmHg)
11	93.88	74.21	78.04	3.83
12	84.50	76.80	75.94	0.86
13	97.55	81.20	78.51	2.69
14	89.87	75.32	77.30	1.98
15	72.49	71.25	71.40	0.15
16	80.57	71.58	74.68	3.10
17	95.11	69.75	78.31	8.56
18	100.57	69.46	78.77	9.31
19	88.51	84.54	76.99	7.55
20	90.80	72.54	77.49	4.95
Average	89.39	74.67	76.74	4.30

The accuracy of Meth4 is calculated based on equation (5-2) [73]:

$$\text{The Meth4 Accuracy} = 100\ \% \times \left(1 - \left(\frac{4.30}{74.67}\right)\right) = 94.24\ \%$$

The estimated MAP values of Meth4, Meth3, Meth2, Meth1 and real MAP values are illustrated graphically in figure 6.9:

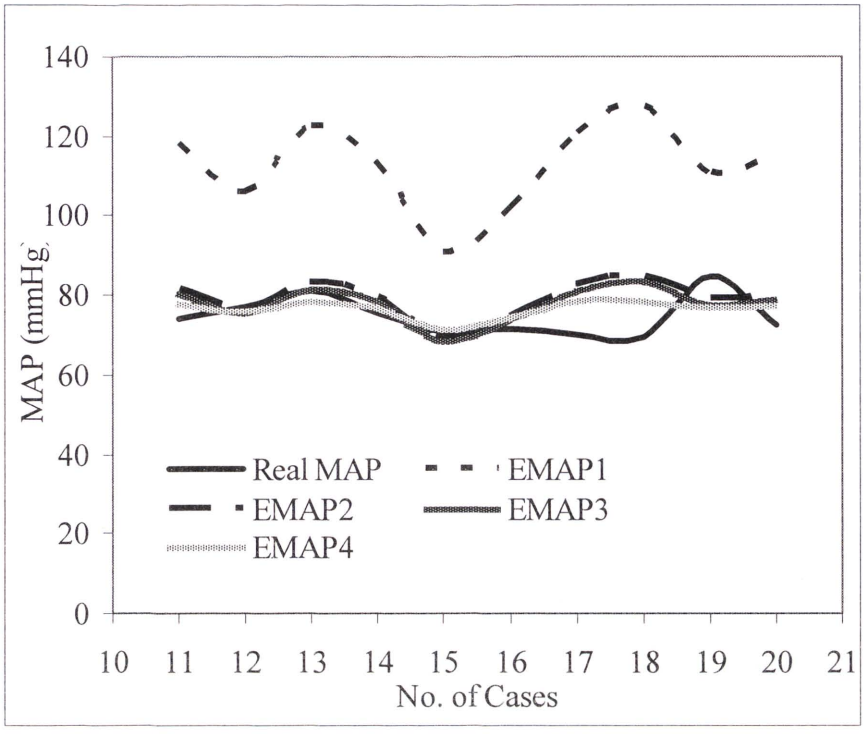

Figure 6.9: The estimated MAP of Meth4 Meth3, Meth2, Meth1 and real MAP values

As can be observed in figure 6.9, the estimated MAP values by Meth4 are the closest to real MAP values than estimated MAP values by Meth1, Meth2 and Meth3, also Meth4 accuracy equals 94.24% is higher than the accuracy of Meth3, Meth2 and Meth1; hence, Meth4 can be considered as practical method.

Likewise previous methods, the achievements of Meth4 for remaining ten cases' records are illustrated graphically by the B&A plot method [74]. The B&A plot is prepared by calculating the Mean and SD of (EMAP4 - Real MAP), of table (6.7). The Mean and SD values are 2.08 and 5.11 respectively, then the B&A plot for MAP Values for Meth4 is shown in figure 6.10.

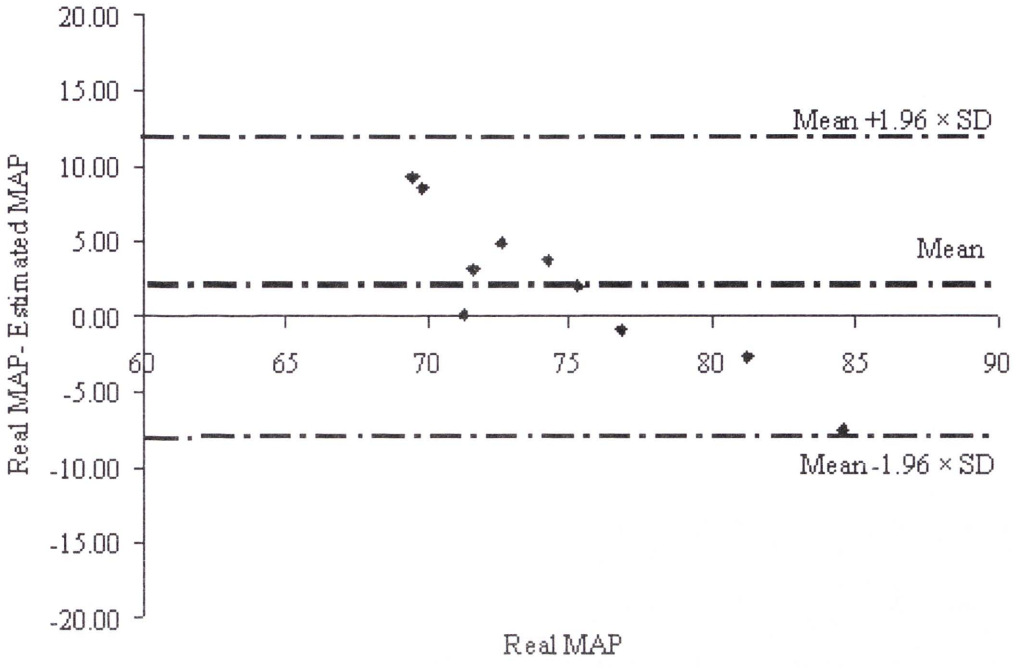

Figure 6.10: B&A plot for MAP Values for Meth4

Through the previous four methods the MAP values are estimated and the average of absolute differences between estimated MAP values and real MAP values for testing subjects is reduced form 37.979 mmHg to 4.30 mmHg that is mean the methods, that are developed and improved, increase the accuracy up to 94.24% and achieve near accurate estimated MAP.

These three proposed method are estimated MAP parameter of blood pressure parameters only. Therefore, to complete the design of Cardiovascular Parameters Long Term Monitoring System (CPLTMS) based on PPG signal; the researcher proposes a new model to predict the other blood pressure parameters: SBP and DBP, and these are clarified in the next section.

6.3. **Utilize type-2 Fuzzy for Blood pressure parameters estimation**

As mentioned before, blood pressure parameters, Systolic, Diastolic and Mean Blood Pressures, have a high correlation relationship with the heart rate (HR). This relationship is complex, nonlinear, multimode, and a multi-uncertainty relationship. In

reality, there is no direct forward mathematical expression to express the relationship between BPPs and Heart rate (HR). To handle this complex relationship a novel Interval Type-2 Fuzzy system (IT2FS) is designed to predict BPPs by processing the HR values.

Clinically, two different (IT2FSs) are designed to estimate Systolic Blood Pressure (SBP) and Diastolic Blood Pressure (DBP) based on HR values, the output for first IT2FS is SBP and the output for second IT2FS is DBP.

Both IT2FSs have the same structure and the same input but they have a different output, both systems are designed along the following steps:

1- The possible range of HR values, as input is fuzzified to five singletons Gaussian Interval Type-2 (Type-1) PMFs with the same standard deviation for all PMFs. PMFS take linguistic expressions; very Low, Low, Healthy, High and very High as shown in figure 6.11. The PMFs' of HR are initialized according to the American Health Association (AHA) standards [82].

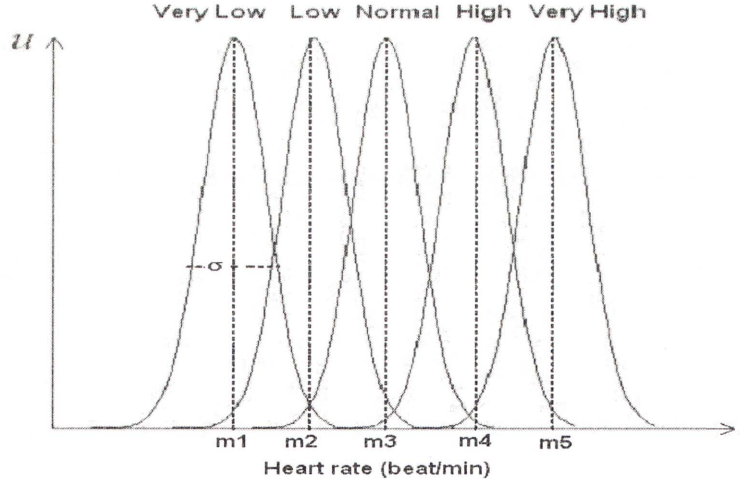

Figure 6.11: Fuzzification of Heart Rate to five singleton Interval Type-2 fuzzy sets

2- The possible range of SBP and DBP (BPP) values, as output, is represented by five Gaussian Interval type-2 PMFs, two means for each PMF and same standard deviation for all PMFs. These PMFs take the linguistic expressions:

very Low, Low, Healthy, High and very High as shown in figure 6.12. The PMFs' parameters for SBP and DBP are initialized according to AHA standards.

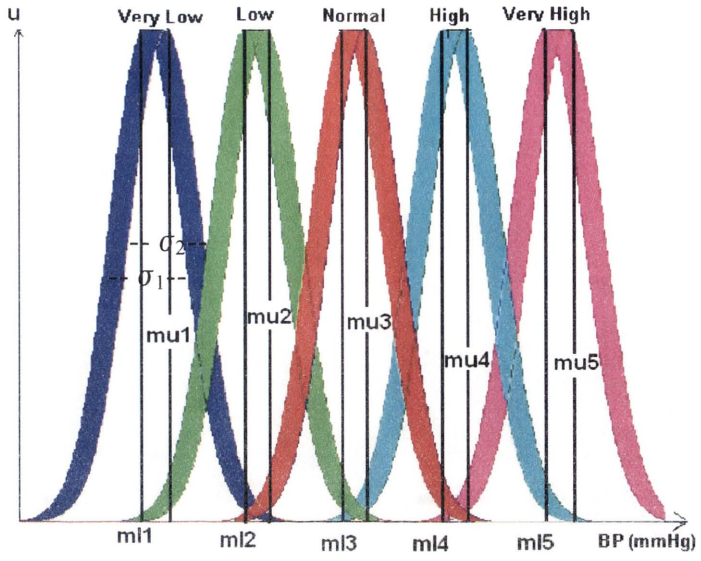

Figure 6.12: Fuzzification of SBP or DBP to five Interval Type-2 fuzzy sets

3- Fuzzy rules are located as one rule for each input fuzzy set, where each rule has the expression: "IF HR is Ã, THEN BPP is G̃".

4- The Inference engine combines the rules and forms a mapping between HR fuzzy sets and BPPs' fuzzy sets, finds non-zero membership function values of HR, and generates the T2 fuzzy set of BPP depends on non-zero membership function values of HR and specified inference method which is the product sum inference method in this design;

5- The Defuzzification process is implemented by following two steps [49];

a- Descend the T2 fuzzy set of BPP by computing upper MF (y_r) by using the equation:

$$y_r = \frac{\sum_{i=1}^{M} f^i y_r^i}{\sum_{i=1}^{M} f^i} \quad \text{..... (6-8)}$$

Where y_r upper MF of output

i is variable value changed from 1 to N

N is number of non-zero membership function values for input value created by firing the fuzzy rules

f^i is fuzzy membership value(s) of input value

y^i_r is mean value of matching output upper MF based on fuzzy rules

and lower MF y_l by next equation:

$$y_l = \frac{\sum_{i=1}^{N} f^i y^i_l}{\sum_{i=1}^{N} f^i} \quad \text{..... (6-9)}$$

y_l is lower MF of output

y^i_l is mean value of matching output lower MF based on fuzzy rules

b- compute the output of IT2FS by using Centre of Sums as defuzzifiction method as expressed in next equation:

$$y = \frac{y_l + y_r}{2} \quad \text{..... (6-10)}$$

y is output of Fuzzy system

Then the out put of IT2FS is y = SBP or DBP.

Subsequently, the MAP parameter is computed based on equation (2-1) [5]:

$$\text{MAP} = \text{DBP} + \frac{1}{3} \times (\text{SBP} - \text{DBP}) \quad \text{..... (2-1)}$$

6.3.1. Estimating BPPs for Unhealthy subjects

The designed IT2FS are implemented on database of twenty unhealthy subjects; which were randomly chosen from MIMIC database [80]. MIMIC database is available in Physio-bank web site, and it includes continuous records of cardiovascular signals and interrupted measurements; such as HR and MAP values, of subjects at intensive care unit (ICU), for every second through more than 10 hours; that means 36000 records for each case, at least. These records are extracted from bedside monitors that were attached to subjects and from subjects' medical records.

The mean of HR, SBP and DBP values of each subject are given in table (6.5):

Table (6.5): Mean of HR and BPPs values of unhealthy subjects

No. of Cases	HR b/m	SBP mmHg	DBP mmHg	No. of Cases	HR b/m	SBP mmHg	DBP mmHg
1	132	161	91	11	82	114	53
2	78	129	76	12	72	112	54
3	60	122	64	13	81	106	58
4	68	129	68	14	71	113	50
5	98	142	55	15	74	123	61
6	137	166	96	16	93	103	76
7	72	129	53	17	103	107	64
8	95	90	71	18	59	98	55
9	108	152	65	19	90	110	61
10	80	92	56	20	65	104	61

6.3.1.1 Estimating SBP for Unhealthy subjects

SBP values are estimated by utilizing IT2FS and twenty unhealthy subjects' readings which are divided into two groups: ten subjects' readings of HR and SBP are used for training the designed IT2FS by using MPSO algorithm while the remaining ten subjects' readings are used for testing the trained IT2FS.

The PMF parameters' values of IT2FS; m1, m2, m3, m4, m5, ml1, ml2, ml3, ml4, ml5, mu1, mu2, mu3, mu4, mu5, σ, σ_1 and σ_2, as shown in figures 6.11 and 6.12, are assumed as the means of AHA parameters' ranges for each parameter for SBP. MPSO is utilized to find the optimum parameters' values within the AHA parameters' ranges [82] by adjusting parameters' values within the parameters' ranges to achieve the smallest average of absolute differences between real and estimated values of SBP. The following steps explain how the MPSO algorithm was utilized to optimize PMF parameters' values of IT2FS:

1- Set the problem domain for the MPSO as the database of ten cases and boundaries of each range for each parameter; which were set by AHA [82];

2- Assign different swarm population for each PMF parameter of input; m1, m2, m3, m4, m5 and σ;

3- Assign different swarm population for each PMF parameter of output; ml1, ml2, ml3, ml4, ml5, mu1, mu2, mu3, mu4, mu5, σ_1 and σ_2;

4- Set the population for each swarm of steps 2 and 3 within the recommended range [61, 62]; In this system, fifty particles are proposed to consider whole problem domain; n = 1 ... 50;

5- Initialize fifty random values for each parameter within the boundaries of each range; for example **m4** initial fifty random values are located within the boundaries of **High** range, and the same for all other parameters;

6- Initialize same fifty random velocities for all parameters within range of [0, 1] with 0.02 step change and set constant value for V_{max} = 0 or 1;

7- Set constant values for parameters; χ = 1 and $\varphi_1 = \varphi_2 = 2$, to use them in equation (4-2) for each Swarm;

8- Utilize two particles' topologies gbest and pbest to achieve the optimal solution or near optimal solution for all parameters, where the initial pbest vectors are equal to the combination of initial fifty particles' random values. While the initial gbest vector is equal to the initial pbest vector, that achieves the smallest mean of absolute differences between estimated SBP (ESBP) values by designed IT2FS and Real SBP values for ten cases' readings;

9- Start the searching part of MPSO; where number of iterations is 100; t = 1 … 100;

10- Evaluate the vector of gbest by designed IT2FS. If the mean of absolute differences between ESBP and Real SBP values for training ten cases' records is zero, where real HR and Real SBP values equal the mean of real HR and Real SBP records for each case's of the ten cases' records and if the initial gbest vector passes the evaluation check, then the optimal value is achieved so the algorithm processing is stopped or else the algorithm processing continues;

11- Update the particle's velocity for each swarm separately by following step 9 as explained in page 90;

12- Update the particle's position for each swarm separately by following step 10 as explained in page 90;

13- Repeat steps 11 and 12 with other particles to update the $V_n(t+1)$, $X_n(t+1)$ values for other 49 particles to use them as the new values for $V_n(t)$, $X_n(t)$ in equations (4-2) and (4-3) during next iteration;

14- Update the $pbest_n$ vector; which will be used as the new $pbest_n$ vector in equation (4-2) during next iteration, based on using the updated particles' values for each parameter; which are achieved from equation (4-3), to estimate SBP values by designed IT2FS for ten cases' records. If the average of absolute differences between ESBP and Real SBP values for ten cases with the combination of new

particles' positions is less than the average of absolute differences between ESBP and Real SBP values for ten cases with the combination of previous particles' positions, then the combination of new particles' positions is assigned as new value for $pbest_n$ vector. Otherwise new $pbest_n$ vector equals the previous $pbest_n$ vector;

15- Update the gbest vector which equals the $pbest_n$ vector that achieves the smallest mean of absolute differences between ESBP by IT2FS and Real SBP values; where each value of that vector will be used as a new gbest value for corresponding swarm respectively in equation (4-2) during next iteration;

16- Test the new gbest vector by the evaluation check as in step 10;

17- Repeat steps 10, 11, 12, 13, 14 and 15 to update the $V_n(t+1)$, $X_n(t+1)$ for each particle and for all swarms also to update the $pbest_n$ vectors and the gbest vector for whole system during every iteration till pass the evaluation check and the achieved optimal values or reach the maximum iteration ($t = 100$);

18- Finally assigns each value of gbest vector to corresponding PMF parameter, respectively. These values of PMF parameters form the trained IT2FS.

Later, the trained IT2FS that is generated by the Multi-PSO algorithm is used to estimate SBP (ESBP) values for testing the remaining ten subjects' records. These ESBP values, HR values, Real SBP values and the absolute differences between ESBP and Real SBP for test group are shown in table (6.6).

Table (6.6): ESBP values, HR values, Real SBP values for remaining ten subjects and the absolute differences between ESBP and Real SBP

No. of Cases	HR (b/m)	Real SBP (mmHg)	ESBP (mmHg)	|ESBP - Real SBP| (mmHg)
11	82.00	114.00	113.75	0.25
12	72.00	112.00	110.50	1.50
13	81.00	106.00	113.61	7.61
14	71.00	113.00	110.50	2.50
15	74.00	123.00	110.50	12.50
16	93.00	103.00	115.50	12.50
17	103.00	107.00	119.11	12.11
18	59.00	98.00	95.32	2.68
19	90.00	110.00	115.50	5.50
20	65.00	104.00	101.32	2.68
Average	79.00	109.00	110.56	5.98

The accuracy of trained IT2FS is calculated by equation (5-2) [73]:

$$\text{The trained IT2FS accuracy} = 100\ \% \times \left(1 - \left(\frac{5.98}{109}\right)\right) = 94.51\%$$

The estimated SBP values of trained IT2FS and real SBP values are illustrated graphically in figure 6.13:

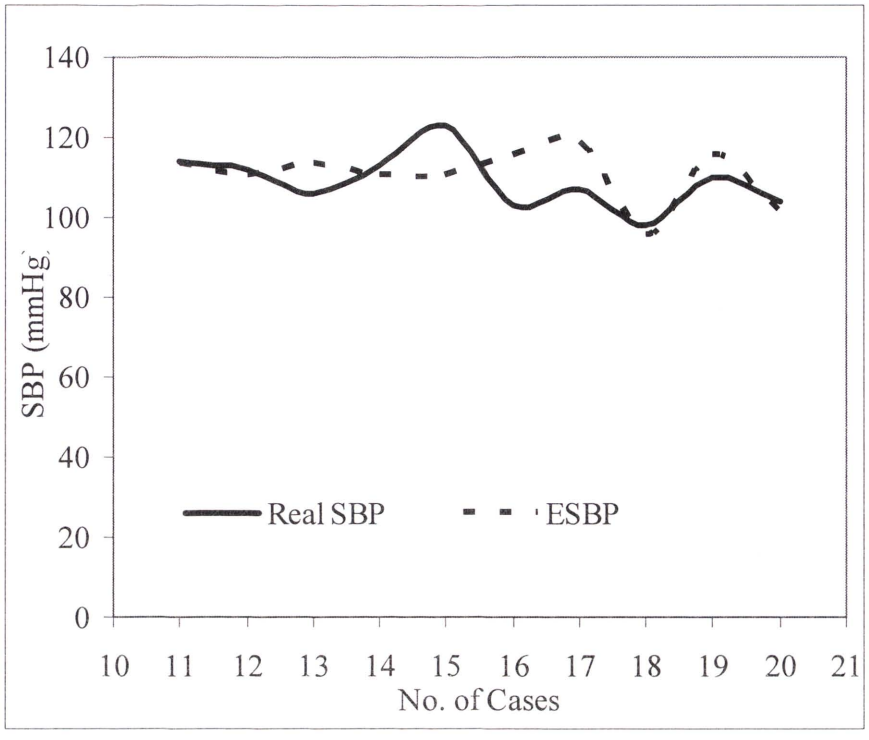

Figure 6.13: The estimated SBP values of trained IT2FS and real SBP values

As can be observed from figure 6.13, the estimated SBP values by trained IT2FS are very close to real SBP values; also the trained IT2FS accuracy equals 94.51 %; hence, trained IT2FS can be considered as a reliable and practical method.

Similarly, the achievements of trained IT2FS are illustrated graphically by the B&A plot method [74] to check if trained IT2FS can be used as an alternative method instead of benchmark methods that are already used to measure SBP in ICU. The B&A plot is prepared by calculating the Mean and SD of (ESBP - Real SBP) from table (6.6). The Mean and SD values are 1.56 and 7.79 respectively. The B&A plot of ESBP Values for trained IT2FS is shown in figure 6.14.

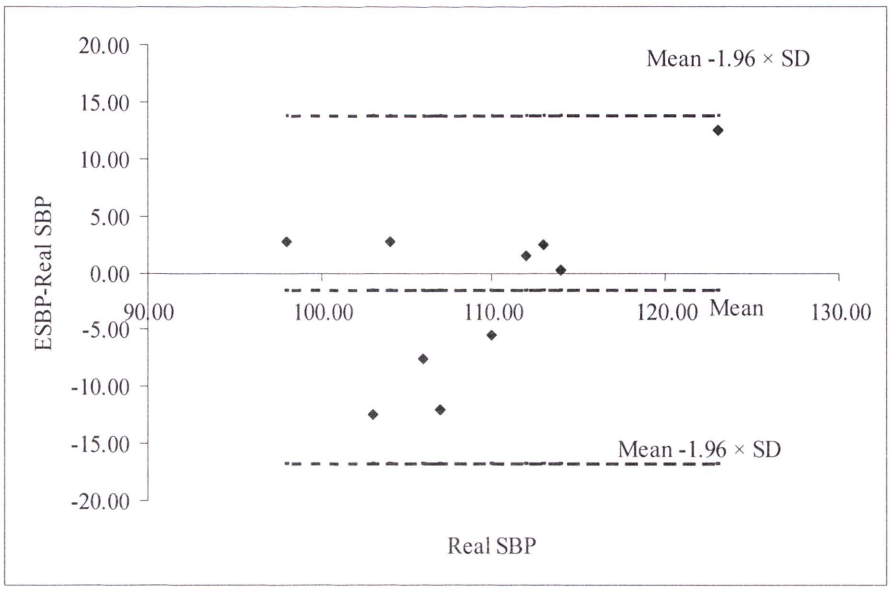

Figure 6.14: B&A plot of ESBP Values

In the B&A plot of SBP that are shown in figure 6.14, all estimated values are located close to mean of difference and within the border of (mean ± 1.96 SD) and all of these differences are within 95% of Gaussian distribution limit. According to these results, the IT2FSs achieve 94.51% accuracy for estimating SBP so IT2FSs can be used as alternative method to measure the SBP values instead of benchmark methods that are already used to measure SBP in ICU.

6.3.1.2 Estimating DBP for unhealthy subjects

The DBP values are estimated by new IT2FS by using same twenty unhealthy subjects' readings [80] which are divided to two groups: ten subjects' readings of HR and DBP are used for training the IT2FS by using multi-PSO algorithm whilst the remaining ten subjects' readings are used for testing the trained IT2FS.

The PMF parameters' values of IT2FS are assumed as the means of AHA parameters' ranges for each parameter for DBP. Multi-PSO is utilized to find the optimum parameters' values within the AHA parameters' ranges [82].

The PMF parameters of IT2FS were adjusted within AHA ranges of DBP by using same multi-PSO algorithm as detailed in section 6.3.1.1 to achieve the smallest average of absolute differences between real and estimated values of DBP.

Likewise, the new IT2FS, which is trained by multi-PSO, is used to estimate DBP (EDBP) values for the test group. These EDBP values, HR values, Real DBP values and the absolute differences between EDBP and Real DBP are shown in table (6.7).

Table (6.7): EDBP values, HR values, Real DBP values for remaining ten subjects and the absolute differences between EDBP and Real DBP

No. of Cases	HR b/m	Real DBP mmHg	EDBP mmHg	|EDBP - Real DBP| mmHg
11	82.00	53.00	60.82	7.82
12	72.00	54.00	52.75	1.25
13	81.00	58.00	60.76	2.76
14	71.00	50.00	52.75	2.75
15	74.00	61.00	61.31	0.31
16	93.00	76.00	68.84	7.16
17	103.00	64.00	74.15	10.15
18	59.00	55.00	60.34	5.34
19	90.00	61.00	68.66	7.66
20	65.00	61.00	66.34	5.34
Average	79.00	59.3	62.67	5.05

The accuracy of trained IT2FS for DBP is calculated by equation (5-2) [73]:

$$\text{The trained IT2FS for DBP accuracy} = 100\ \% \times \left(1 - \left(\frac{5.05}{59.3}\right)\right) = 91.48\ \%$$

The estimated DBP values of trained IT2FS and real DBP values are illustrated graphically in figure 6.15:

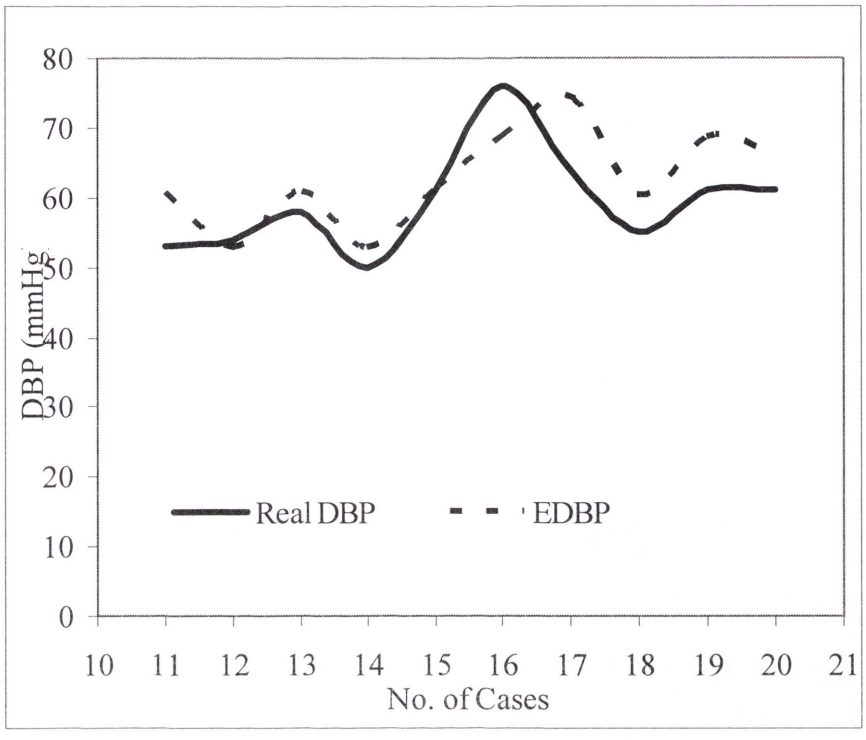

Figure 6.15: The estimated DBP values of trained IT2FS and real DBP values

As can be observed from figure 6.15, the estimated DBP values by trained IT2FS are very close to real DBP values also trained IT2FS accuracy equals 91.48 %; hence, trained IT2FS can be considered as a practical method.

The successes of trained IT2FS for DBP are illustrated graphically by the B&A plot method [74]. The B&A plot is prepared by calculating the Mean and SD of (EDBP - Real DBP), of table (6.7), are 3.37 and 5.1 respectively; afterwards the B&A plot of EDBP values for trained IT2FS is shown in figure 6.16.

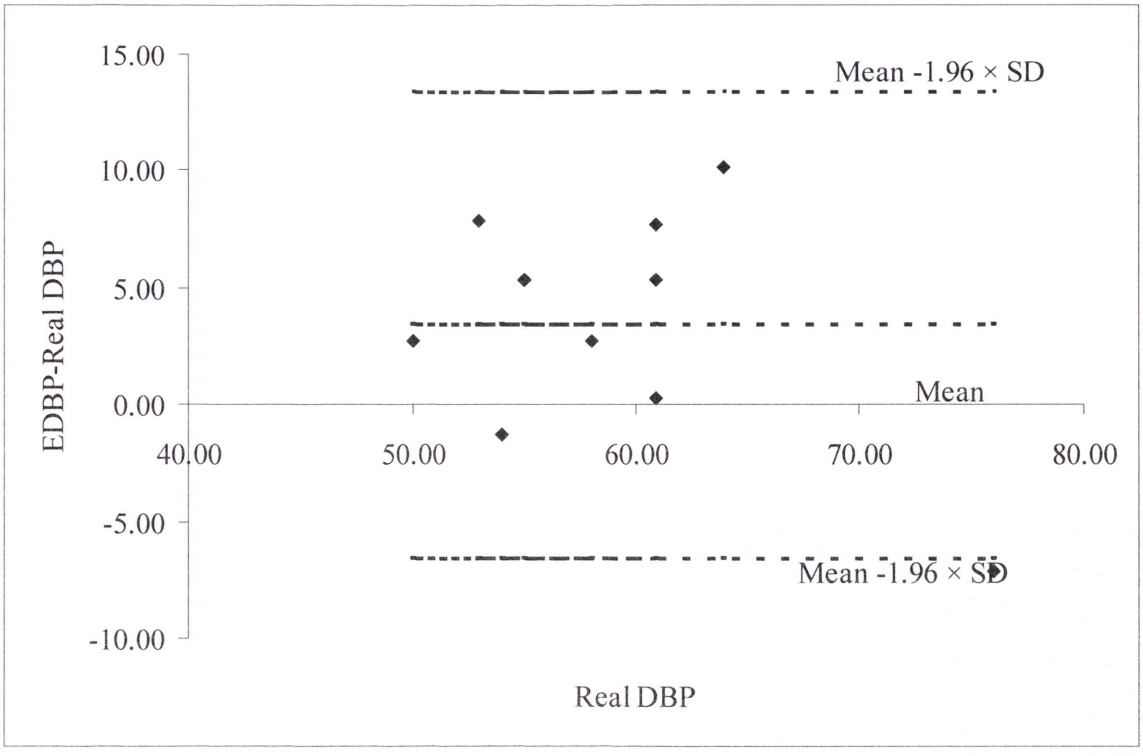

Figure 6.16: B&A plot of EDBP Values

In the B&A plot of DBP that are shown in figure 6.16; all estimated values are located close to mean of difference and within the border of (mean ± 1.96 SD) and all of these differences are within 95% of Gaussian distribution limit. Also, IT2FSs achieve 91.48% accuracy for estimating DBP. Hence, the trained IT2FS for DBP can be used as an alternative method to measure the DBP values instead of benchmark methods that are already used to measure DBP in ICU.

6.3.1.3 Estimating MAP for unhealthy subjects

After estimating SBP and DBP values, the MAP values can be computed based on ESBP, EDBP and equation (2-1): $MAP = DBP + \frac{1}{3} \times (SBP - DBP)$ --- ------- (2-1)

The estimated MAP (EMAP) values, HR values, Real MAP [80] values and the absolute differences between EMAP and Real MAP for test group are shown in table (6.8).

Table (6.8): EMAP values, HR values, Real MAP values for remaining ten subjects and the absolute differences between EMAP and Real MAP

No. of Cases	HR b/m	Real MAP mmHg	EMAP mmHg	|EMAP - Real MAP| mmHg
11	82.00	73.33	78.46	5.13
12	72.00	73.33	72.00	1.33
13	81.00	74.00	78.38	4.38
14	71.00	71.00	72.00	1
15	74.00	81.67	77.71	3.96
16	93.00	85.00	84.39	0.61
17	103.00	78.33	89.14	10.81
18	59.00	69.33	72.00	2.67
19	90.00	77.33	84.27	6.94
20	65.00	75.33	78.00	2.67
Average	79	75.87	78.64	3.95

The accuracy of estimated MAP values is calculated by equation (5-2) [73]:

Hence, Accuracy of estimated MAP values = $100\ \% \times \left(1 - \left(\frac{3.95}{75.87}\right)\right) = 94.79\ \%$

The estimated MAP values and real MAP values are illustrated in figure 6.17:

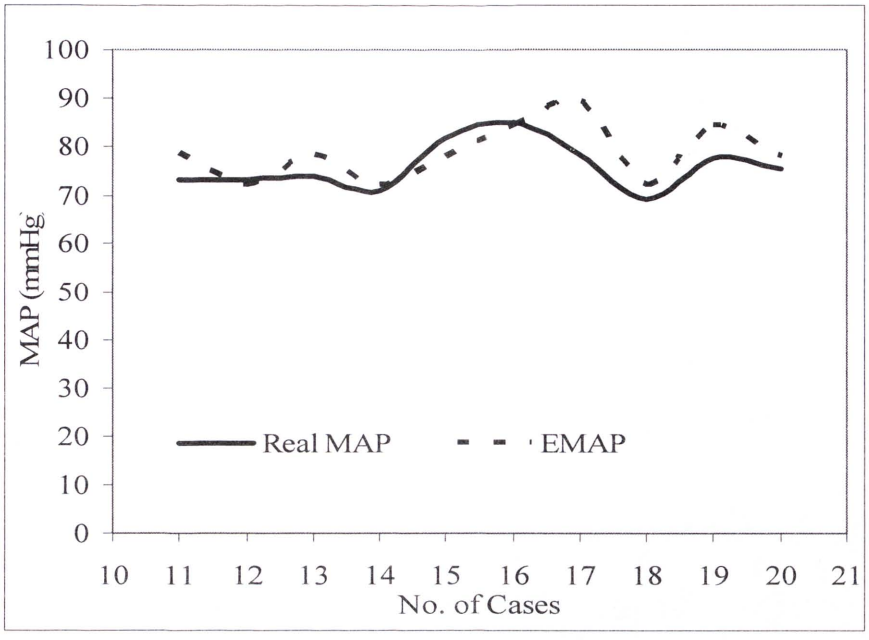

Figure 6.17: The estimated MAP values and real MAP values

As can be observed in figure 6.17; the estimated MAP values are very close to real MAP values also the accuracy equals 94.79%; hence, trained IT2FS can be considered as a practical method.

The achieved EMAP values are illustrated graphically by the B&A plot method [74]. The B&A plot is prepared by calculating the Mean and SD of (EMAP - Real MAP), of table (6.8). The Mean and SD of (EMAP - Real MAP) are 2.77 and 4.31. The B&A plot of EMAP Values for trained IT2FS is shown in figure 6.18.

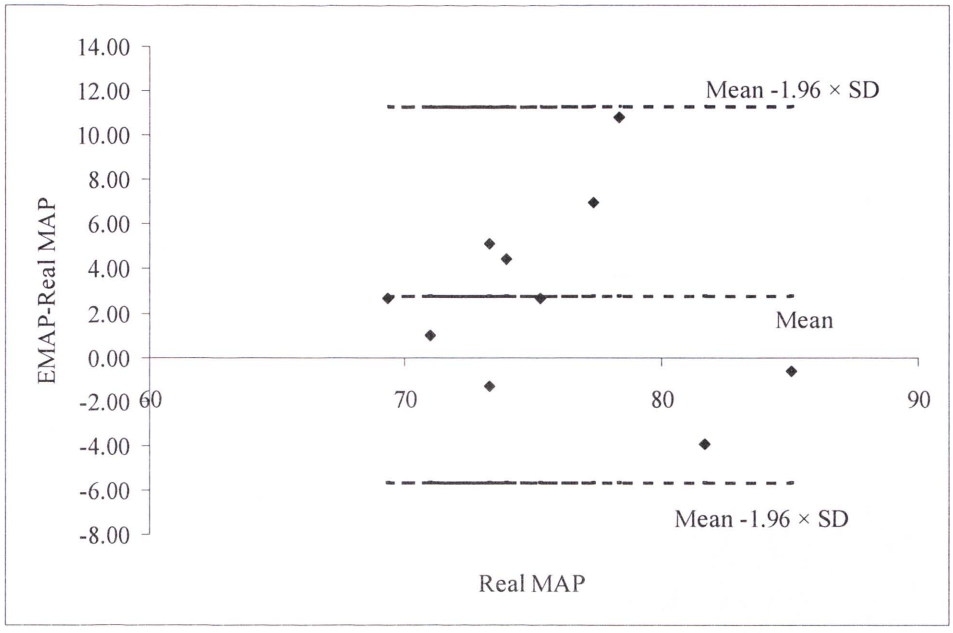

Figure 6.18: B&A plot of EMAP Values

In the B&A plot of MAP that are shown in figure 6.18, all estimated values are located close to mean of difference and within the border of (mean ± 1.96 SD) and all of these differences are within 95% of Gaussian distribution limit. Hence, IT2FSs achieve 94.79% accuracy for estimating MAP so IT2FSs can be used as an alternative method to measure the MAP values instead of benchmark methods that are already used to measure MAP in ICU.

6.3.1.4 Estimating MAP for unhealthy subjects by Meth4

On other hand, the MAP values for this data set of unhealthy subjects, that data set is different from the data set was used in section 6.3.1, are computed by using Meth4 that is explained in section 6.1.3 based on equation (6-7):

$$MAP = SV_0 \times TPR \times HR \times (A \times HR+1)$$

Where A = -0.0048, SV_0 = 81.67 ml and TPR = 0.01844 mmHg.min/ml, these values are achieved by Multi-PSO algorithm.

The mean of estimated MAP values by using Meth4 (EMAP4), HR values, Real MAP values, and the absolute differences between EMAP and Real MAP for test group are shown in table (6.9).

Table (6.9): Mean of EMAP4 values, HR values, Real MAP values for remaining ten subjects and the absolute differences between EMAP and Real MAP

No. of Cases	HR b/m	Real MAP mmHg	EMAP mmHg	EMAP4 mmHg	|EMAP4 - Real MAP| mmHg
11	82.00	73.33	78.46	74.89	1.56
12	72.00	73.33	72.00	70.96	2.37
13	81.00	74.00	78.38	74.56	0.56
14	71.00	71.00	72.00	70.49	0.51
15	74.00	81.67	77.71	71.86	9.81
16	93.00	85.00	84.39	77.54	7.46
17	103.00	78.33	89.14	78.43	0.10
18	59.00	69.33	72.00	63.69	5.64
19	90.00	77.33	84.27	76.99	0.34
20	65.00	75.33	78.00	67.35	7.98
Average	79	75.87	78.64	72.67	3.63

Mean of estimated MAP values by IT2FS, EMAP4 and real MAP values are illustrated in figure 6.19:

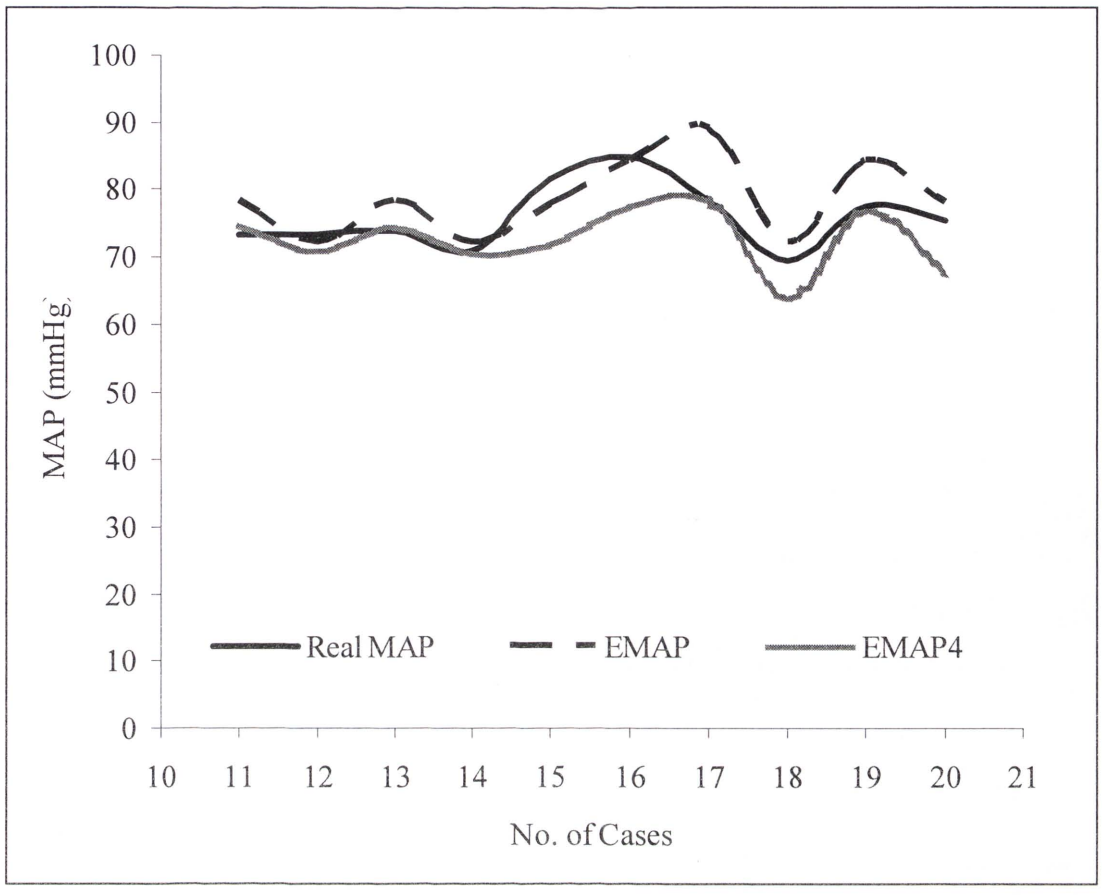

Figure 6.19: Mean of estimated MAP values by IT2FS, EMAP4 and real MAP values

The accuracy of estimated MAP4 values is calculated by equation (5-2) [73]:

$$\text{Hence, Accuracy of estimated MAP values} = 100\ \% \times \left(1 - \left(\frac{3.63}{75.87}\right)\right) = 95.21\ \%$$

As observed in figure 6.19, EMAP4 are closer to real MAP values than the estimated MAP values by IT2FSs; also the accuracy of EMAP4 is 95.21 % and it is better than the accuracy that is achieved by IT2FSs which equals 94.79%. Hence, Meth4 is better than the IT2FS. However, Meth4 is only utilized to estimate MAP while IT2FS is utilized to estimate SBP, DBP and MAP. In conclusion, IT2FS can be considered as more practical than Meth4 because it can be used to estimate SBP, DBP and MAP.

6.3.2. Estimating BBP for Healthy subjects

After continuing the design of CPLTMS, by designing and trained IT2FS through utilizing available database for unhealthy subjects, the researcher attends to utilizing the novel CPLTMS on collecting a new database for healthy subjects. This database is acquired from 30 healthy Adult subjects who are picked randomly from local volunteer people with an unknown medical history record.

The new database has been acquired by Othman and I based on our PPG sensor and following the ethical approval that attached in appendix 1. This new database consists of three readings of heart rate with simultaneous three readings of all blood pressure parameters of thirty Adult healthy subjects of six males and twenty-four females aged between 17-68 years old and weighted between 45-92 Kg.

The three readings of heart rate are prepared based on PPG signal frequency and equation (5-1); where the PPG signal is acquired by attaching a PPG sensor on subject finger as shown in figure 5.3.

While the three readings of blood pressure parameters are acquired by digital automatic blood pressure instrument, "OMRON IAIB Model HEM-7000-C1L" is made by OMRON Healthcare Japan [16].

The three readings of blood pressure parameters and PPG signal are taken, simultaneously, from each subject in a sitting posture with 20 minutes between each reading. The average of systolic and diastolic blood pressures and also heart rate readings of each subject are given in table (6.10).

The new database for Twenty subjects are used to train two IT2FSs through adjusting the PMFs' parameters by using multi-PSO within AHA standards to achieve smallest errors between real and estimated SBP and DBP as explained in subsection 6.3.1.1.

Both the trained IT2FSs are used to estimate SBP and DBP for the remaining ten healthy subjects, which used as test data, and are computed by equation (2-1).

Table (6.10): Average of HR and BP readings of Healthy subjects

No. of Cases	HR b/m	SBP mmHg	DBP mmHg	No. Of Cases	HR b/m	SBP mmHg	DBP mmHg
1	79.33	96.33	63.00	16	77.33	122.67	85.67
2	87.67	100.67	58.67	17	88.67	122.67	92.00
3	76.00	112.67	75.33	18	70.33	110.00	82.00
4	71.00	110.00	78.67	19	88.00	120.33	78.67
5	83.67	107.33	78.00	20	85.67	99.33	60.67
6	100.3	104.00	76.67	21	76.00	121.33	84.67
7	88.67	144.00	83.33	22	70.67	125.33	80.33
8	72.00	105.00	72.33	23	86.00	79.33	50.00
9	67.00	118.67	70.33	24	84.00	122.67	74.00
10	79.00	129.00	85.00	25	90.67	105.33	73.67
11	63.33	112.00	72.00	26	68.67	97.33	64.33
12	88.00	156.33	89.33	27	74.33	110.00	68.67
13	74.00	141.67	77.33	28	82.33	119.67	77.33
14	86.00	114.00	71.33	29	79.67	125.67	78.33
15	83.67	124.00	85.67	30	66.33	108.00	71.33

The estimated values of SBP by trained IT2FSs are shown in table (6.11):

Table (6.11): Estimated SBP for remaining ten healthy subjects

No	HR	ESBP (mmHg)	Real SBP (mmHg)	|ESBP- Real SBP| (mmHg)
21	72.00	110.50	105.00	5.50
22	86.00	115.50	114.00	1.50
23	63.33	110.50	112.00	1.50
24	74.33	111.50	110.00	1.50
25	82.33	113.80	119.70	5.90
26	71.00	110.80	110.00	0.80
27	76.00	112.10	112.70	0.60
28	66.33	110.50	108.00	2.50
29	88.00	115.50	120.30	4.80
30	70.33	110.50	110.00	0.50
Average	74.97	112.12	112.17	2.51

The accuracy of estimated SBP values is calculated by equation (5-2) [73]:

Hence, accuracy of estimated SBP values = $100\ \% \times (1-(\frac{2.51}{112.17}))$ = 97.76 %

The estimated SBP values and real SBP values, which are shown in table (6.11), are illustrated in figure 6.20:

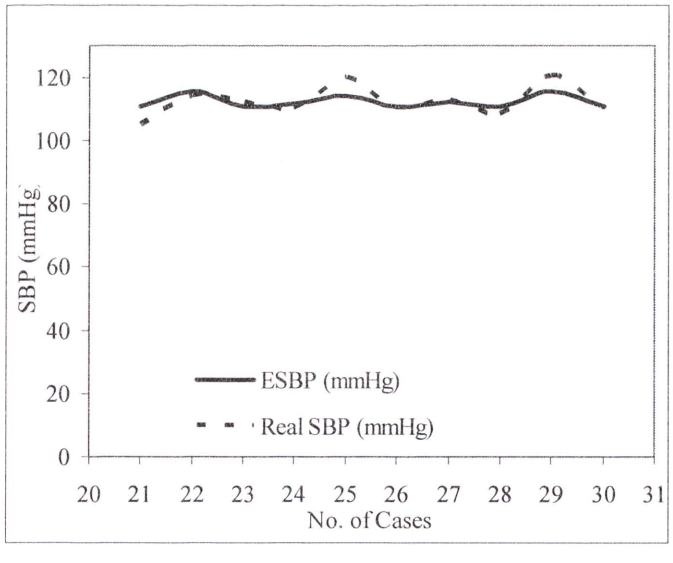

Figure 6.20: The estimated SBP values real SBP values for Healthy Subjects

As can be noticed from figure 6.20, the estimated SBP values are very close to real SBP values also the accuracy equals 97.76 %; hence, trained IT2FS can be consider as a practical method.

The achieved ESBP values are illustrated graphically by the B&A plot method [74]. The B&A plot is prepared by calculating the Mean and SD of (ESBP - Real SBP), that is shown in table (6.11), the Mean and SD values of (ESBP - Real SBP) are -0.05 and 3.37, respectively; then B&A plot of ESBP Values is shown in figure 6.21.

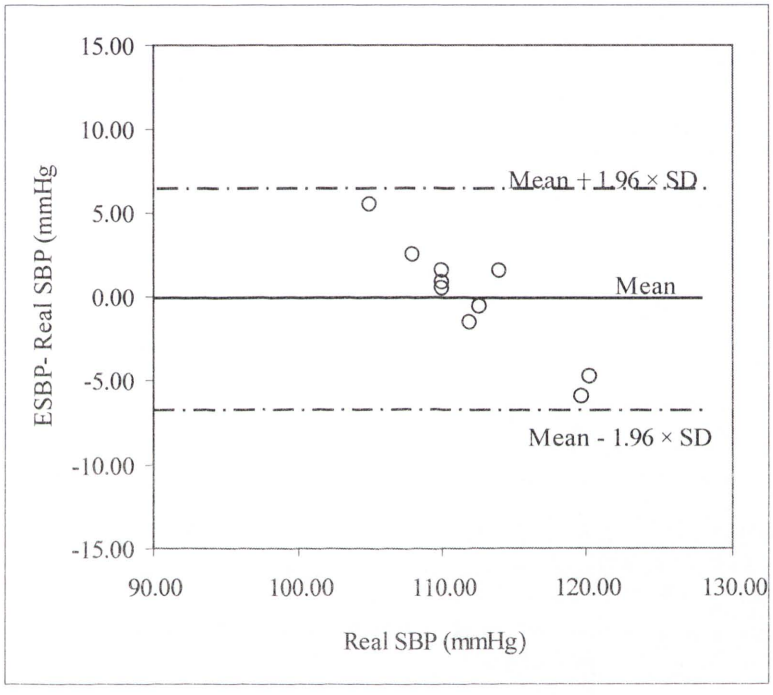

Figure 6.21: B&A plot of SBP for Healthy Subjects

In the B&A plot of SBP that are shown in figure 6.21, all estimated values are located close to the mean of difference and within the boundaries of (mean ± 1.96 SD) and all of these differences are within 95% of Gaussian distribution limit. Moreover, IT2FSs achieve 97.76% accuracy for estimating SBP. Hence, IT2FSs can be used as an alternative method to calculate the SBP values instead of benchmark methods that are already used to measure SBP in ICU.

Furthermore, the estimated values of DBP for healthy subjects by trained IT2FSs are shown in table (6.12):

Table (6.12): Estimated DBP for remaining ten healthy subjects

No	HR	EDBP (mmHg)	Real DBP (mmHg)	|EDBP- Real DBP| (mmHg)
21	72.00	76.6	72.3	4.3
22	86.00	81.4	71.3	10.1
23	63.33	73.7	72	1.7
24	74.33	79.3	68.7	10.6
25	82.33	84.4	77.3	7.1
26	71.00	76.6	78.7	2.1
27	76.00	81.8	75.3	6.5
28	66.33	76.6	71.3	5.3
29	88.00	86.9	78.7	8.2
30	70.33	76.7	82	5.3
Average	74.97	79.4	74.76	6.12

The accuracy of estimated DBP values is calculated by equation (5-2) [73]:

Hence, Accuracy of estimated DBP values = $100\ \% \times (1-(\frac{6.12}{112.17}))$ = 91.81 %

The estimated DBP values and real DBP values, which are shown in table (6.12), are illustrated in figure 6.22.

As can be noticed from figure 6.22, the estimated DBP values are very close to real DBP values also the accuracy equals 91.81 %; hence, trained IT2FS can be considered as a practical method.

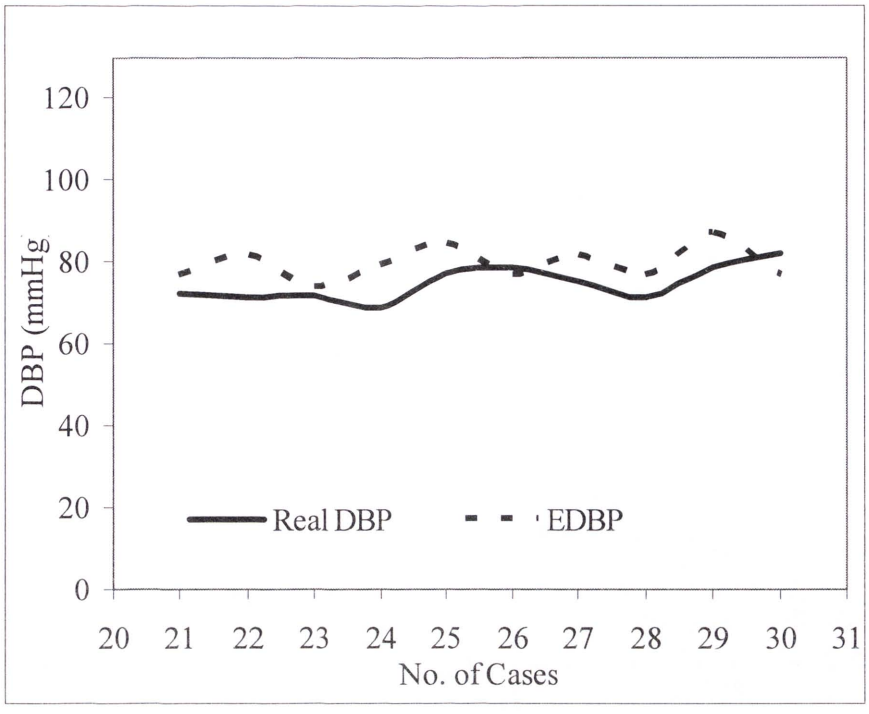

Figure 6.22: The estimated DBP values real DBP values for Healthy Subjects

The achieved EDBP values are illustrated graphically by the B&A plot method [74]. The B&A plot is prepared by calculating the Mean and SD of (EDBP - Real DBP), that shown in table (6.12), the Mean and SD values of (EDBP - Real DBP) are 4.64 and 5.17 respectively; then B&A plot of EDBP Values for trained IT2FS is shown in figure 6.23.

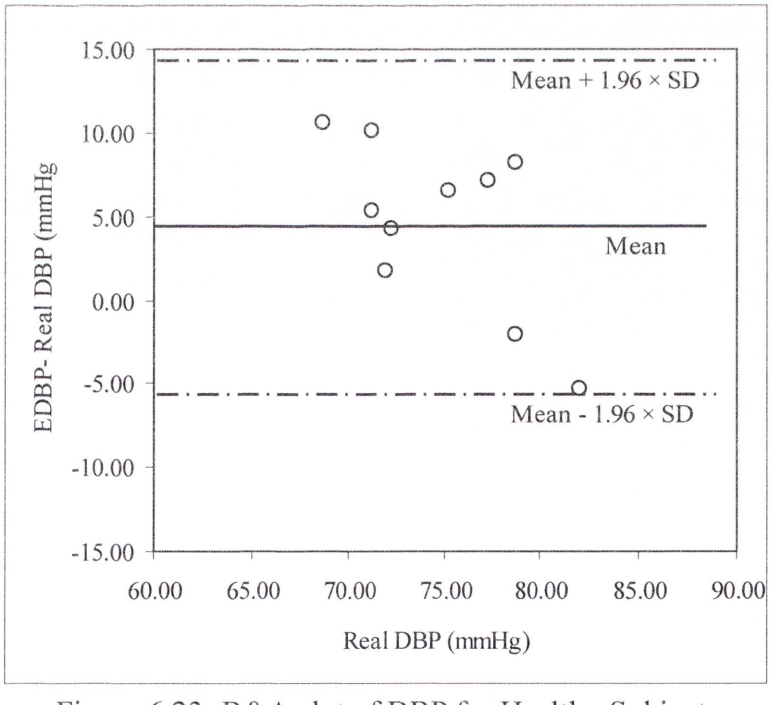

Figure 6.23: B&A plot of DBP for Healthy Subjects

In B&A plot of DBP that are shown in figure 6.22, all estimated values are located close to the mean of difference and within the boundaries of (mean ± 1.96 SD) and all of these differences are within 95% of Gaussian distribution limit also IT2FSs achieve 91.81% accuracy for estimating DBP. Hence, IT2FSs can be used as alternative method to calculate the DBP values instead of benchmark methods that are already used to measure DBP for healthy subjects.

At last, the estimated values of MAP for healthy subjects by trained IT2FSs are shown in table (6.13):

Table (6.13): Estimated MAP for remaining ten healthy subjects

No	HR	EMAP (mmHg)	Real MAP (mmHg)	|EMAP- Real MAP| (mmHg)
21	72.00	87.9	88.7	0.8
22	86.00	92.8	92.7	0.1
23	63.33	86	92	6
24	74.33	90	89.3	0.7
25	82.33	94.2	98.5	4.3
26	71.00	87.9	94.3	6.4
27	76.00	91.9	94	2.1
28	66.33	87.9	89.7	1.8
29	88.00	96.4	99.5	3.1
30	70.33	87.9	96	8.1
Average	74.97	90.29	93.47	3.34

The accuracy of estimated MAP values is calculated by equation (5-2) [73]:

$$\text{The accuracy of estimated MAP values} = 100\ \% \times \left(1-\left(\frac{3.34}{93.47}\right)\right) = 96.43\ \%$$

The estimated MAP values and real MAP values, which are shown in table (6.13), are illustrated in figure 6.24:

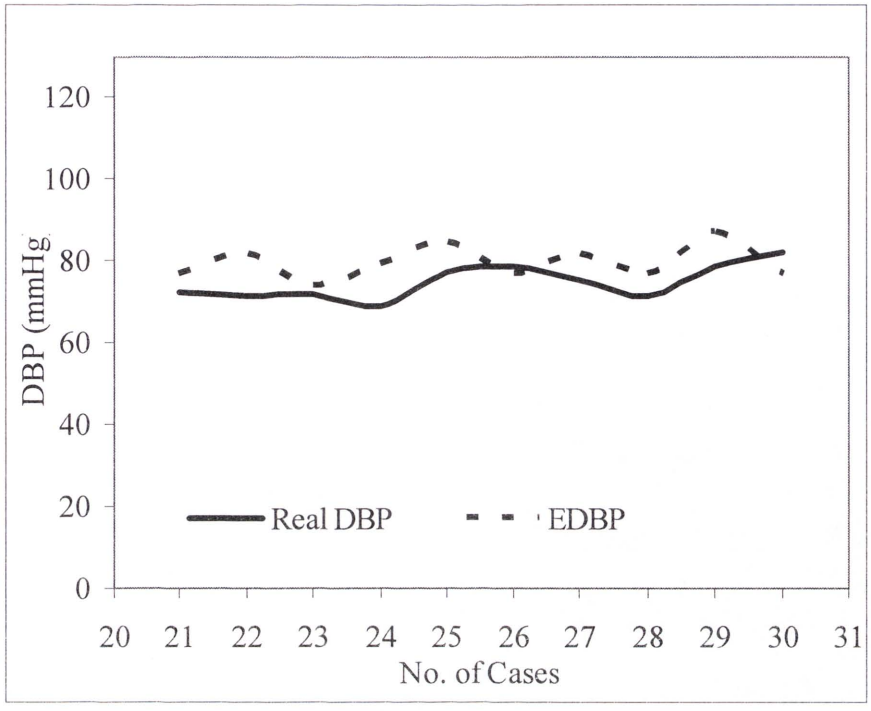

Figure 6.24: The estimated MAP values real MAP values for Healthy Subjects

As can be seen from figure 6.24, the estimated MAP values are very close to real MAP values also the accuracy equals 96.43 %; hence, trained IT2FS can be considered as a practical method.

The achieved EMAP values are illustrated graphically by the B&A plot method [74]. The B&A plot is prepared by calculating the Mean and SD of (EMAP - Real MAP), that is shown in table (6.13), the Mean and SD values of (EMAP - Real MAP) are -3.18 and 2.95 respectively; then B&A plot of EMAP values is shown in figure 6.25.

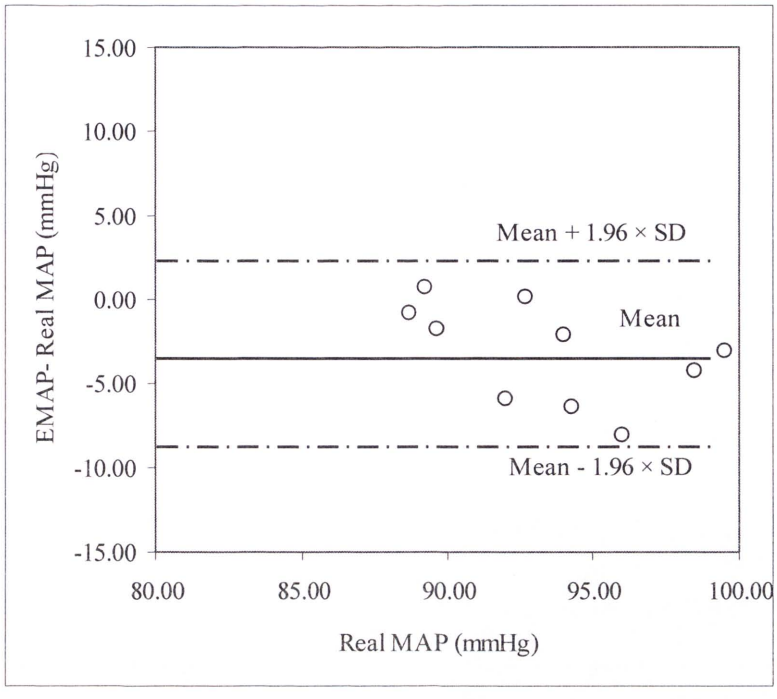

Figure 6.25: B&A plot of MAP for Healthy Subjects

In the B&A plot of MAP that are shown in figure 6.25, all estimated values are located close to the mean of difference and within the border of (mean ± 1.96 SD) and all of these differences are within 95% of Gaussian distribution limit also IT2FSs achieve 96.43 % accuracy for estimating MAP. Hence, IT2FSs can be used as alternative method to calculate the MAP values instead of benchmark methods that are already used to measure MAP for healthy subjects.

6.3.2.1. Estimating MAP for Healthy subjects by Carr's expression

The MAP values for this data set of Healthy subjects are computed by using Carr's expression based on equation (6-5).

Where SV = 70 ml and TPR = 0.018 mmHg.min/ml [5], these values are the SV and TPR for healthy subject.

The estimated MAP (EMAP) values, HR values, Real MAP values, and the absolute differences between EMAP and Real MAP for test group are shown in table (6.14).

Table (6.14): EMAP values, HR values, Real MAP values for remaining ten subjects and the absolute differences between EMAP and Real MAP

No. of Cases	HR b/m	Real MAP mmHg	EMAP mmHg	|EMAP - Real MAP| mmHg
21	72.00	88.7	90.72	2.02
22	86.00	92.7	108.36	15.66
23	63.33	92	79.80	12.20
24	74.33	89.3	93.66	4.36
25	82.33	98.5	103.73	5.24
26	71.00	94.3	89.46	4.84
27	76.00	94	95.76	1.76
28	66.33	89.7	83.58	6.12
29	88.00	99.5	110.88	11.38
30	70.33	96	88.62	7.38
Average	74.97	93.47	94.46	7.10

The estimated MAP values and real MAP values are illustrated in figure 6.26:

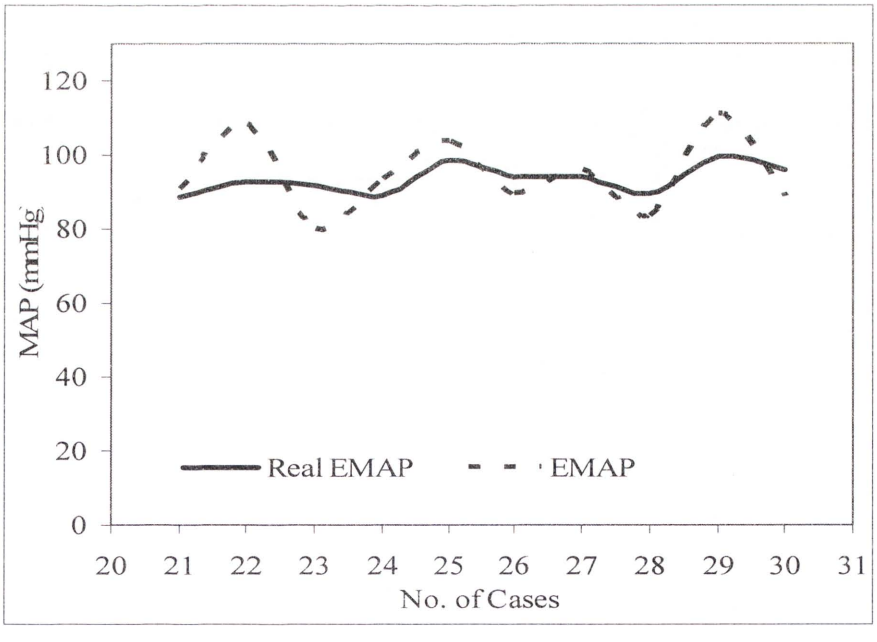

Figure 6.26: The estimated MAP values by Carr's expression and real MAP values

The accuracy of estimated MAP values is calculated by equation (5-2) [73]:

Hence, Accuracy of estimated MAP values = 100 % × (1- ($\frac{7.1}{93.47}$)) = 92.41 %

As observed in figure 6.26, the estimated MAP values by IT2FS are closer to real MAP values than the estimated MAP values by Carr's expression also the accuracy of IT2FS equals 96.43 % and it is higher than the accuracy of Carr's expression [41]; hence, IT2FS is more practical than the Carr's expression. Moreover, IT2FS is utilized to estimate SBP, DBP and MAP.

6.4. Summary

This chapter presented suggested algorithms to overcome some of blood pressure measurement limitations by designing Cardiovascular Parameters Long Term Monitoring System (CPLTMS) based on heart rate (HR) that acquired from Photo-plethysmography (PPG) signal.

The development of methods, performing experiments and achieved results of these methods were clarified, explained, discussed and illustrated by procedures steps, flowcharts, tables, figures and discussion arguments in this chapter .

Chapter 7. Conclusion and Future research

This thesis has established a new methodology by designing the Cardiovascular Parameters Long Term Monitoring System (CPLTMS) based on the correlation between plethysmography's features and cardiovascular parameters as well as employing particle swarm optimization and Interval type 2 fuzzy system alone or both of them to compute or estimate some of the cardiovascular parameters; such as heart rate, oxygen saturation level, also systolic diastolic, and mean blood pressures

The designed CPLTMS consists of two main parts; firstly, the prototype of an electrical circuit. The electrical circuit acquires the amplified and cleaned PPG signals of the subject's finger, analyses the acquired PPG signals' features. Secondly, it has developed a novel algorithm to compute and estimate some of the cardiovascular parameters based on analysed features.

Many experiments have been accomplished to investigate, train and test CPLTMS. This chapter presents the conclusions of the experiments on the developed algorithms and discuss and their results.

7.1. Experiments' results of Heart rate

HR values have been calculated by CPLTMS based on equation (5-1) and PPG signal's frequencies that were extracted of Mimic database. The calculated HR values are compared with real HR values and the achieved accuracy is 99.53%.

Moreover, the agreement of designed CPLTMS is checked by the Bland and Altman (B&A) plot method. The mean of difference between calculated HR values and real HR values equals -0.173 and the standard deviation (SD) equals 0.44; also all the calculated HR values by CPLTMS are located within the agreement boundaries; the mean $\pm$ 1.96 $\times$ SD. Hence, CPLTMS can be used to measure HR values.

7.2. Experiments' results of oxygen saturation level

OSL values have been computed by CPLTMS based on equations (5-12) and (5-13) as well as the amplitudes of alternate current components and direct current components of two acquired PPG signals for two subjects in healthy and deep breath situations. The achieved OSL values of CPLTMS are compared with measured OSL values by a standard device and the achieved accuracy equals 98.91%. Hence, CPLTMS can be used as to evaluate OSL values.

7.3. Experiments' results of mean arterial blood pressure

MAP values have been estimated based on HR values that were extracted of Mimic database and many methods; Meth1: Carr's expression (equation (6-5)), Meth2: our developed expression (equation (6-7)) where the adjustment coefficient of stroke volume (SV) variability influence (A) is determined by the Fit value method. Meth3: our developed expression (equation (6-7)) where A is determined by basic PSO. Meth4: our developed expression (equation (6-7)) where A, SV and total peripheral resistance is simultaneously determined by multi PSO.

The estimated MAP values by Meth1, which is considered as a benchmark method, are compared with MAP real reading values that were extracted from the Mimic database and the achieved accuracy equals 53.83%.

Moreover, the agreement of Meth1 is checked by the B&A plot method. The mean of difference between estimated MAP values and real MAP values equals 34.63 and SD equals 12.2. The calculated MAP values by Meth1 has very high mean difference, hence, Meth1 cannot be used as alternative method to estimate MAP values.

The estimated MAP values by our proposed Meth2 are compared with MAP values that were extracted from Mimic database and the achieved accuracy is equal to 92.00%.

Moreover, the agreement of Meth2 was checked by the B&A plot method. The mean of difference between calculated MAP values and real MAP values equals 4.499 and SD equals 6.42, also all the calculated MAP values by Meth2 are located within the agreement boundaries. Hence, Meth2 can be used as alternative method to estimate MAP values.

The achieved accuracy, however, was improved through determined A by a PSO in our proposed Meth3.

The estimated MAP values by Meth3 achieved accuracy equals 92.58%, when compared with MAP real recorded values that were extracted of Mimic database.

Moreover; Meth3 was checked by B&A plot method. The mean of difference between estimated MAP values and real MAP values equals 3.31 and SD equals 6.44, as well as all the calculated MAP values by Meth3 are located within the agreement boundaries. Hence, Meth3 can be used as alternative method to estimate MAP values. The achieved accuracy, however, had been improved when A, SV and total peripheral resistance is simultaneously determined by multi PSO in our proposed Meth4.

The estimated MAP values by our proposed Meth4 are compared with MAP values that were extracted of Mimic database and achieved accuracy was 94.24%.

Moreover, Meth4 was checked by B&A plot method. The mean of difference between estimated MAP values and real MAP values equals 2.08 and SD equals 5.11, besides, all the calculated MAP values by Meth4 are located within the agreement boundaries. Hence, Meth4 can be used as alternative method to estimate MAP values.

All the achieved accuracies for methods that were used to estimate MAP values are demonstrated in figure 7.1.

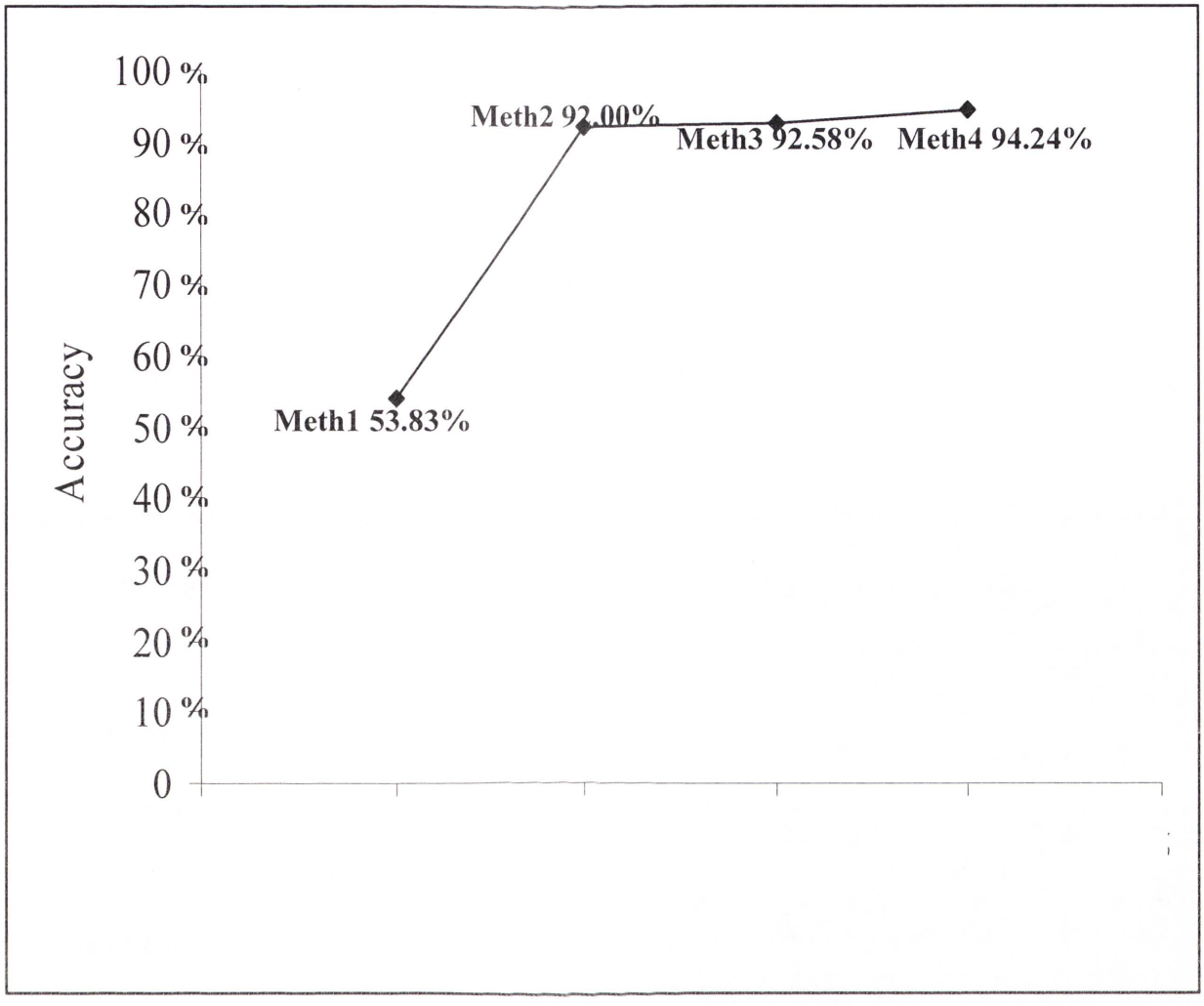

Figure 7.1 The achieved accuracies of MAP methods

From figure 7.1, it can be seen that the achieved accuracies is highly improved by our developed expression and it is slightly improved based on each method that used to optimize the values of expression's factors; adjustment coefficient of SV (A), SV and total peripheral resistance.

7.4. Experiments' results of systolic blood pressure

Essentially, there is no expression to estimate SBP and DBP values based on heart rate; thus, IT2FS has been adopted to estimate and predict SBP and DBP values based on HR values.

The IT2FS has been designed to estimate SBP values based on HR values. Then IT2FS has been trained by updating the parameters of its primary membership functions based on multi PSO on two data sets of unhealthy subjects and healthy subjects.

For unhealthy subjects, the estimated SBP values by trained IT2FS are compared with real recorded SBP values that were extracted of Mimic database and the achieved accuracy equal to 94.51%.

Moreover; the IT2FS designed system was checked by B&A plot method. The mean of difference between estimated SBP values and real SBP values equals 1.56 and SD equals 7.79, besides all the estimated SBP values are located within the agreement boundaries.

For healthy subjects, the estimated SBP values by trained IT2FS are compared with SBP values that were extracted of our collected data and the achieved accuracy equal to 97%.

The designed IT2FS is checked by B&A plot method. The mean of difference between estimated SBP values and real SBP values equals -0.05 and SD equals 3.37; besides all the estimated SBP values are located within the agreement boundaries. Hence, trained IT2FS can be used as an alternative method to estimate SBP values for unhealthy and healthy subjects.

7.5. Experiments' results of diastolic blood pressure

As SBP values, DBP values had been estimated by another IT2FS. The other IT2FS has been designed to estimate DBP values based on HR values then IT2FS has been trained by updating the parameters of its primary membership functions based on multi PSO on two data sets of healthy subjects and unhealthy subjects.

For unhealthy subjects, the estimated DBP values based on trained IT2FS are compared with real DBP values that were extracted of Mimic database and the achieved accuracy of 91.48 %.

The DBP IT2FS system was checked by B&A plot method. The mean of differences between estimated DBP values and real DBP values are equal to 3.37 and SD equal was 5.1, besides all the estimated DBP values are located within the agreement boundaries.

For healthy subjects, the estimated DBP values based on trained IT2FS are compared with real DBP values that were extracted from our collected data and the achieved accuracy was 91.81%.

Moreover, the IT2FS system was checked by B&A plot method. The mean of differences between estimated DBP values and real DBP values equals 4.64 and SD equals 5.17, besides all the estimated DBP values are located within the agreement boundaries. Hence, our proposed trained IT2FS can be used as alternative method to estimate DBP values for unhealthy and healthy subjects.

On other hand, MAP values have been evaluated based on equation (2-1) by using the estimated values of SBP and DBP of trained IT2FSs.

For unhealthy subjects, the evaluated MAP values based on trained IT2FS are compared with MAP values that were extracted of Mimic database and the achieved accuracy was 94.79 %.

Moreover, the evaluated MAP values were checked by the B&A plot method. The mean of differences between evaluated MAP values and real MAP values equals 2.77 and SD equals 4.31, besides all the estimated DBP values are located within the agreement boundaries.

For healthy subjects, the evaluated MAP values based on trained IT2FS are compared with MAP values that were extracted of our collected data and the achieved accuracy was 96.43%.

Again, the evaluated MAP values are checked by B&A plot method. The mean of differences between evaluated estimated MAP values and real MAP values equals -3.18

and SD equals 2.95, besides all estimated MAP values are located within the agreement boundaries. Hence, trained IT2FS can be used as alternative method to estimate MAP values for unhealthy and healthy subjects.

7.6. Future work

There are a number of directions in which CPLTMS could be extended. Here we describe few of these directions.

Improving the system utility and reliability:

The current achieved accuracies of CPLTMS can be more reliable and more widespread.

Labeling the achieved results by understandable words:

The current achieved results of CPLTMS are displayed by numbers only. These numbers are not completely understood by the general public and unspecialized people. These include some language terms, such as normal, high, very high, low and others, to represent these numbers will make them more easily understood by the general public and unspecialized people.

Building a complete stand alone device:

The current methods and algorithms of CPLTMS can be programmed into a microcontroller and a PPG sensor can be integrated with microcontroller to acquire PPG signal of subjects and with display to show the values of cardiovascular parameters with understandable words. This device will facilitate the measurements of heart rate, oxygen saturation level, and blood pressure parameters.

Connecting the device with medical records at hospital:

The achieved results of CPLTMS can be transmitted to a hospital or medical centres and recorded those results in the subject's records. The subjects can be monitored to help them and to protect them from any developments of unpredictable cardiovascular parameters deflections.

8. Appendix

Ethical report:

17 August 2006

Dr Adel Al-Jumaily
CB02.06.05
Faculty of Engineering
UNIVERSITY OF TECHNOLOGY, SYDNEY

Dear Adel,

UTS HREC REF NO 2006-82 – AL-JUMAILY, Dr Adel, DONOGHUE, Professor Judith (for AL-JAAFREH, Mr Moha'med PhD student) - "Cooperative Multi-Agent System for Real-time Continuous Estimation of Cardiovascular Parameters"

Thank you for your response to my email dated 18 April 2006. Your response satisfactorily addresses the concerns and questions raised by the Committee, and I am pleased to inform you that ethics clearance is now granted, subject to the provision of approval letter from the hospitals.

Your clearance number is UTS HREC REF NO. 2006-82A

Please note that the ethical conduct of research is an on-going process. The *National Statement on Ethical Conduct in Research Involving Humans* requires us to obtain a report about the progress of the research, and in particular about any changes to the research which may have ethical implications. This report form must be completed at least annually, and at the end of the project (if it takes more than a year). The Ethics Secretariat will contact you when it is time to complete your first report.

I also refer you to the AVCC guidelines relating to the storage of data, which require that data be kept for a minimum of 5 years after publication of research. However, in NSW, longer retention requirements are required for research on human subjects with potential long-term effects, research with long-term environmental effects, or research considered of national or international significance, importance, or controversy. If the data from this research project falls into one of these categories, contact University Records for advice on long-term retention.

If you have any queries about your ethics clearance, or require any amendments to your research in the future, please do not hesitate to contact the Ethics Secretariat at the Research and Innovation Office, on 02 9514 9615.

Yours sincerely,

Professor Jane Stein-Parbury
Chairperson
UTS Human Research Ethics Committee

9. References

[1] P. Sachford, *A stitch in time saves nine, Prevention mote Cure*, the phantom writers in *http://www.thephantomwriters.com/freecontent/d/s/prevention-health-beats-cure.shtml, Access date* [*12-11-2008*].

[2] Australian Bureau, *National Health Survey: Summary of Results, Australia, 2004-05*, Vol.: no.4364.0, Canberra, Australian Bureau of Statistics, 2006.

[3] AIHW, *Living dangerously: Australians with multiple risk factors for cardiovascular disease*, Vol.: Bulletin no. 24, AUS 57, Canberra, Australian Institute of Health and Welfare, 2005.

[4] L. Steiner, et al., "Validation of a tonometric noninvasive arterial blood pressure monitor in the intensive care setting", *Anaesthesia*, Vol.: 58, No.: (5), pp.: 448-454, 2003.

[5] J.D. Bronzino, *The biomedical engineering handbook*, 3rd. ed., Electrical engineering handbook series., Boca Raton, FL, CRC Press/Taylor & Francis, 2006.

[6] J. DeLisa and W.C. Stolov, *Significant Body Systems*, Handbook of Severe Disability, W.C. Stolov and M.R. Clowers, Department of Education, Rehabilitation Services Administration, USA, pp.: 36-41, 1981.

[7] C.P. Anthony and G.A. Thibodeau, *Textbook of Anatomy & Physiology*, St. Louis, Mosby, pp.: 390-495, 1983.

[8] K. Jan, *Hemodynamic Princibles*, Physiology, in *http://www.columbia.edu/~kj3/Chapter2.htm, Access date* [*21 - 12 - 2007*].

[9] NHLBI, "What Is Blood Pressure", in *http://www.nhlbi.nih.gov/health/dci/Diseases/Hbp/HBP_WhatIs.html, Access date [18 - 06 -2007].*

[10] J.T. Cacioppo, L.G. Tassinary and G.G. Berntson, *Handbook of psychophysiology*, 2nd ed., New York, USA, Cambridge University xiii, 1039 pages, 2000.

[11] AHA, *About High Blood Pressure*, American Heart Association National Center, in *http://www.americanheart.org/presenter.jhtml?identifier=468, Access date* [*18 - 04 - 08*].

[12] S.C. Smeltzer and B.G. Bare, *Brunner and Suddarth's Textbook of Medical and Surgical Nursing*, 8th ed., Philadelphia, Lippincott-Raven 1996.

[13] D. Beecher, et al., *Blood Pressure Monitoring*, non-invasive blood pressure monitoring, in *http://www.medphys.ucl.ac.uk/teaching/undergrad/projects/2003/group_03/history.html, Access date* [*15 - 07 - 2007*].

[14] A. Roguin, "Rene Theophile Hyacinthe Laennec (1781-1826): The Man Behind the Stethoscope", *Clinical Medicine and Research*, Vol.: 4, No.: (3), pp.: 230-235, 2006.

[15] E. O'Brien and K. O'Malley, *Essentials of blood pressure measurement*, Edinburgh, New York, USA, Churchill Livingstone, x, 69 pages, 1981.

[16] O. Healthcare, *Blood Pressure Monitor*, Japan, Omron healthcare company, *http://www.omronhealthcare.com*, 2008.

[17] P. èOberg, et al., "Sensors in medicine and health care", xxiv, 420 pages, in *http://www.lib.uts.edu.au/sso/goto.php?url=http://dx.doi.org/10.1002/35276014 14, Access date [12 - 10 -2007].*

[18] K.-I. Yamakoshi, H. Shimazu and T. Togawa, "Indirect Measurement of Instantaneous Arterial Blood Pressure in the Human Finger by the Vascular Unloading Technique", *IEEE Transactions on Biomedical Engineering*, Vol.: BME-27, No.: (3), pp.: 150-155, 1980.

[19] M. Mizumoto and K. Tanaka, "Some properties of fuzzy sets of type 2", *Information and Control*, Vol.: 31, pp.: 312-340, 1976.

[20] M. Nakagawara and K. Yamakoshi, "Development of a finger cuff unit for a non-invasive blood-pressure monitoring system based on the volume-compensation method", *Journal of Medical Electrical and Biomedical Engineering*, Vol.: 38, pp.: 283-290, 2000.

[21] J. Penaz, "Photo-electric Measurement of blood pressure, Volume and Flow in the Finger", *Digest of the 10-th International Conference on Medical and Biological Engineering*, Dresden, 1973.

[22] B.P.M. Imholz, et al., "Continuous non-invasive blood pressure monitoring: reliability of Finapres device during the valsalva manoeuvre", *Cardiovasc Researce*, Vol.: 22, pp.: 390-397, 1988.

[23] T. Togawa, H. Mizutani and T.Tamura, "Physical monitoring techniques for home health care", *Biomedical Scientific Instrument*, Vol.: 28, pp.: 105 - 110, 1992.

[24] J.W. Remington, *The physical of the aorta and major arteries*, Handbook of Physiology, pp.: 685-692, 1961.

[25] D. Hughes, et al., "Measurement of Young's modulus of elasticity of the canine aorta with ultrasound", *Ultrasonic Imaging*, Vol., pp.: 356-367, 1979.

[26] W. Chen, et al., "Continuous estimating of Systolic blood pressure using the pulse arrival time and intermittent calibration", *Medical and Biological Engineering and Computer*, Vol.: 38, pp.: 569-574, 2000.

[27] J.W. Severinghaus and J.F. Kelleher, "Recent developments in pulse oximetry", *Anesthesiolog*, Vol.: 76, No.: (6), pp.: 1018-1038, 1992.

[28] J.W. Severinghaus and Y. Honda, "History of blood gas analysis.VII. Pulse oximetry" *Journal of Clinical Monitoring*, Vol.: 3, No.: (2), pp.: 135-138, 1987.

[29] M. Hayes and P. Smith, "Artefact Reduction in Photoplethysmography", *Optical Society of America*, Vol.: 37, No.: (31), pp.: 7437-7446, 1998.

[30] Y. Zhang, *Cuff-less continuous monitoring of beat-to-beat blood pressure using a Kalman filter and sensor fusion*, Massachusetts Institute of Technology. Dept. of Mechanical Engineering, Vol.: Massachusetts Institute of Technology. Dept. of Electrical Engineering and Computer Science, 60 leaves, 2000.

[31] Y. Zhang, B. Yang and H. Asada, "Continuous Blood Pressure Measurement by Using a Kalman Filter", *Proceedings of World Congress on Medical Physics and Biomedical Engineering*, Chigaco, USA, 2000.

[32] S. Rhee, B. Yang and H. Asada, "Artifact-Resistant Power-Efficient Design of Finger-Ring Plethysmographic Sensors", *IEEE Transaction on Biomedical Engineering*, Vol.: 48, No.: (7), pp.: 795 - 805, 2001.

[33] H. Asada, et al., "Mobile Monitoring with Wearable PPG-BioSensors", *IEEE Engineering in Medicine and Biology Magazine*, Vol.: 22, No.: (3), pp.: 28-40, 2003.

[34] P.Y.S. Cheang and P.R. Smith, *An Overview of Non-contact Photoplethysmography*, Department of Electronic and Electrical Engineering, Loughborough University, Loughborough, 2003.

[35] X.F. Teng and Y.T. Zhang, "Continuous and Non-invasive Estimation of Arterial Blood Pressure Using a Photo-plethysmographic Approach", *25th Annual International Conference of the IEEE EMBS*, Cancun, Mexico, 2003.

[36] C.M. Lee and Y.T. Zhang, "Cuffless and Noninvasive Estimation of blood pressure Based on a Wavelet Transform approach", *IEEE EMBS Asian-Pacific Conference*, pp.: 148-149, 2003.

[37] M. Yan and Y. Zhang, "Noninvasive Estimation of Blood Pressure Using Photo-plethysmographic Signals in the Period Domain", *27th Annual International Conference in Medicine and Biology Society*, Shanghai, China, pp.: 3583 - 3584, 2005.

[38] T. Ma and Y. Zhang, "A Correlation Study on the Variabilities in Pulse Transit Time, Blood Pressure, and Heart Rate Recorded Simultaneously from Healthy Subjects", *Proceedings of 27th Annual International Conference in Medicine and Biology Society*, Shanghai, China, pp.: 996 - 999, 2005.

[39] C. Poon and Y. Zhang, "Cuff-less and Noninvasive Measurements of Arterial Blood Pressure by Pulse Transit Time", *Proceedings of 27th Annual International Conference in Medicine and Biology Society*, Shanghai, China, pp.: 5877 - 5880, 2005.

[40] P.A. Shaltis, A.T. Reisner and H.H. Asada, "Cuffless Blood Pressure Monitoring Using Hydrostatic Pressure Changes", *Biomedical Engineering, IEEE Transactions on*, Vol.: 55, No.: (6), pp.: 1775-1777, 2008.

[41] J.J. Carr and J.M. Brown, *Introduction to biomedical equipment technology*, 4th ed., Upper Saddle River, N.J., Prentice Hall, xv, 743 pages, 2001.

[42] S. Jayaraman and C. North, *A Radial Focus +Context Visualization for Multi-Dimensional Functions*, Conference on Visualization, San Jose, California, USA, 443 – 450, 2002.

[43] P. McSharry, M. McGuinness and A. Fowler, "Confronting a cardiovascular system model with heart rate and blood pressure data", *Journal of Computers in Cardiology*, Vol.: 32, pp.: 587-590, 2005.

[44] N. Karnik and J. Mendel, "Introduction to type-2 fuzzy logic systems", *IEEE International Conference on World Congress on Computational Intelligence*, pp.: 915-920, 1998.

[45] J. Mendel and Q. Liang, *Pictorial Comparisons of Type-1 and Type-2 Fuzzy Logic Systems*, International Conference on Intelligent Systems & Control IASTED, Santa Barbara, CA, 1999.

[46] L. Zadeh, "Fuzzy sets", *Information and Control*, Vol.: 8, pp.: 338-352, 1965.

[47] H. Ying, *Fuzzy Control and Modeling*, Analytical Foundations and Applications, Wiley-IEEE Press, pp.: 1-13, 2000.

[48] T. Henk, *Understanding Probability*, Cambridge University, New York, USA, 2004.

[49] M. Mendel, *Uncertain rule-based fuzzy logic systems: introduction and new directions*, Upper Saddle River, New Jersey, USA, Prentice Hall PTR, 2001.

[50] S. Coupland and R.I. John, "Geometric Type-1 and Type-2 Fuzzy Logic Systems", *IEEE Transactions on Fuzzy Systems*, Vol.: 15, No.: (1), pp.: 3-15, 2007.

[51] L. Zadeh, "The concept of a linguistic variable and its application to approximate reasoning", *Information Sciences*, Vol.: 8, pp.: 199-249, 1975.

[52] J. Mendel, R. John and F. Liu, "Interval Type-2 Fuzzy Logic Systems Made Simple, IEEE Transactions on Fuzzy Systems", 14, pp.: 808-821, 2006.

[53] R. John, "Type-2 fuzzy sets: an appraisal of theory and applications", *International Journal of Uncertainty, Fuzziness and Knowledge-Based Systems*, Vol.: 6, pp.: 563 - 576, 1998.

[54] R. John and C. Czarnecki, "A type-2 adaptive fuzzy inferencing system", *IEEE International Conference on Systems for Man and Cybernetics (SMC'98)*, pp.: 2068 - 2073, 1998.

[55] O. Mendoza, P. Melin and G. Licea, "Fuzzy Inference Systems Type-1 and Type-2 for Digital Images Edge Detection", *Journal of Engineering Letters*, Vol.: 15, No.: (1), pp.: 45-52, 2007.

[56] R. John, P. Innocent and M. Barnes, "Type-2 fuzzy sets and Neuro-fuzzy clustering of radiographic tibia images", *International Conference of IEEE Congress on Computational Intelligence on Fuzzy Systems*, pp.: 1373 - 1376, 1998.

[57] C. Own, et al., "Adaptive type-2 fuzzy median filter design for removal of impulse noise Imaging Science", *Imaging Science Journal*, Vol.: 54, No.: (1), pp.: 3 - 18, 2006.

[58] T. Baeck, "Generalized convergence models for tournament and (mu, lambda)-selection", *the Sixth International Conference on Genetic Algorithms*, San Francisco, California, USA, Morgan Kaufmann Publishers, pp.: 2-7, 1995.

[59] J. Kennedy, R.C. Eberhart and Y. Shi, *Swarm intelligence*, San Francisco, California, USA, Morgan Kaufmann Publishers, 2001.

[60] R.C. Eberhart and J. Kennedy, "A new optimizer using particle swarm theory", *Sixth International Symposium on Micro-machine and Human Science*, Nagoya, Japan, pp.: 39-43, 1995.

[61] S. Panda and N.P. Padhy, "Comparison of Particle Swarm Optimization and Genetic Algorithm for TCSC-based Controller Design", *International Journal of Computer Science and Engineering*, Vol.: 1, No.: (1), 2008.

[62] J. Robinson and Y. Rahmat-Samii, "Particle Swarm Optimization in Electromagnetics", *IEEE Transactions on Antennas and Propagations*, Vol.: 52, No.: (2), pp.: 397-407, 2004.

[63] J. Salerno, *Using the particle swarm optimization technique to train a recurrent neural model*, IEEE International Conference on Tools with Artificial Intelligence, 45-49, 1997.

[64] R. Eberhart and X.Hu, "Human tremor analysis using particle swarm optimization", *IEEE Congress on evolutionary computation (CEC 1999)*, pp.: 1927-1930, 1999.

[65] Y. Fukuyama, et al., "A particle swarm optimization for reactive power and voltage control in electric power systems", *the Genetic and Evolutionary Computation Conference*, Orlando, Florida, USA, pp.: 1523-1528, 1999.

[66] S. Kannan, et al., "Application of particle swarm optimization technique and its variants to generation expansion planning problem", *Electric Power Systems Research*, Vol.: 70, No.: (3), pp.: 203-210, 2004.

[67] K. Pilt, et al., *An Experimental Study of PPG Probe Efficiency Coefficient Determination on Human Body*, IFMBE Proceedings, Vol.: 20, Springer Berlin Heidelberg, 2008.

[68] K.W. Sum, Y.P. Zheng and A.F.T. Mak, "Vital Sign Monitoring for Elderly at Home: Development of a Compound Sensor for Pulse Rate and Motion", *Personalised Health Management Systems: The Integration of Innovative Sensing, Textile, Information and Communication Technologies*, Vol.: 117, pp.: 43-50, 2005.

[69] Y.Y. Gu, Y. Zhang and Y.T. Zhang, "A novel biometric approach in human verification by photo-plethysmographic signals", *4th International IEEE EMBS Conference on Information Technology Applications in Biomedicine*, pp.: 13-14, 2003.

[70] A. Johansson, "Neural network for photo-plethysmographic respiratory rate monitoring", *Medical and Biological Engineering and Computing*, Vol.: 41, No.: (3), pp.: 242-248, 2003.

[71] H. Pispati, *Concise textbook of physiology for dental students*, New Delhi ; Oxford, Oxford University Press, viii, 424 pages, 2001.

[72] G.Y. Jeong, K.H. Yu and N.G. Kim, "Continuous Blood Pressure Monitoring using Pulse Wave Transit Time", *ICCAS2005 Conference*, Gyeonggi-Do, Korea, KINTEX.2005.

[73] J.S. Armstrong, "Relative Accuracy of Judgmental and Extrapolative Methods in Forecasting Annual Earnings", *Journal of Forecasting*, Vol.: 2, pp.: 437-447, 1983.

[74] J.M. Bland and D.G. Altman, "Measuring agreement in method comparison studies", *Statistical Methods in Medical Research*, Vol.: 8, pp.: 135-160, 1999.

[75] J. Walker, D. Halliday and R. Resnick, *Fundamentals of physics*, 8th ed., Hoboken, NJ, John Wiley & sons, xxii, 1248 pages, 2008.

[76] A. Hurch, et al., "Limitations of pulse oximetry", *Lancet*, Vol.: 1, pp.: 357-358, 1988.

[77] J.D. Ingle and S.R. Crouch, *Spectrochemical analysis*, Englewood Cliffs, N.J, Prentice Hall, xv, 590 pages, 1988.

[78] J.G. Kim, X. Mengna and L. Hanli, "Extinction coefficients of hemoglobin for near-infrared spectroscopy of tissue", *Engineering in Medicine and Biology Magazine, IEEE*, Vol.: 24, No.: (2), pp.: 118-121, 2005.

[79] S.L. Schutz, *Oxygen Saturation Monitoring by Pulse Oximetry*, AACN Procedure manual for Critical Care, D.J. Lynn-McHale and K.K. Carlson, W.B. Saunders, Philadelphia, pp.: 77-82, 2001.

[80] PhysioNet, *Mimic database*, Massachusetts Institute of Technology (MIT), Cambridge, USA, 1999.

[81] D.S. O'Leary and R.A. Augustyniak, "Muscle metaboreflex increases ventricular performance in conscious dogs", *Am J Physiol Heart Circ Physiol*, Vol.: 275, No.: (1), pp.: H220-224, 1998.

[82] AHA, "American heart association", in *http://www.americanheart.org*, Access date [18 - 08 -2008].